ALKALI FELDSPARS: ORDERING, COMPOSITION AND OPTICAL PROPERTIES

by

Shu-Chun Su

Dissertation submitted to the Faculty of the
Virginia Polytechnic Institute and State University
in partial fulfillment of the requirements for the degree of
Doctor of Philosophy
in
Geology

APPROVED:

F. Donald Bloss, Co-chairman

Paul H. Ribbe, Co-chairman

Gerald V. Gibbs

David B. Stewart

Hans Wondratschek

March 1986

Blacksburg, Virginia

ALKALI FELDSPARS: ORDERING, COMPOSITION AND OPTICAL PROPERTIES

by

Shu-Chun Su

F. Donald Bloss, Co-chairman
Paul H. Ribbe, Co-chairman

Geological Sciences

(ABSTRACT)

For the **entire** alkali feldspar series, Σt_1 (total Al content in the T_1 sites, a quantitative measure of structural state or Al,Si long-range ordering) can be closely estimated from X_{Or} (mole fraction of $KAlSi_3O_8$) and V_x (one half of the optic axial angle $2V_x$) by use of a simple determinative diagram based on the model

$$\Sigma t_1 = \frac{b_0 + b_1 X_{Or} + b_2 X_{Or} \sin^2 V_x + b_3 \sin^2 V_x}{a_0 + a_1 X_{Or} + a_2 X_{Or} \sin^2 V_x + a_3 \sin^2 V_x} .$$

Three sets of coefficients for this equation are required to account for three cases: (A) where $X_{Or} \leq 0.6$; (B) where $X_{Or} > 0.6$ and O.A.P. (optical axial plane) $\sim \perp$ (010); and (C) where $X_{Or} > 0.6$ and O.A.P. = (010). They are (multiplied by 1000):

Case	a_0	a_1	a_2	a_3	b_0	b_1	b_2	b_3
A	4.08	-2.35	0.95	-1.28	1.52	-0.18	-1.74	2.88
B	1.69	1.63	-2.33	0.69	0.11	2.17	-2.70	3.46
C	-1.69	-1.63	-0.70	2.38	-0.11	-2.17	-0.53	3.57

Tested by the data from 109 alkali feldspars in the literature and the author's experiments, this model estimates Σt_1 (given X_{Or} and V_x) with a standard error of 0.02, which is essentially the same as when Σt_1 is estimated from refined lattice parameters determined by X-ray diffraction methods.

The model was developed by assuming that the principal refractive indices for sodium light – symbolized as n_a, n_b, and n_c dependent upon whether the corresponding principal vibration axis was parallel or most nearly parallel to crystallographic axes *a*, *b* and *c* – varied linearly with Σt_1 for the high-sanidine to low-microcline series and for the low albite to high albite (or analbite) series. However, for the high albite to high sanidine solid solution series, as well as the low albite to low microcline series, neither density nor principal refractive indices vary linearly across the entire composition range,but they closely approached linearity between $0.0 \leq X_{Or} < 0.6$ and $0.6 < X_{Or} \leq 1.0$.

ACKNOWLEDGEMENTS

It is with deepest appreciation that I thank Professor F. Donald Bloss and this Department as well as this University for having offered me this opportunity to pursue my doctoral program. It means so much to me. With the same appreciation I thank all members of my advisory committee for their tireless guidance and valuable criticism throughout all stages of this study. Few doctorate candidates in mineralogy have been privileged to have so many eminent mineralogists and crystallographers serving on their advisory committee.

Special thanks are due to Co-chairmen Professors Bloss and Paul H. Ribbe not only for their primary contribution to guiding this dissertation, but also for their spiritual support during a period of trial in my life; without it I can hardly imagine how I could have accomplished this work. The extensive knowledge and pioneer thinking of Dr. David B. Stewart (U. S. Geological Survey) and Prof. Ribbe in feldspar problems and the questioning mind and penetrating insight of Prof. Bloss in unraveling crystal-chemical controls of optical properties have greatly improved the depth and quality of this work. Prof. Gerald V. Gibbs' stimulating teaching and thorough understanding of modern crystal chemistry and crystallography have proved to be invaluable to my research. The late inspired some original thinking about the relationships between thermodynamical properties and optical properties of rock-forming silicates. He has been keenly missed. The vacancy left by his sudden and tragic death was ably filled by Prof. Hans Wondratschek, Director of the Institute of Crystallography, University of Karlsruhe, West Germany. The inspiring discussions with Prof. Wondratschek have always been very helpful and rewarding.

Special thanks are also due to my noble-hearted wife , who defied the "revolutionaries" by marrying me, a "counter-revolutionary," in the darkest period of Chinese history, for her selfless sacrifices, and for her unfailing support to me.

It would be unforgivable not to acknowledge the financial support received in the form of research assistantships from the National Science Foundation and a Cunningham Fellowship administered by this University. More properly, these came from the people of this great nation, and without this support it would have been impossible for me to come to study in the United States, an opportunity I never took for granted. I am grateful to CNRS (Centre Nationale de la Recherche Scientifique), France, for the generous fellowship which enabled me to present a paper at the 3rd NATO Advanced Study Institute on Feldspars and Feldspathoids held in Rennes, France, 1983. Financial support to me from the Caswell Silver Foundation of the Department of Geology, University of New Mexico, during my fruitful stay there with Prof. Bloss from July 1981 to May 1982 is also gratefully acknowledged.

skillful typing of this dissertation on the word processor is highly appreciated and warmly acknowledged. Also I would like to thank and for the high quality of their drafting of all the figures.

I am indebted to and for their technical support and valuable help in various phases of data collection.

I thank for their generosity in providing feldspar samples for this study.

Lastly but not least importantly, I give my thanks to , my host family in Albuquerque. Their love to me and my family has been a source of strength that has never left me since I stepped on this land in 1981.

TABLE OF CONTENTS

LIST OF FIGURES

LIST OF TABLES

CHAPTER 1. PROCEDURES AND COMPUTER PROGRAMS TO REFINE THE DOUBLE VARIATION METHOD

Introduction

The precision and accuracy with which the refractive indices of a solid can be determined by the immersion method depend upon the precision and accuracy with which the refractive indices of the immersion oil are known. If the double variation method is to be used, the change of the oil's refractive index (n) with wavelength ($dn/d\lambda$) and with temperature (dn/dt) must also be known with comparable precision and accuracy. These data, although sometimes supplied by the manufacturer, may change as the oil ages. Indeed, sometimes after a manufacturer's supply of a given immersion oil has been exhausted, the refractive index of the replacement oil may precisely match that of its predecessor only at the wavelength 589 nm. Consequently, its printed label, if that of its predecessor, may indicate refractive indices that no longer pertain at the other wavelengths. For precise and accurate determination of the refractive indices of solids by the double variation method, therefore, it is necessary to calibrate the immersion oils to be used.

This paper describes the techniques and supporting computer programs used by the writer to calibrate immersion media and to suppress random errors when determining the refractive indices of solids by the double variation method. It also describes procedures for reducing systematic errors through use of glass standards whose refractive indices are accurately known to the fifth or sixth decimal place. Only touched upon is the use of a spindle stage (Bloss, 1981), mounted on a polarizing microscope, so as to orient anisotropic crystals so that their principal refractive indices can be measured without significant error from misorientation.

Equipment

High accuracy refractometer

A high-accuracy Abbe refractometer, model 60/HR from Bellingham and Stanley, Ltd., has proven ideal for immersion oil calibration. It differs from conventional types of Abbe refractometers in that (1) it does not have a built-in prism to compensate for dispersion so that it can only be used with monochromatic light sources, and (2) its read-out scale is graduated in degrees and, with help of a micrometer drum, can be read to one-thousandth of a degree. The manufacturer provides four conversion tables whereby a critical angle reading may be converted into its corresponding refractive index at each of the four wavelengths, 435.84, 546.07, 589.60, and 643.85 nm, respectively. For other wavelengths, as well as the foregoing, the conversion of critical angle (α) to refractive index N_L can be calculated from

$$N_L = 0.866025 + [N_P^2 - \sin(\alpha - 29.5°)]^{1/2} + 0.5 \sin[(\alpha - 29.5°)] \quad , \qquad (1)$$

where

$$N_P = 1.860682 + 1.91832 \times 10^{-2} \times \lambda^{-2} + 1.029446 \times 10^{-4} \times \lambda^{-4} \quad . \qquad (2)$$

While the refractometer is in use, the temperature of the oil between its prisms must be monitored to within 0.1°C. Considering that dn/dt for Cargille oils in the 1.500-1.700 index range may equal as much as -0.0006 per degree Celsius, a temperature error of 0.2°C would cause an error of approximately 0.0001 in the measured refractive index. To maintain a stable temperature for the prism box of the refractometer, room-temperature water from a reservoir is circulated through the prism box. The temperature of the

immersion oil being calibrated is monitored by a chromel-alumel thermocouple inserted into a channel hollowed out in the cement surrounding the refractometer's illuminating prism.

Light source

Rather than using a monochromator to illuminate the refractometer, we use a set of three metal-vapor spectral bulbs that provide high purity and high intensity light at wavelengths 435.84 nm (Hg bulb with blue filter), 546.07 nm (Hg bulb with green filter), 589.60 nm (Na bulb), and 643.85 nm (Cd bulb with red filter). A heat filter placed between the bulb and the refractometer greatly reduces heat transfer to the refractometer by infrared radiation from the bulb.

Monochromator and oil cell

When employing the double variation (λ,T) method to measure the refractive indices of solid unknowns, we control the wavelength of illumination by means of a Schott wedge-interference filter as made by Leitz. Alternatively, any continuously variable monochromator or a series of narrow-band-pass filters with peak wavelengths at 5 nm intervals can be used. A heatable oil cell (Bloss, 1981, p. 139) changes the oil temperature and is monitored by a built-in thermocouple.

Spindle stage

A spindle stage, mounted on a polarizing microscope, plus the techniques of Bloss (1981) will serve to orient anisotropic crystals so that their principal refractive indices can be measured without significant error due to misorientation. A spindle stage is even valuable if the unknown grain is isotropic. By its means one can orient the grain so that it best shows a Becke line or an oblique shadow when comparing the refractive indices of the grain and oil.

Calibration Procedures

Immersion oils

To calibrate the oil we make at leasat 10 critical-angle measurements at each of four wavelengths (643.85, 589.60, 546.07 and 435.84 nm). The measurements at 643.85 and 435.84 nm are difficult because of the eye's lesser sensitivity to these wavelengths. Consequently, it is necessary to work in a darkened room and to prevent stray light from the light source from entering the observer's eyes. For each critical-angle measurements, the oil's temperature (t) is also determined. The computer program OIL, written by the author, converts each measured critical angle to its corresponding refractive index (n_t). OIL then corrects this index to its value at 25°C ($n_{25,\lambda}$) by inserting the values of t and n_t, plus dn/dt of the oil into the equation

$$n_{25} = n_t - (t - 25°)(dn/dt) \quad . \qquad (3)$$

Using a least-squares method, OIL next fits to the n_{25} values thus obtained for each wavelength (in nanometers) the Cauchy dispersion equation

$$n_{25,\lambda} = c_1 + \frac{c_2}{\lambda^2} + \frac{c_3}{\lambda^4} \quad . \tag{4}$$

After the intercept c_1 and the regression coefficients c_2 and c_3 are obtained, the calibrated oil's refractive index for any wavelength and temperature ($n_{t,\lambda}$) can be calculated from

$$n_{t,\lambda} = c_1 + \frac{c_2}{\lambda^2} + \frac{c_3}{\lambda^4} + (t - 25)(dn/dt) \quad . \tag{5}$$

If the Cargille oils used in our laboratory are kept tightly closed and protected from light between each use, their Cauchy constants (c_1, c_2, c_3) have remained unchanged, within the experimental error, for at least a year.

Measuring system

The precision and accuracy with which a solid's refractive indices can be measured depend upon (1) the sensitivity of the criterion of match between the indices of grain and oil and (2) knowledge of the exact refractive index of the oil at the conditions of match. Louisnathan et al. (1978) addressed item (1). Item (2) depends upon how precisely and accurately one knows (a) the temperature and wavelength of match and (b) dn/dt of the oil, and its Cauchy constants (c_1, c_2, c_3) so that equations (3) and (4) can serve to calculate the refractive index of the oil for the temperature and wavelength of match. Although statistical analysis of the data may reduce the effect of random experimental errors, systematic errors may also affect the determinations of the temperature and the

wavelength of match. Moreover, if only a few oils are used during the double variation procedures, errors in dn/dt and the Cauchy constants for these oils will themselves become systematic errors. In our laboratory our measuring system is calibrated by means of standard optical glasses whose refractive indices at various wavelengths are accurately known to the sixth decimal place.

To calibrate our measuring system so as to reduce systematic errors, we use 13 highly homogeneous optical glasses kindly supplied to our laboratory by the Corning Glass Company. For these 13 glasses, whose indices range from 1.51 to 1.80, the refractive indices were measured to the sixth decimal at wavelengths 435.8, 546.1, 587.6 and 632.8 nm by Drs. C.J. Parker and Al Werner (pers. comm.) of Corning through the use of the minimum deviation method and a specially designed spectrometer.

In determining the refractive indices of an unknown solid, we first select that Corning glass whose refractive index n_D is closest to the refractive index to be measured for the solid. We next select the three **calibrated** oils whose refractive indices are slightly higher, almost equal, and slightly lower than that for the Corning glass selected. Using these oils, successively, we measure the Corning glass by the double variation method. For each match between glass and oil, essentially determined as discussed by Louisnathan et al. (1978), the wavelength (λ) and temperature (T) is recorded. Approximately 100 to 150 readings, evenly distributed over the visible range (486-656 nm), are made within the 20-30°C temperature range. These λ,t data are then processed by the FORTRAN program SOLID which, through least-squares regression methods, determines the values for the Cauchy constants c_1, c_2 and c_3 by fitting equation (4) to the data. SOLID similarly determines values for the constants a_0 and a_1 in the linearized Sellmeier equation (Louisnathan et al., 1978; Bloss, 1981),

$$y = a_0 + a_1 x \quad , \tag{6}$$

where x equals λ^{-2}, y equals $(n_\lambda^2 - 1)^{-1}$, and n_λ equals the refractive index at wavelength λ. The resultant constants we call observed Cauchy and Sellmeier constants and symbolize them as $c_{1,obs}$, $c_{2,obs}$, $c_{3,obs}$ and as $a_{0,obs}$ and $a_{1,obs}$, respectively. Similarly, we fit the refractive indices measured at the four wavelengths by Parker and Werner.to equations (4) and (6) to obtain constants which we symbolize as $c_{1,cal}$, $c_{2,cal}$, $c_{3,cal}$, $a_{0,cal}$, and $a_{1,cal}$ where the subscript "cal" indicates that the constant was calculated from the minimum deviation data of Parker and Werner. Equation (4) and the two sets of Cauchy constants for the Corning glass standard – $c_{1,obs}$, $c_{2,obs}$, $c_{3,obs}$ and $c_{1,cal}$, $c_{2,cal}$, $c_{3,cal}$ – permit n_{obs} and n_{cal} to be calculated at any wavelength λ. The correction value Δn_λ can thus be determined for any wavelength λ since

$$\Delta n_\lambda = n_{obs} - n_{cal} \quad . \tag{7}$$

Similarly, for this Corning glass standard, equation (6) and the two sets of linearized Sellmeier constants – $a_{0,obs}$, $a_{1,obs}$ and $a_{0,cal}$, $a_{1,cal}$ – also permit n_{obs} and n_{cal} to be determined for any wavelength λ. The correction value Δn_λ can thus be again calculated for any wavelength λ by use of equation (7).

When an unknown solid is measured, then n_{25}, its refractive index at 25°C for the wavelength at which a match occurred, can be calculated from n_t, the refractive index of the oil for the wavelength of match, and t, the temperature of match. Thus by inserting n_t, t and dn/dt into equation (3), we obtain n_{25}. Systematic error in this value is reduced by subtracting from it Δn_λ as calculated (eqn. 7) for the same wavelength as that of match. Thus,

$$n_{25,\,corrected} = n_{25} - \Delta n_\lambda \quad .$$

Each match observed by the double variation method within the 20-30°C range for the unknown thus results in a wavelength of match λ and a corresponding corrected refractive index of match $n_{25,\,corrected}$. Typically, 30 or more such matches for a principal refractive index are obtained over the 486 to 656 nm wavelength range. These pairs of data are then analyzed by the computer, and either Equation (4) or (6) is fitted to the data pairs by the method of least square. In actuality, we merely submit to the program SOLID, the λ and t values for the 30 or so matches, as well as dn/dt and n_{25} for the oil. It then applies the temperature correction (eqn. 3) and the correction for systematic error based on the appropriate Corning glass standard (eqn. 7). It then fits respectively a Cauchy equation (eqn. 4) and linearized Sellmeier equation (eqn. 6) to the $(\lambda, n_{25,\,corrected})$ data pairs to obtain the constants c_1, c_2, c_3 and a_0, a_1 that will permit the unknown's refractive index to be calculated for any wavelength within the visible range (and perhaps slightly beyond).

REFERENCES

Bloss, F.D. (1981) The Spindle Stage: Principles and Practice. Cambridge University Press, Cambridge, England, 340 p.

Louisnathan, S.J., Bloss, F.D., and Korda, E.J. (1978) Measurement of refractive indices and their dispersion. American Mineralogist, 63, 394-400.

APPENDIX

User's Guide for OIL

OIL is a program written in FORTRAN IV for processing the refractive index (R.I.) data measured at different wavelengths (at least four) and temperatures of a liquid or immersion oil collected on a B & S 60/HR high precision refractometer. It fits the data into Cauchy and linearized Sellmeier dispersion equations by using least-squares regression methods and derives the Cauchy and Sellmeier dispersion constants for the liquid or oil measured. This program has its own least-squares analysis subroutines and therefore does not call any subroutines from any statistical packages.

Input data file

Card Type I TITLE Format (3F10.5), One card only

Columns	Variable	Description
1-10	LABEL	The refractive index value on the label of the immersion oil bottle.
11-20	DNDTLT	dn/dt for temperatures lower than 25°C.
21-30	DNDTHT	dn/dt for temperatures higher than 25°C.

Comment: The dn/dt values are negative. In this line the negative signs of dn/dt,s must not be entered. The program will treat them as negative values.

Card Type II OBSERVED DATA Format (3F10.5), Up to 100 cards

Columns	Variable	Description
1-10	SCLRED	Scale reading of the B & S 60/HR refractometer.
11-20	WLNM	Wavelength (in nm) of the light sources.
21-30	TMV	Temperature reading. Depending on the type of temperature measurement devices, TMV may be entered either as degrees in centigrade (°C) or as millivolts (mV).

Comments: 1.If TMV entered as millivolt(s), the statement of Line #69 in the main program should be changed according to the parameters of the thermocouple used.
2. Starting on the second observed data card, if any of the variables (SCLRED, WLNM and TMV) is identical to the previous one, it can be represented by blanks.

User's Guide for SOLID

SOLID is a program written in FORTRAN IV for processing the experimental data collected by double (or single) variation method. It fits the data into Cauchy and linearized Sellmeier dispersion equations by using least-squares regression methods and derives the Cauchy and Sellmeier dispersion constants for the solid measured. This program has its own least-squares analysis subroutines and therefore does not call any subroutines from any statistical packages. It can also make corrections to the observed data based on the results of measuring system calibration using Corning optical glasses to reduce the systematic errors.

Input data file

Card Type I TITLE Format (18A4), One card only

Columns	Variable	Description
1-72	TITLE	Any alphanumeric information.

Card Type II CAUCHY CONSTANTS Format (6F10.7), One card only

Columns	Variable	Description
1-10	C1CAL	Cauchy constants c_1, c_2 and c_3, calculated from the minimum deviation data provided by Corning Co. for the optical glass used in system calibration.
11-20	C2CAL	
21-30	C3CAL	
31-40	C1OBS	Cauchy constants c_1, c_2 and c_3 of the Corning optical glass derived in the system calibration.
41-50	C2OBS	
51-60	C3OBS	

Comment: If no corrections are to be applied to the observed data, this line must be left as a blank line.

Card Type III SELLMEIER CONSTANTS Format (2(F10.7, F10.3)), One card only

Columns	Variable	Description
1-10	A0CAL	Sellmeier constants a_0 and a_1 calculated from minimum deviation data provided by Corning Co. for the optical glass used in system calibration.
11-20	A1CAL	
21-30	A0OBS	Sellmeier constants a_0 and a_1 of the Corning optical glass derived in the system calibration.
31-40	A1OBS	

Comments: 1. If no corrections are to be aplied to the observed data, this line must be left as a blank line.
2. The a_1 value is based on the wavelength in nm instead of μm.

Card Type IV — WEDGE AND THERMOCOUPLE PARAMETERS Format (5F10.7), One card only

Columns	Variable	Description
1-10	WEDGE1	Leitz interference wedge filter parameters derived from the data provided by the manufacturer.
11-20	WEDGE2	
21-30	WEDGE3	
31-40	THERM1	Thermocuple parameters.
41-50	THERM2	

Comments: See Bloss (1981) for detailed procedures of deriving these wedge constants.

Card Type V — OIL CONSTANTS Format (6F10.7), Up to 5 cards.

Columns	Variable	Description
1-10	LABEL	The refractive index value on the label of the immersion oil bottle.
11-20	DNDTL0	dn/dt for temperatures lower than 25°C.
21-30	C10	Cauchy constants c_1, c_2 and c_3 of the oil used.
31-40	C20	
41-50	C30	
51-60	DNDTH0	dn/dt for temperatures higher than 25°C.

Card Type VI — OBSERVED DATA Format (10X, 2F10.7), Up to 200 cards.

Columns	Variable	Description
11-20	WLR	The wavelength reading at the match point. Depending on the type of the monochromator used, WLR may be entered either as Messort number (in mm) if a Leitz interference wedge filter is used or as wavelength (in nm) if a monochromator with direct wavelength scale is used.
21-30	TMV	The temperature reading at the match point. Depending on the type of temperature measurement devices, TMV may be entered either as degrees in centigrade (°C) or as millivolts (mV).

Comments:
1. OIL CONSTANTS card is followed by a series of OBSERVED DATA cards.
2. If WLR or TMV is identical to the previous observation, it can be represented by blanks.

CHAPTER 2. OPTICAL AXIAL ANGLE, A PRECISE MEASURE OF AL,SI ORDERING IN T_1 TETRAHEDRAL SITES OF K-RICH ALKALI FELDSPARS[1]

Introduction

It is well known that the optic axial angle $2V_x$ is strongly dependent on the long-range order of Al,Si in the tetrahedral sites of K-rich feldspars, and in fact $2V_x$ has been used to designate relative "structural states" for many years (see Smith, 1974, Chapter 8, for a review). Conventionally, the highly disordered, monoclinic **high sanidines** (HS) have optic axial planes (O.A.P.'s) parallel to (010) with $2V_x$ ranging from ~60° to 0°; **low sanidines** (LS) have O.A.P.'s normal to (010) with $0° < 2V_x < ~36°$; **orthoclases** (OR) also have O.A.P.'s $\perp$ (010), but with $~36° < 2V_x < ~80°$. Triclinic **microclines** (MC) have O.A.P.'s approximately normal to (010) with $2V_x$ values overlapping the orthoclases and vary from ~38° (**intermediate microclines**) to ~85° for completely ordered **low** or **maximum microcline** (LM).[2] Thus, combined with the change in orientation of the optic plane, $2V_x$ varies through a total of 145° as Al,Si ranges from disordered to ordered in K-rich alkali feldspars.

The crystal structures of potassic feldspars are well documented by 15 or more modern structural refinements of C2/m sanidines and orthoclases and another 15 of $C\bar{1}$ microclines. These have led to a detailed understanding of the response of unit cell parameters – notably *b*, *c*, α^* and γ^* – to changes in Al,Si distribution within the two tetrahedral sites (T_1 and T_2) of monoclinic potassic feldspars and among the four tetra-

---

[1] Published as Su et al. (1984), American Mineralogist, 69, 440-448.

[2] Optically positive microclines ("iso-microclines") have been reported, but we have examined the specimens of Blasi (1972) by microprobe X-ray scanning methods and found them to be mechanical mixtures of exsolved low microcline ($2V_x$ = 85°) and low albite ($2V_x$ = 103°). For a detailed review of alkali feldspar optics, see Stewart and Ribbe (1983).

hedral sites (T_1o, T_1m, T_2o and T_2m) of triclinic ones. Using the symbols t_1, t_2, t_1o, t_1m, t_2o and t_2m to designate the average Al/(Al + Si) contents of these sites (as determined from mean T-O bond lengths in the aforementioned structural refinements), we may make the following statements about K-rich alkali feldspars: (1) For C2/m monoclinic specimens: $2t_1 + 2t_2 = 1.0$. (2) For $C\bar{1}$ triclinic specimens: $t_1o + t_1m + t_2o + t_2m = 1.0$. (3) The most disordered high sanidine has $2t_1 = 2t_2 = 0.5$ (although this has never been observed in a natural specimen). (4) In low sanidines and orthoclases $2t_1$ becomes increasingly greater than $2t_2$ as ordering increases. (5) Microclines have $t_1o > t_1m > t_2o \cong t_2m$ or $t_1o > t_1m \cong t_2o \cong t_2m$. (6) Ordered low microcline has $t_1o = 1.0$, $t_1m = t_2o = t_2m = 0.0$. Kroll and Ribbe (1983) give details on how to estimate Al contents of T sites from crystal structure data and from unit cell parameters determined by X-ray single-crystal or powder diffractometry. In this paper, however, we present the **quantitative** relationship between the total Al content of the T_1 sites, $\Sigma t_1 \equiv 2t_1$ or $(t_1o + t_1m)$, and $2V_x$, thus establishing a rapid and precise method of determining the structural state of separated grains of K-rich alkali feldspars (using a spindle stage) or from point to point on grains in thin section (using a universal stage).

The Relation of Optical Properties to Al,Si Distribution

Disordered high sanidine ($\Sigma t_1 \cong 0.5$) and ordered low microcline ($\Sigma t_1 \cong 1.0$) differ markedly in optic orientation (Fig. 2.1). Consequently, to facilitate comparison of principal refractive indices for light vibrating along **similar** crystallographic directions in these two structures (and in those of intermediate structural states), we use n_b to symbolize the principal index for light vibrating parallel or nearly parallel to the crystallographic axis *b*. In this we follow Hewlett (1959), who used the symbol "b" (see also

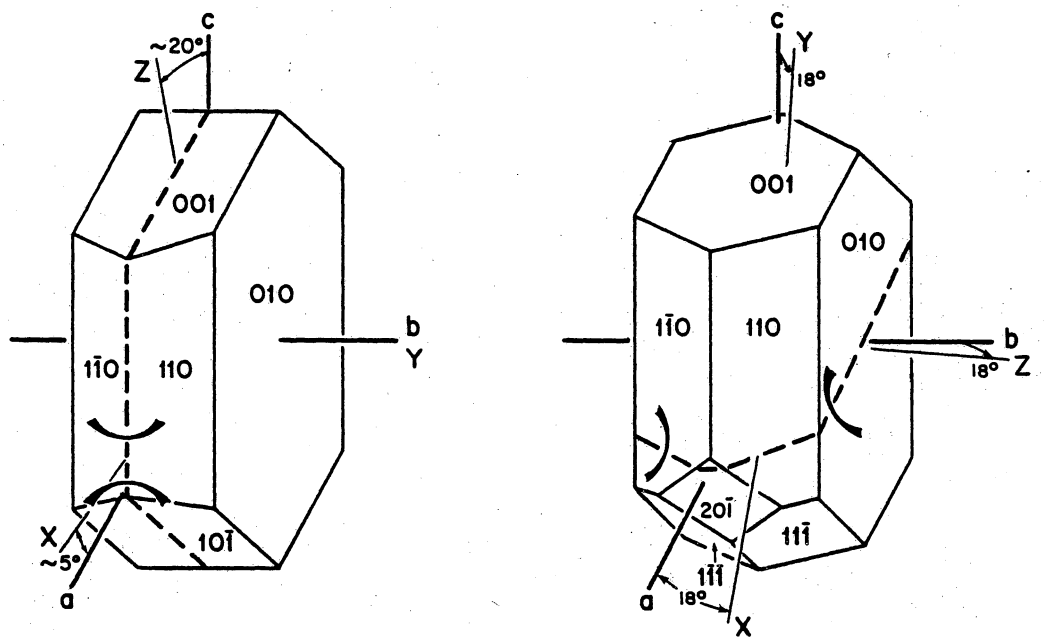

Figure 2.1. The optic orientations of high sanidine and low microcline: Dashed lines are the traces of the optic axial planes.

Finney and Bailey, 1964). We extend this convention by using n_a and n_c to indicate the principal refractive indices for light vibrating most nearly parallel to the *a* and *c* crystallographic axes, respectively, even though these vibrations may be at appreciable angles to *a* and *c*.

Refractive indices versus unit cell edges

If at opposite ends of a "structural state" scale we plot the principal refractive indices for high sanidine (HS) and low microcline (LM) and label them n_a, n_b, n_c instead of α, β, γ, and if we simplistically assume that n_a , n_b and n_c vary linearly with total Al content of the T_1 sites, the lower portion of Figure 2.2 results. The general correctness of this model over that in which γ_{HS} is traditionally connected to γ_{LM} and β_{HS} to β_{LM} , is readily apparent. It indicates that, for O.A.P. = (010) in HS, $2V_x$ decreases from ~60° to 0° with increased Al,Si ordering. With continued Al,Si ordering beyond the point where n_b equals n_c, the O.A.P. becomes perpendicular to (010) or nearly so, and $2V_x$ increases from 0° toward its maximum value of ~85° for LM. Cell-edge data for HS and LM also corroborate this model. If we add these data to Figure 2.2 and for simplicity assume linear variation, we note a reciprocal relationship between each cell edge and the principal refractive index for light vibrating most nearly parallel to it. Thus, as Al,Si ordering increases from HS to LM, a marked increase in n_b accompanies a marked decrease in *b*, a slight increase in n_a accompanies a slight decrease in *a*, and a marked decrease in n_c accompanies a marked increase in *c*. This principle of the inverse relationship between cell-edge length and corresponding refractive index was first demonstrated convincingly for the andalusite-kanonaite series by Gunter and Bloss (1982) and, indeed, aided our insight into the alkali feldspars. In Figure 2.2 we arbitrarily chose to plot *b* and *c* so that they cross at the Σt_1 value for which $n_b = n_c$ in our model. This

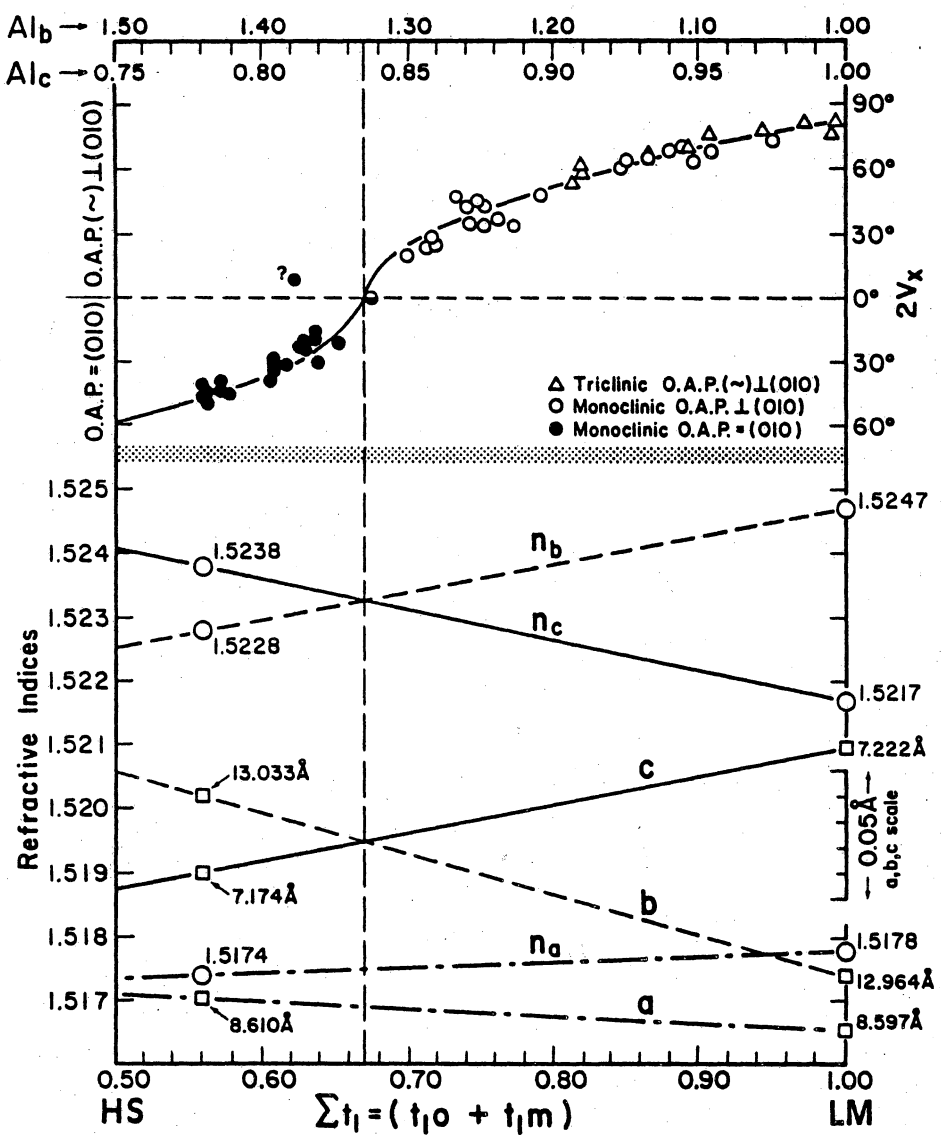

Figure 2.2. The refractive indices, n_a, n_b , n_c (open circles), and unit cell dimensions, *a*, *b*, *c* (open squares), are plotted for high sanidine (HS) and low microcline (LM), and simple linear variations are assumed for each parameter: The n values for HS were determined by refinement of values extrapolated from data given by Smith (1974, Figs. 8-9, p. 386); the corresponding $2V_x$ = 46.4°. The n values for LM are those of the Pellotsalo specimen of Brown and Bailey (1964); $2V_x$ = 82.3 °. The cell dimensions of HS ($2t_1$ = 0.56) and LM (t_1o = 1.0) are those chosen by Kroll and Ribbe (1983) as standard reference values for alkali feldspars [see their paper (pp. 71 and 74 and Table 4) for details and reasons for choosing to plot HS at Σt_1 = 0.56; this choice controls the values of α_s, β_s, γ_s , and the coefficients in Equations 8 and 9.

emphasizes the reciprocity between the refractive index and its corresponding cell edge by causing the triangles formed by the intersection of lines *b* and *c* to be very similar to the two formed by the intersection of lines n_c and n_b .

Hewlett (1959) recognized that the d_{010} and d_{001} spacings varied nearly linearly with structural state of K-rich feldspars, and Stewart and Ribbe (1969) quantified these relationships for the *b* and *c* cell edges of all alkali feldspars. In Figure 2.3 it can be seen that the Al contents encountered in any six contiguous tetrahedral sites along *b* (≡ Al_b) and any three along *c* (≡ Al_c) are:

$$Al_b = t_1o + t_1m + 4\,t_2 \quad , \tag{1}$$

$$Al_c = t_1o + t_1m + t_2 \quad , \tag{2}$$

where t_2 represents t_2o or t_2m for triclinic feldspars (in which all structure analyses to date have shown $t_2o = t_2m$). Because

$$t_1o + t_1m + t_2o + t_2m = 1$$

$$\text{or } \Sigma t_1 + t_2o + t_2m = 1 \, ,$$

and since $t_2o = t_2m$,

$$t_2 = \frac{1}{2}\,(1 - \Sigma t_1) \quad . \tag{3}$$

Equations 1 and 2 may be rewritten

$$Al_b = \Sigma t_1 + 2(1 - \Sigma t_1) = 2 - \Sigma t_1 \quad , \tag{4}$$

and

$$Al_c = \Sigma t_1 + (1 - \Sigma t_1)/2 = (1 + \Sigma t_1)/2 \quad . \tag{5}$$

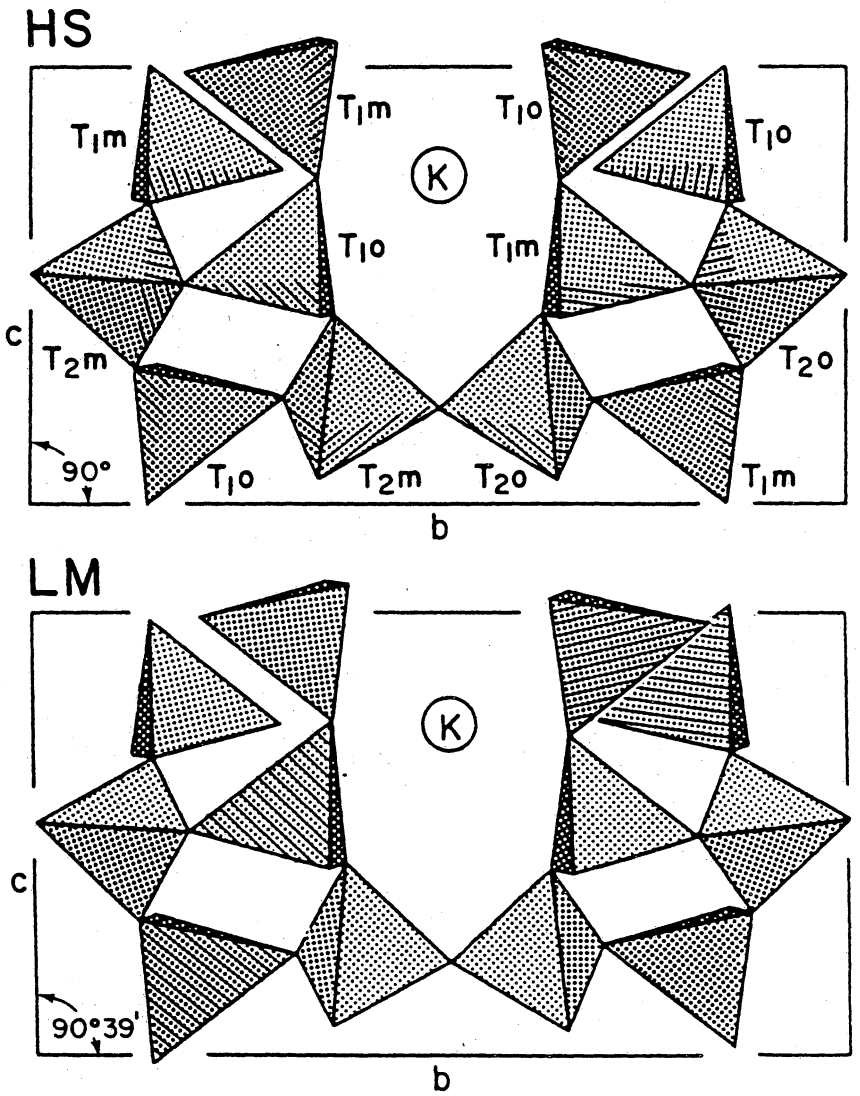

Figure 2.3. The arrangement of tetrahedra along *b* and *c* in similar regions of the unit cells of high sanidine (HS) and low microcline (LM): The tetrahedra are ruled roughly in proportion to their Al content (0.25 for each T site in HS; 1.0 for T_1o in ordered LM).

To a first approximation, therefore, the amounts of Al encountered along *b* and *c* are **linear** functions of Σt_1(see upper abscissa in Fig. 2.2), Al_b **decreasing** from 1.5 for HS to 1.0 for LM and Al_c **increasing** exactly half as much, that is, from 0.75 for HS to 1.0 for LM. Because the effective size of Al is larger than Si (mean T-O bonds are ~1.74 A for Al sites, ~1.61 A for Si sites), Stewart and Ribbe (1969) were able to show that the cell edges *b* and *c* vary proportionately with Σt_1, as now confirmed by approximately 30 crystal structures (Kroll and Ribbe, 1983). By contrast, the cell edge *a* varies only slightly with Al,Si ordering because

$$Al_a = t_1o + t_1m + t_2o + t_2m = 1.0 \quad ,$$

and the actual distribution of Al among these sites is essentially irrelevant to the length of *a*.

Sigmoidal 2Vx curve

We now assume that the refractive indices and their linear variation with Al,Si ordering are reasonably correct. From these refractive index trends, we can calculate $2V_x$ using the exact equation

$$\sin^2 V_x = \frac{\beta^{-2} - \gamma^{-2}}{\alpha^{-2} - \gamma^{-2}} \qquad (6)$$

or, to within a few tenths of a degree for crystals of low birefringence like potassic feldspars, using the approximate equation

$$\sin^2 V_x = \frac{\gamma - \beta}{\gamma - \alpha} \quad . \tag{7}$$

Plotting $2V_x$ values calculated from the linearly varying refractive indices against Σt_1 produces the sigmoidal curve shown near the top of Figure 2.2. To this curve we added data from the literature for which $2V_x$ and unit cell parameters were both reported (Table 2.1) so that t_1o and t_1m could be calculated for each specimen using the [110],[1$\bar{1}$0] translation method of Kroll (1980, reported in Kroll and Ribbe, 1983). Most of these data points fall very close to the sigmoidal curve. In fact, the estimated standard error in Σt_1 is 0.02 for 52 specimens, 19 of which have known crystal structures that confirm the Σt_1 values calculated by Kroll's method (see Table 2.2).

The agreement between the sigmoidal model and the crystal data is all the more remarkable because: (1) No consideration was given to whether the crystal symmetry was monoclinic or triclinic; (2) no correction for albite content was made even though some specimens contained up to 20 mol % Ab, in addition to minor amounts of Ca, Ba, Sr, and Fe; (3) some of the specimens are submicroscopically twinned and/or exsolved; (4) some specimens may be strained; (5) the sigmoidal curve, in the final analysis, was derived from just two sets of data points (HS and LM; data on Fig. 2.2) together with the simplistic assumption that refractive indices n_a, n_b , and n_c vary linear with Al,Si ordering between HS and LM; (6) for 32 of these data, cell parameters were measured on powdered specimens and $2V_x$ on separate crystals, and even some of the specimens whose crystal structures were determined had their $2V_x$ values measured on separate single crystals. Only eight of the nine feldspars in the superb suite of Dal Negro et al. (1978) and DePieri (1979) are certain to have had $2V_x$ and Σt_1 (from both cell parameters and structure analyses) measured on the same grain In fact, some of the specimens in Table 2.1 had $2V_x$ measured by Spencer (1937) and cell parameters measured by powder

Table 2.1. Potassium-rich alkali feldspars, their compositions (in mol % Or), $2V_x$ values and unit cell dimensions: For $2V_x$, a minus sign indicates that the optic axial plane is parallel to (010). Var = structural classification: MC = microcline, OR = orthoclase, LS = low sanidine, HS = high sanidine. An asterisk indicates the feldspar is metrically monoclinic, but topochemically triclinc. Ref = references, as listed at the bottom of the table.

No.	Sample	Or	Var	$2V_x$	*a*, Å	*b*, Å	*c*, Å	α (°)	β (°)	γ (°)	Ref
1	PELLOTSALO	95.0	MC	82.5	8.560	12.964	7.215	90.65	115.83	87.70	2
2	CA1E	88.6	MC	82.0	8.558	12.963	7.217	90.52	115.93	87.98	4
3	RC20C	85.5	MC	78.5	8.566	12.961	7.217	90.43	116.00	88.48	4
4	PONTISKALK	98.0	MC	77.0	8.573	12.962	7.218	90.57	115.92	87.75	5
5	SP-U	87.6	MC	76.0	8.578	12.960	7.211	90.30	115.97	89.12	1
6	P1C	90.0	MC	71.0	8.574	12.971	7.212	90.33	116.03	88.78	4
7	CA1B	88.6	MC	65.0	8.559	12.976	7.211	90.30	116.03	89.02	4
8	SP-H	86.3	MC	61.5	8.577	12.963	7.190	90.26	116.06	89.48	9
9	A1D	90.4	MC	53.0	8.563	12.984	7.201	90.13	116.02	89.50	4
10	SP-M	85.6	OR	73.7	8.637	12.895	7.185	90.00	116.24	90.00	9
11	SP-Z	90.1	OR	71.8	8.570	12.965	7.207	90.00	116.03	90.00	9
12	SP-I	90.2	OR	69.1	8.622	12.927	7.192	90.00	116.15	90.00	9
13	SP-B	90.0	OR	68.5	8.554	12.970	7.207	90.00	116.01	90.00	11
14	7007	88.1	OR	65.0	8.545	12.967	7.201	90.00	116.00	90.00	6
15	SP-V	90.7	OR	63.5	8.571	12.973	7.202	90.00	116.01	90.00	9
16	HIMALAYA	88.1	OR	63.0	8.563	12.963	7.210	90.00	116.07	90.00	8

(to be continued)

(continued)

No.	Sample	Or	Var	$2V_x$	*a* Å	*b*, Å	*c*, Å	α (°)	β (°)	γ (°)	Ref
17	SP-K	88.3	OR	61.4	8.605	12.944	7.186	90.00	116.10	90.00	9
18	CA1A	88.6	OR*	60.0	8.563	12.984	7.204	90.00	116.03	90.00	4
19	P2A	93.1	OR*	49.0	8.583	12.989	7.202	90.00	116.05	90.00	4
20	SP-F	74.9	OR	49.0	8.522	12.976	7.183	90.00	116.11	90.00	9
21	SP-D	80.5	OR	46.2	8.538	12.982	7.185	90.00	116.02	90.00	9
22	P50-56	87.7	OR	44.0	8.561	12.995	7.194	90.00	115.99	90.00	11
23	SP-C	90.8	OR*	43.6	8.562	12.996	7.193	90.00	116.01	90.00	3
24	P2B	93.1	OR	38.0	8.589	12.995	7.198	90.00	116.02	90.00	4
25	SP-A	93.9	OR	34.8	8.582	12.989	7.198	90.00	116.04	90.00	9
26	2B11-1	95.0	LS	35.0	8.574	13.003	7.199	90.00	116.02	90.00	7
27	2B31	92.0	LS	34.0	8.567	12.997	7.199	90.00	116.05	90.00	7
28	2B131	92.0	LS	28.0	8.568	13.004	7.195	90.00	116.04	90.00	7
29	2B12	94.0	LS	26.0	8.573	13.005	7.195	90.00	116.02	90.00	7
30	2B11-2	92.0	LS	25.0	8.569	13.003	7.192	90.00	116.02	90.00	7
31	2B6	94.0	LS	20.0	8.573	13.008	7.194	90.00	116.04	90.00	7
32	SV-17	90.0	LS	9.0	8.549	13.028	7.188	90.00	116.02	90.00	10
33	2B15-1	93.0	HS	0.0	8.572	13.011	7.190	90.00	116.03	90.00	7
34	S1A43-1	90.0	HS	-15.0	8.555	13.020	7.185	90.00	115.99	90.00	12
35	2B15-2	95.0	HS	-16.0	8.574	13.014	7.191	90.00	116.01	90.00	7
36	S1A33-1	91.0	HS	-20.0	8.557	13.024	7.184	90.00	115.97	90.00	12
37	2B4-1	93.0	HS	-20.0	8.574	13.017	7.185	90.00	116.03	90.00	7
38	2B4-2	93.0	HS	-22.0	8.570	13.018	7.188	90.00	116.01	90.00	7
39	7002	85.4	HS	-22.0	8.539	13.015	7.179	90.00	115.99	90.00	6

(to be continued)

(continued)

No.	Sample	Or	Var	$2V_x$	*a* Å	*b*, Å	*c*, Å	α (°)	β (°)	γ (°)	Ref
40	S1A44-1	89.0	HS	-24.0	8.553	13.021	7.183	90.00	115.98	90.00	12
41	S1A43-2	90.0	HS	-28.0	8.554	13.025	7.181	90.00	115.98	90.00	12
42	S1A33-2	91.0	HS	-30.0	8.558	13.025	7.182	90.00	115.99	90.00	12
43	2A4	93.0	HS	-30.0	8.570	13.017	7.186	90.00	116.04	90.00	7
44	S1A43-3	88.0	HS	-31.0	8.554	13.019	7.180	90.00	116.00	90.00	12
45	S1A44-2	89.0	HS	-34.0	8.555	13.023	7.181	90.00	116.00	90.00	12
46	S1A43-4	90.0	HS	-38.0	8.555	13.026	7.180	90.00	115.96	90.00	12
47	S1A33-3	89.0	HS	-39.0	8.551	13.032	7.179	90.00	116.00	90.00	12
48	SV-17T	89.0	HS	-41.0	8.546	13.037	7.178	90.00	115.97	90.00	10
49	S1A33-4	90.0	HS	-44.0	8.558	13.032	7.177	90.00	115.97	90.00	12
50	SAN-SP-C	90.8	HS	-44.5	8.565	13.030	7.175	90.00	115.99	90.00	3
51	1B1	92.0	HS	-45.0	8.567	13.031	7.181	90.00	116.03	90.00	7
52	5A1	94.0	HS	-50.0	8.574	13.032	7.178	90.00	116.02	90.00	7

1. Bailey (1969)
2. Brown & Bailey (1964)
3. Cole et al. (1949)
4. DePieri (1979)
5. Finney & Bailey (1964)
6. Phillips & Ribbe (1973)
7. Priess (1982)
8. Prince et al. (1973).
9. Stewart (1974)
10. Weitz (1972)
11. Wright & Stewart (1968)
12. Zeipert & Wondratschek (1981)

Table 2.2. The Al/(Al + Si) contents of the T_1 sites of specimens in Table 2.1: Column 1 = Σt_1 as determined from mean T-O bond lengths using structural data (Kroll and Ribbe, 1983, Tables 2 and 3). Column 2 = Σt_1 calculated by the [110],[1$\bar{1}$0] method of Kroll (1980). Column 3 = Σt_1 predicted by our sigmoidal model. Column 4 is the residual of [column 2 - column 3], subject to round-off errors. Column 5 = Σt_1 predicted by our linear model. Column 6 = [column 2 - column 5].

No.	Sample	$2V_x$	1	2	3	4	5	6
1	PELLOTSALO	82.5	1.01	1.00	1.00	0.00	0.97	0.02
2	CA1E	82.0	0.97	0.97	1.00	-0.02	0.97	0.00
3	RC20C	78.5	0.96	0.94	0.97	-0.02	0.95	-0.01
4	PONTISKALK	77.0	0.99	0.99	0.96	0.03	0.94	0.05
5	SP-U	76.0	0.91	0.91	0.95	-0.04	0.93	-0.03
6	P1C	71.0	0.87	0.90	0.92	-0.02	0.90	-0.01
7	CA1B	65.0	0.90	0.87	0.88	0.00	0.87	0.00
8	SP-H	61.5	.	0.82	0.85	-0.04	0.85	-0.03
9	A1D	53.0	0.82	0.81	0.81	0.01	0.81	0.01
10	SP-M	73.7	.	0.95	0.93	0.02	0.92	0.03
11	SP-Z	71.8	.	0.89	0.92	-0.03	0.91	-0.02
12	SP-I	69.1	.	0.91	0.90	0.01	0.89	0.02
13	SP-B	68.5	0.83	0.88	0.90	-0.02	0.89	-0.01
14	7007	65.0	0.85	0.87	0.88	-0.01	0.87	0.00

(to be continued)

(continued)

No.	Sample	$2V_x$	1	2	3	4	5	6
15	SP-V	63.5	.	0.85	0.87	-0.02	0.86	-0.01
16	HIMALAYA	63.0	0.90	0.90	0.86	0.03	0.86	0.04
17	SP-K	61.4	.	0.85	0.85	-0.01	0.85	-0.01
18	CA1A	60.0	0.84	0.82	0.85	-0.03	0.84	-0.02
19	P2A	49.0	0.78	0.79	0.79	0.00	0.79	0.00
20	SP-F	49.0	.	0.73	0.79	-0.05	0.79	-0.05
21	SP-D	46.2	.	0.75	0.77	-0.03	0.77	-0.03
22	P50-56	44.0	.	0.75	0.76	-0.01	0.76	-0.01
23	SP-C	43.6	0.72	0.74	0.76	-0.02	0.76	-0.02
24	P2B	38.0	0.73	0.76	0.74	0.02	0.74	0.02
25	SP-A	34.8	.	0.77	0.73	0.05	0.73	0.05
26	2B11-1	35.0	.	0.74	0.73	0.01	0.73	0.01
27	2B31	34.0	.	0.75	0.73	0.03	0.73	0.03
28	2B131	28.0	.	0.72	0.71	0.01	0.71	0.01
29	2B12	26.0	.	0.72	0.70	0.02	0.70	0.02
30	2B11-2	25.0	.	0.71	0.70	0.01	0.70	0.01
31	2B6	20.0	.	0.70	0.69	0.01	0.69	0.01
32	SV-17	9.0	0.64	0.62	0.67	-0.06	0.67	-0.05
33	2B15-1	0.0	.	0.68	0.67	0.01	0.66	0.01
34	S1A43-1	-15.0	.	0.64	0.66	-0.02	0.65	-0.02

(to be continued)

(continued)

No.	Sample	$2V_x$	1	2	3	4	5	6
35	2B15-2	-16.0	.	0.68	0.66	0.02	0.65	0.02
36	S1A33-1	-20.0	.	0.63	0.65	-0.03	0.64	-0.02
37	2B4-1	-20.0	.	0.64	0.65	-0.01	0.64	-0.01
38	2B4-2	-22.0	.	0.65	0.65	0.00	0.64	0.01
39	7002	-22.0	0.60	0.63	0.65	-0.02	0.64	-0.01
40	S1A44-1	-24.0	.	0.63	0.64	-0.01	0.63	-0.01
41	S1A43-2	-28.0	.	0.61	0.63	-0.02	0.62	-0.02
42	S1A33-2	-30.0	.	0.61	0.63	-0.02	0.62	-0.01
43	2A4	-30.0	.	0.64	0.63	0.01	0.62	0.02
44	S1A43-3	-31.0	.	0.62	0.62	-0.01	0.61	0.00
45	S1A44-2	-34.0	.	0.61	0.61	0.00	0.60	0.00
46	S1A43-4	-38.0	.	0.60	0.60	0.01	0.59	0.02
47	S1A33-3	-39.0	.	0.57	0.59	-0.02	0.59	-0.01
48	SV-17T	-41.0	0.54	0.56	0.59	-0.03	0.58	-0.02
49	S1A33-4	-44.0	.	0.57	0.57	0.00	0.57	0.01
50	SAN-SP-C	-45.0	0.54	0.56	0.57	-0.01	0.56	0.00
51	1B1	-45.0	.	0.58	0.57	0.01	0.56	0.01
52	5A1	-50.0	.	0.56	0.54	0.02	0.54	0.02

methods **on the K-rich phase only** (Stewart and Wright, 1974); these parameters were used to calculate Σt_1. Since "geologic evidence is abundant for a range in $2V_x$ of tens of degrees in one feldspar crystal, and of 50° or more among the crystals in a single hand specimen" (Stewart and Ribbe, 1983, p. 133), it is remarkable how good the agreement is with the sigmoidal curve.

A corollary of the assumed linear variation of n_a, n_b and n_c relative to Σt_1 (Fig. 2.2) is that the birefringences $(\gamma - \alpha)$, $(\gamma - \beta)$ and $(\beta - \alpha)$ also vary linearly with Σt_1. These linear relationships, if used in conjunction with equation 6, will lead to the following general equations for the sigmoidal curve (after considerable mathematical manipulation). Thus, for O.A.P. = (010) we obtain:

$$\Sigma t_1 = 0.44 \left[\frac{(\gamma_s - \beta_s) - (\gamma_s - \alpha_s) \sin^2 V_x}{[(\gamma_m - \beta_m) + (\gamma_s - \beta_s)] + [(\beta_m - \alpha_m) - (\gamma_s - \alpha_s)] \sin^2 V_x} \right] + 0.56 \quad (8)$$

For O.A.P. $\perp$ (010) or $\sim \perp$ (010) we obtain:

$$\Sigma t_1 = 0.44 \left[\frac{(\gamma_s - \beta_s) - (\beta_s - \alpha_s) \sin^2 V_x}{[(\gamma_m - \beta_m) + (\gamma_s - \beta_s)] + [(\gamma_m - \alpha_m) - (\beta_s - \alpha_s)] \sin^2 V_x} \right] + 0.56 \quad (9)$$

Here the subscripts **s** and **m** respectively are abbreviations for HS and LM. To the extent that the refractive index data plotted in Figure 2.2 are correct, equation 8 becomes

$$\Sigma t_1 = 1.686 - \frac{1.626}{1.600 - \sin^2 V_x} , \quad (10)$$

and equation 9 becomes

$$\Sigma t_1 = -1.024 + \frac{4.517}{2.667 - \sin^2 V_x} . \quad (11)$$

Also, to the extent these refractive indices and equations 10 and 11 are valid, the cross-over point of the sigmoidal curve (i.e., the point where $V_x = 0°$) occurs at $\Sigma t_1 = 0.67$.

Linear model: Σt_1 versus $\sin^2 Vx$

Equation 7 indicates that $\sin^2 V_x$ represents the quotient of two birefringences. Even if both birefringences vary linearly with Σt_1, their quotient and thus $\sin^2 V_x$ would not do so (see the discussion by Bloss, 1952). Equations 10 and 11 also indicate that Σt_1 is related nonlinearly to $\sin^2 V_x$ Nevertheless, given the magnitude of the coefficients in Equations 10 and 11, and the fact that $0° \leq V_x \leq 45°$ so that $0 \leq \sin^2 V_x \leq 0.5$, the relationship between Σt_1 and $\sin^2 V_x$ is nearly linear. This explains why a **linear** regression performed on the data on Table 2.1, using $\sin^2 V_x$ as the independent variable and Σt_1 as the dependent variable, yields a coefficient of determination, $r^2 = 0.962$ (see Fig. 2.4). The resulting equation is split into two segments. For O.A.P. = (010),

$$\Sigma t_1 = 0.665(3) - 0.711(17) \sin^2 V_x \quad , \qquad (12a)$$

and for O.A.P. perpendicular to (010), or nearly so

$$\Sigma t_1 = 0.665(3) + 0.711(17) \sin^2 V_x \quad , \qquad (12b)$$

with numbers in parentheses referring to the estimated standard deviations (**esd**) for the respective coefficients. Each indicates, as for the sigmoidal model, that if V_x equals 0°, then $\Sigma t_1 = 0.665$ (**esd** = 0.02). These equations predict that $2V_x$ will equal 57.6° for a completely disordered high sanidine ($\Sigma t_1 = 0.5$) and 86.7° for a completely ordered low microcline ($\Sigma t_1 = 1.0$). These compare to literature values of 54° and 82°. It should be noted that the largest $2V_x$ value reported for a sanidine, 63°, is for a specimen syn-

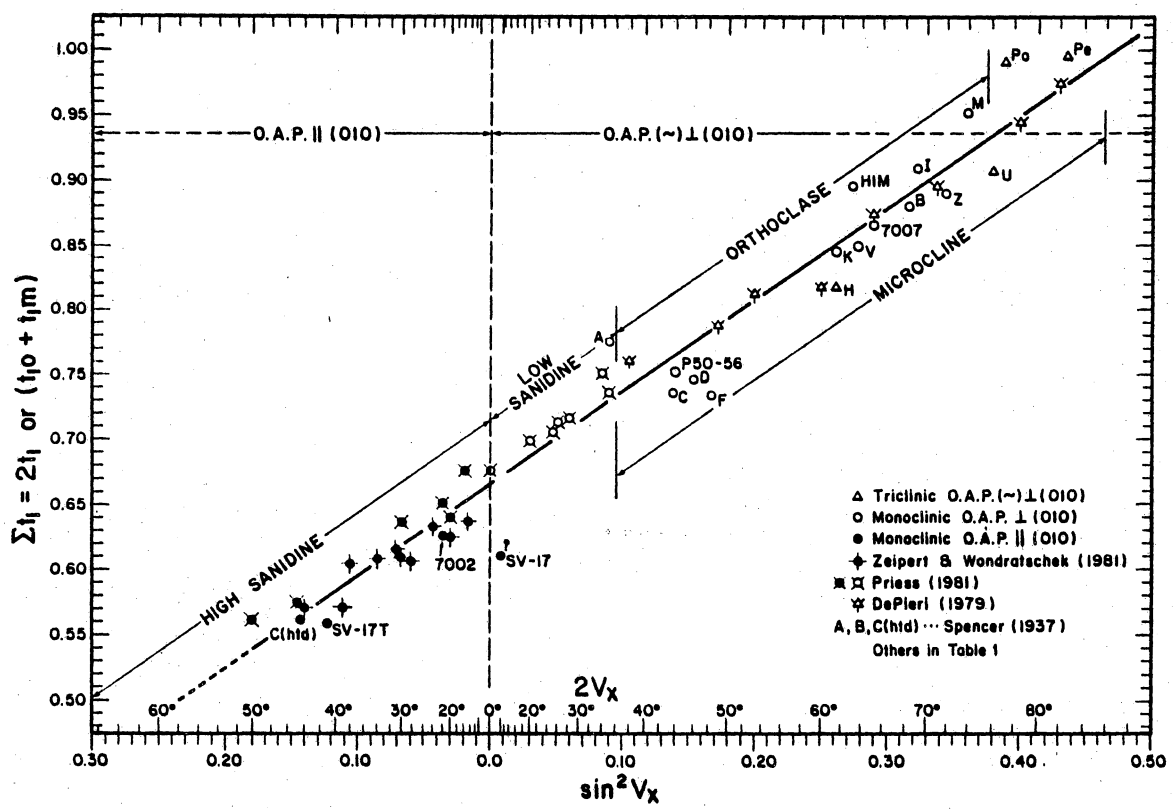

Figure 2.4. Sin^2V_x and $2V_x$ versus Σt_1: The Σt_1 values were determined by the [110],[1$\bar{1}$0] method of Kroll (1980), as discussed by Kroll and Ribbe, 1983): The line represents a least-squares regression fit to the data for 52 specimens in Table 2.1. See Equations 12a and b, and cf. Su et al. (1983b) for an earlier version.

thesized by Tuttle (1952). Optically positive "isomicroclines" ($2V_x > 90°$) were discussed in Footnote 2.

Linear model: Σt_1 versus $\tan^2 Vx$

Priess (1981) and Ott (1982) found linear relationships for Σt_1 or t_1 and t_2 versus $\tan^2 V_x$ for suites of **monoclinic** K-rich feldspars between $2V_x \sim 50°$ [O.A.P. = (010)] and $2V_x \sim 63°$[O.A.P. $\perp$ (010)]. We tested $\tan^2 V_x$ with our suite of 52 monoclinic **and** triclinic specimens and obtained an equation which may be split into two segments. For O.A.P. = (010),

$$\Sigma t_1 = 0.664(4) - 0.473(14) \tan^2 V_x \quad , \qquad (13a)$$

and for O.A.P. $\perp$ or nearly $\perp$ to (010),

$$\Sigma t_1 = 0.664(4) + 0.473(14) \tan^2 V_x \quad , \qquad (13b)$$

with $r^2 = 0.958$ and **esd** = 0.03 (just slightly higher than the **esd** of 0.02 for equation 6 A).

The rationale for near-linearity in the relationship between Σt_1 and $\tan^2 V_x$ is similar to that for Σt_1 and $\sin^2 V_x$, because equations similar to 8 through 11 can be derived for the $\tan^2 V_x$ function. The greater range of values of $\tan^2 V_x$ (from 0.0 to 1.0) accounts for the smaller r^2 and larger **esd** for equation 13 over equation 6 A.

Discussion and Summary

Earlier work and partial birefringences

Finney and Bailey (1964, Fig. 2, p. 426) plotted the distant order function,

$$S = \sum_{i\,1}^{i\,4} \left[\frac{|0.25 - t_i|}{1.50} \right]$$

against $2V_x$ for all five structures of K-rich feldspars available at that time. Ribbe and Gibbs (1969, p. 86) recognized flaws in this and other distant order parameters and suggested that they be abandoned in favor of some more direct measure of the Al/(Al + Si) content of the tetrahedral sites (for example, those used by Weitz (1972) and DePieri (1979)). But Finney and Bailey's result was nonetheless an important contribution.

As may be demonstrated mathematically, S will be linearly related **only** to t_1o when t_1m is <0.25, whereas, if $t_1m > 0.25$ or if the feldspar is monoclinic, S will be linearly related to Σt_1. Of course, Σt_1 is the parameter we find to be rather precisely predictable from $2V_x$. Finney and Bailey (1964, Figs. 3 and 4) obtained a good nonlinear correlation of $2V_x$ and "b"-α and a nearly perfect linear correlation of S and "b"-α, where the birefringence value "b"-α, as first proposed by Hewlett (1959), is equivalent to our $(n_b - n_a)$. Although they stated that their "diagrams should not be interpreted too vigorously . . . at this stage of our knowledge," Finney and Bailey's ideas have proven to be correct. If we were to suggest a partial birefringence most sensitive to order-disorder in K-rich feldspars, it would be $(n_b - n_c)$, which passes through zero at $2V_x = 0$. Values for a Σt_1 versus $(n_b - n_c)$ plot may be derived from Figure 2.2.

Complete characterization of Al,Si distribution in triclinic K-feldspar

A measurement of $2V_x$ (or partial birefringence, $(n_b - n_c)$) permits easy determination of t_1 or $(t_1o + t_1m)$, and thus, using equation 3, of t_2 or $t_2o = t_2m$. However, the individual Al contents of T_1o and T_1m in triclinic potassic feldspars are **not** available from these measurements alone. Brown (1962, Fig. 2, p. 32) and Stewart (1974, Fig. 2, p. 158) suggested that the extinction angle α' or X′ to the trace of (010) on (001) cleavage fragments may be linearly related to the difference $(t_1o - t_1m)$. A few data suggest a correlation between this extinction angle and the γ^* reciprocal lattice angle (Brown, 1962). In turn, γ^* is well known to be linearly correlated to $(t_1o - t_1m)$ (see Kroll and Ribbe, 1983, Fig. 5, p. 80). Marfunin (1966) hinted at the utility of angles between the individual optic axes and the normal to (010) in differentiating structural states of K-rich feldspars, but confirmation from lattice parameters or structure determination is lacking.

It is our intention to obtain complete optical **and** lattice parameter characterization of as many intermediate microclines as possible, so as to be able to fully characterize average Al,Si site distributions in triclinic potassic feldspars using rapid spindle or universal stage methods.

Unusual potassic feldspars

Bambauer and Laves (1960) studied a large (> 1 cm) adularia "crystal" from Val Casatscha, Switzerland. This specimen exhibited coarse lamellar domains whose $2V_x$ angles and α^* and γ^* angles (recorded by X-ray precession methods) suggested a range of structural states from "(high) sanidine . . . (axial plane ~ $\parallel$ (010), $2V_x \cong 50°$) . . . to microcline . . . (axial plane ~ $\perp$ (010), $2V_x \cong 50°$. Between these extremes a continuous series of intermediate optical orientations was found" (p. 178). These unusual orien-

tations, representing a range of intermediate microclines with triclinic symmetry, are not accomodated by our model. Carefully correlated structural, optical, and electron microscope studies of these and similar specimens are now under way to resolve the discrepancies.

Summary

Values of $2V_x$ measured for potassic feldspars in thin sections, plus the observations of whether $r < v$, which indicates the optic plane to be parallel to (010), or $r > v$, which indicates the optic plane to be perpendicular to (010) or nearly so, should suffice to determine t_1 and t_2 (for monoclinic) or ($t_1o + t_1m$) and $t_2o = t_2m$ (for triclinic crystals) from grain to grain (or point to point). Further study is needed to confirm or establish more certainly the relationship between ($t_1o - t_1m$) and extinction angles, especially X′ on (001), which has the greatest potential. The K-rich feldspars of "unusual" optic orientation require special attention.

We urge that all investigators measure and report full optical orientation data for crystals on which structures are determined or that investigators in possession of such crystals (or for that matter, any known intermediate microclines) send them to FDB or PHR for further study.

REFERENCES

Bailey, S.W. (1969) Refinement of an intermediate microcline structure. American Mineralogist, 54, 1540-1545.

Bambauer, H.U. and Laves, F. (1960) Zum Adularproblem. I. Adular von Val Casatscha: Mimetsicher Lamellenbau, Variation von Optik und Gitterkonstanten und ihre genetische Deutung. Schweizerische Mineralogische und Petrografische Mitteilungen, 40, 177-205.

Blasi, A. (1972) < < Iso-microclino > > ed altre varanti strutturali del K-feldspato coesistenti in uno stesso cristallo nei graniti del Massiccio dell' Argentera (Alpi Marittime). Rendiconti della Societa Italiana di Mineralogia e Petrolgia, 28, 375-411.

Bloss, F.D. (1952) Relationship between density and composition in mol percent for some solid solution series. American Mineralogist, 37, 588-599.

Brown, B.E. (1962) Aluminum distribution in an igneous maximum microcline and the sanidine microcline series. Norsk Geologisk Tidsskrift, 42, 25-36.

Brown, B.E. and Bailey, S.W. (1964) The structure of maximum microcline. Acta Crystallographica, 17, 1391-1400.

Cole, W.F., Sörum, H. and Kennard, O. (1949) The crystal structures of orthoclase and sanidinized orthoclase. Acta Crystallographica, 2, 280-287.

Dal Negro, A., DePieri, R., Quareni, S. and Taylor, W.H. (1978) The crystal structures of nine K feldspars from the Adamello Massif (Northern Italy). Acta Crystallographica, B34, 2699-2707.

DePieri, R. (1979) Cell dimensions, optic axial angle and structural state in triclinic K-feldspar of the Adamello massif, Northern Italy. Memorie de Scienze Geologiche, Padova, 32.

Finney, J.J. and Bailey, S.W. (1964) Crystal structure of an authigenic maximum microcline. Zeitschrift für Kristallographie, 119, 413-436.

Gunter, M. and Bloss, F.D. (1982) Andalusite-kanonaite series: lattice and optical parameters. American Mineralogist, 67, 1218-1228.

Hewlett, C.G. (1959) Optical properties of potassic feldspars. Geological Society of America Bulletin, 70, 511-538.

Kroll, H. (1980) Struktur und Metrik der Feldspäte. Habilitations-schrift, Westfalische Wilhelms-Universtitüt, Münster.

Kroll, H. and Ribbe, P.H. (1983) Lattice parameters, composition and Al,Si order in alkali feldspars. In P.H. Ribbe, Ed., Feldspar Mineralogy, Reviews in Mineralogy, 2, 2nd Edition, 57-100. Mineralogical Society of America, Washington, D.C., 362 p.

Marfunin, A.S. (1966) The feldspars: phase relations, optical properties, and geological distribution. (Translated from the Russian edition, 1962.) Israel Program for Scientific Translations, Jerusalem, 317p.

Ott, G. (1982) Röntgenographische Strukturverfeinerungen an getemperten Eifelsanidinen zur Feststellung ihres Ordungszustandes. Diplomarbeit, Institut für Kristallographie der Universität Karlsruhe.

Phillips, M.W. and Ribbe, P.H. (1973) The structures of monoclinic potassium-rich feldspars. American Mineralogist, 58, 263-270.

Priess, U. (1981) Untersuchungen zur Tief-Hoch-Umwandlung von Fe-haltigen Orthoklas-Kristallen aus Madagascar. Neues Jahrbuch für Mineralogie, Abhandlungen, 141, 17-29.

Prince, E., Donnay, G. and Martin, R.F. (1973) Neutron diffraction refinement of an ordered orthoclase structure. American Mineralogist, 58, 500-507.

Ribbe, P.H. and Gibbs, G.V. (1969) Statistical analysis and discussion of mean Al/Si-O bond distances and the aluminum content of tetrahedra in feldspars. American Mineralogist, 54, 85-94.

Smith, J.V. (1974) Feldspar Minerals. I. Crystal Structure and Physical Properties. Springer-Verlag, Heidelberg, 627 p.

Spencer, E. (1937) The potash-soda feldspars. I. Thermal stability. Mineralogical Magazine, 24, 453-494.

Stewart, D.B. (1974) Optic axial angle and extinction angles of alkali feldspars related by cell parameters to Al/Si order and composition. In W.S. MacKenzie and J. Zussman, Eds., The Feldspars, p. 145-161. Manchester University Press, Manchester, 717p.

Stewart, D.B. and Ribbe, P.H. (1969) Structural explanation for variations in cell parameters of alkali feldspar with Al/Si ordering. American Journal of Science, 267-A, 144-462.

Stewart, D.B. and Ribbe, P.H. (1983) Optical properties of feldspars. In P.H. Ribbe, Ed., Feldspar Mineralogy, Reviews in Mineralogy, 2, 2nd Edition, 121-139. Mineralogical Society of America, Washington, D.C., 362 p.

Stewart, D.B. and Wright, T.L. (1974) Al/Si order and symmetry of natural alkali feldspars, and the relationship of strained cell parameters to bulk composition. Bulletin de la Société Française de Minéralogie et de Cristallographie, 97, 356-377.

Su, S.C., Bloss, F.D., Ribbe, P.H. and Stewart, D.B. (1983a) Rapid and precise optical determination of Al,Si ordering in potassic feldspars. Abstr. 3rd NATO Advanced Study Institute on Feldspars and Feldspathoids and Their Parageneses, Rennes, France.

Su, S.C., Bloss, F.D., Ribbe, P.H. and Stewart, D.B. (1983b) Optic axial angle, a precise measure of Al,Si content of the T_1 tetrahedral sites in K-rich alkali feldspar. Geological Society of America, Abstract with Programs, 15, 701.

Tuttle, O.F. (1952) Optical studies on alkali feldspars. American Journal of Science, Bowen volume, 553-567.

Weitz, G. (1972) Die Struktur des Sanidins bei verschiedenen Ordnungsgraden. Zeitschrift für Kristallographie, 136, 418-426.

Wright, T.L. and Stewart, D.B. (1968) X-ray and optical study of alkali feldspars: I. Determination of compositions and structural state from refined unit-cell parameters and 2V. American Mineralogist, 53, 38-87.

Zeipert, C. and Wondratschek, H. (1981) Ein ungewöhnliches Temperverhalten bei Sanidin von Volkesfeld/Eifel. Neues Jahrbuch für Mineralogie Monatshefte, 407-415.

CHAPTER 3. OPTICAL PROPERTIES OF SINGLE CRYSTALS IN THE ORDER-DISORDER SERIES LOW-HIGH ALBITE

Introduction

The structural and thermodynamic aspects of Al,Si order-disorder in albite have received much attention, but few systematic investigations have been conducted on the variation of the optical properties of albites as a function of structural state. Measurements of the optic axial angle 2V (Raase and Kern, 1969) and extinction angles (Raase, 1978) on a series of synthetic albites are the only data available for intermediate structural states. The paucity of data is due to the difficulty in obtaining suitable single crystals, and although the optical measurements of previous workers were done on single grains, the structural state was assessed from unit cell dimensions or the parameter $\Delta 131 \equiv 2\theta(131) - 2\theta(1\bar{3}1)$ determined by X-ray powder methods. However, in this investigation it was possible to carry out both optical measurements and X-ray precession photography on the same single crystal for eight samples of different structural states, produced by a new technique. This provided the first precise characterization of the optical properties of albite as a function of the reciprocal lattice angles α^* and γ^*, which in turn may be used to establish an accurate estimate of the Al,Si order-disorder in each optically characterized crystal (see preliminary report by Su et al., 1985).

Experimental Procedures

An iron- and calcium-free low albite from Clear Creek, California ($Ab_{99.7}Or_{0.3}$, electron microprobe analysis by Ian Steele, University of Chicago) was used as the starting material for this study. Cleavage fragments ranging up to approximately 1 mm in size were embedded in reagent grade Na_2CO_3 and sealed in gold capsules. The carbonate, although supposedly "anhydrous," contains approximately 1 percent H_2O; no water was added. The capsules were run in NaCl pressure cells in piston-cylinder devices at 17-18 kbar. The Na_2CO_3 is adequately plastic so that single crystals large enough for the optical and X-ray work may be readily recovered after the experiment by dissolving the carbonate in 1 molar HCl. The determination of the equilibrium disorder-temperature relations of albite and the preparation at high pressures of albite with any desired degree of Al,Si order ranging from low albite to highly disordered material are described in Goldsmith and Jenkins (1985). In fact, it was Prof. J.R. Goldsmith of the University of Chicago who provided the suite of seven intermediate albites from which single crystals were selected for this study.

These albites were prepared by heating at temperatures of 750° to 1000°C for 6-19 days (Table 3.1), and they cover the range from about 10 to 90% disordered. Of course, modification of structural state by diffusive Al-Si exchange is somewhat slower in relatively large crystals than in fine powders, and this is quite possibly related to rates of hydroxyl or hydrogen diffusion in the albite. But in a study of this sort, it is essential that the crystals used be as homogeneous as possible with respect to structural state. The only nondestructive test we have of this is to examine single crystal X-ray photographs for sharpness of diffraction spots. Although there is some subjectivity in this approach, all of our specimens were selected after examining zero-level precession photographs of each crystal in both the [100] and [001] orientations. Measurements of the

Table 3.1 Heating conditions, reciprocal lattice angles (degrees), Al contents of T sites [$\Delta t_1 = (t_1o - t_1m)$; $\Sigma t_1 = (t_1o + t_1m)$; $t_2o = t_2m$], diffusive order parameter Q_{od} and configurational entropy S_c (J/mol K) of the Clear Creek albites.

Sample	T(°C)	P(kb)	Days	α*	γ*	Δt_1	Σt_1	t_1o	t_1m	t_2o	Q_{od}	S_c
MAB177	1000	17	6	85.87	88.19	0.11	0.58	0.35	0.24	0.21	0.20	18.4
MAB169	780	17	19	85.96	88.52	0.24	0.64	0.44	0.20	0.18	0.38	17.7
MAB176	775	17	19	85.96	88.66	0.30	0.66	0.48	0.18	0.17	0.45	17.2
MAB171	770	17	15	86.14	89.40	0.59	0.80	0.69	0.10	0.10	0.73	13.3
MAB167	760	18	15	86.26	89.99	0.82	0.92	0.87	0.05	0.04	0.90	7.9
MAB172A	750	17	18	86.31	90.04	0.83	0.93	0.88	0.05	0.04	0.90	7.2
MAB151	750	18	12	86.32	90.14	0.87	0.95	0.91	0.04	0.03	0.93	6.0
LA-CC				86.39	90.46	1.00	1.00	1.00	0.00	0.00	1.00	0.0

α^* and γ^* reciprocal lattice angles from these photographs provided the basis for characterizing the structural states of these crystals (see Table 3.1).

It should be pointed out that the degree of Al,Si order in these relatively large crystals is not necessarily that of the equilibrium configuration at the temperature of the run, because equilibration of structural state requires longer run times than with the powdered specimens studied by Goldsmith and Jenkins (1985). Prof. Goldsmith reports that the reaction to jadeite at the surface of the grains is favored in the lower temperature experiments. The presence of Na_2CO_3 produces a silica-undersaturated environment, and jadeite becomes stable and is formed at pressures well below those of the albite $\leftarrow\rightarrow$ jadeite + quartz curve (Holland, 1980). However, satisfactorily homogeneous single crystals of all degrees of order were produced for this study before the cleavage fragments were too badly corroded by the reaction.

From each sample, a single crystal of 200-500 μm in maximum dimension was selected and mounted on a eucentric goniometer head, usually with b^*, the normal to the (010) cleavage face, subparallel to the glass fiber. The goniometer head was attached to a Supper spindle stage mounted on a Leitz ORTHOLUX polarizing microscope, which was in turn equipped with an interference wedge filter to serve as a monochromator and a photomultiplier eyepiece to determine precise extinction positions. The optic axial angle was measured for each crystal at either one peak wavelength, D = 589 nm, or at three different wavelengths, F = 486 nm, D, and C = 656 nm, by determining extinction positions as the dial axis of the spindle stage was rotated through 360° by 10° increments. The extinction data were then processed by the FORTRAN program EXCALIBR (Bloss and Riess, 1973; Bloss, 1981) which calculated, for each wavelength, the optic axial angle and the orientations of the optic axes and the three principal vibration directions. The standard errors of estimate of 2V as calculated by EXCALIBR are 0.1 to

0.5° for the Clear Creek albites. Their changes with wavelength (dispersion) were quantitatively calculated by DISPER, a subroutine of EXCALIBR.

Once the principal vibration directions X, Y and Z were located, each could be successively oriented parallel to the vibration direction of the polarizer so that its associated refractive index could be measured without appreciable error from misorientation. Refractive indices were measured with a refined double variation method on our calibrated system which is supported by computer programs with related statistical analysis capabilities. These permit the indices of colorless crystals like albites in the refractive index range of 1.52-1.60 to be measured with unprecedented accuracy and precision. The standard error of estimate of all indices determined in this study is 0.0001 to 0.0002. For each principal refractive index, n_α, n_β or n_γ, 30 to 70 matches between the refractive index of the immersion oil and that of the crystal were obtained at different temperatures and wavelengths covering the visible range. Using least-squares methods, the match point data were fit into the linearized Sellmeier dispersion equation (see Bloss, 1981, p. 128),

$$\frac{1}{n^2 - 1} = a_0 + a_1\left(\frac{1}{\lambda^2}\right) \quad , \tag{1}$$

where n is the refractive index measured at wavelength λ. The regression coefficients, a_0 and a_1, can be used to calculate the refractive indices at any given wavelength in the visible range.

After the optical data were collected, the goniometer head was transferred to an X-ray precession camera so that *hk*0 and 0*kl* photographs could be taken with Cu or Mo radiation. The locations of X,Y,Z and of a^*,b^*,c^*, obtained from the optical and the X-ray studies, were then jointly plotted on a stereonet after proper conversion of the different settings of the two arcs of the goniometer head during the optical and X-ray

investigations. Thus, the optical orientation as well as extinction angles on the (001) and (010) planes could be derived.

The reciprocal lattice angles α^* and γ^* were measured directly from the *hk*0 and 0*kl* precession photographs, using a measuring device with a vernier of 0.05°. For each angle, at least 10 readings were taken and then averaged to obtain the final value of the angle measured (Table 3.1). Estimated errors of measurement of both α^* and γ^* are less than 0.1°.

Results and Discussion

Angles α^* and γ^* and the estimation of Al,Si distribution

The line relating γ^* to α^* for increasingly disordered Clear Creek albite (Fig. 3.1, left) differs slightly from that (Fig. 3.1, right) by which Kroll and Ribbe (1983) joined the end members low albite (LA) to analbite (AA). This discrepancy is puzzling, particularly since the line joining LA to AA follows the trend for 43 synthetic albites as variously measured by Wright and Stewart (1968), Raase and Kern (1969), Martin (1970), and Kroll et al. (1980). Crystal structure analyses of the partially disordered Clear Creek crystals, soon to be undertaken, may supply an explanation. In the meantime, however, one may derive approximate Al,Si distributions in these albites using a method first quantified for alkali feldspars in general by Stewart and Ribbe (1969) and expressed in the following regression equation by H. Kroll and P.H. Ribbe (manuscript in preparation):

$$\Delta t_1 \equiv (t_1o - t_1m) = \frac{\gamma^* - 44.778 - 0.50246\alpha^*}{6.646 - 0.05061\alpha^*} \quad , \qquad (2)$$

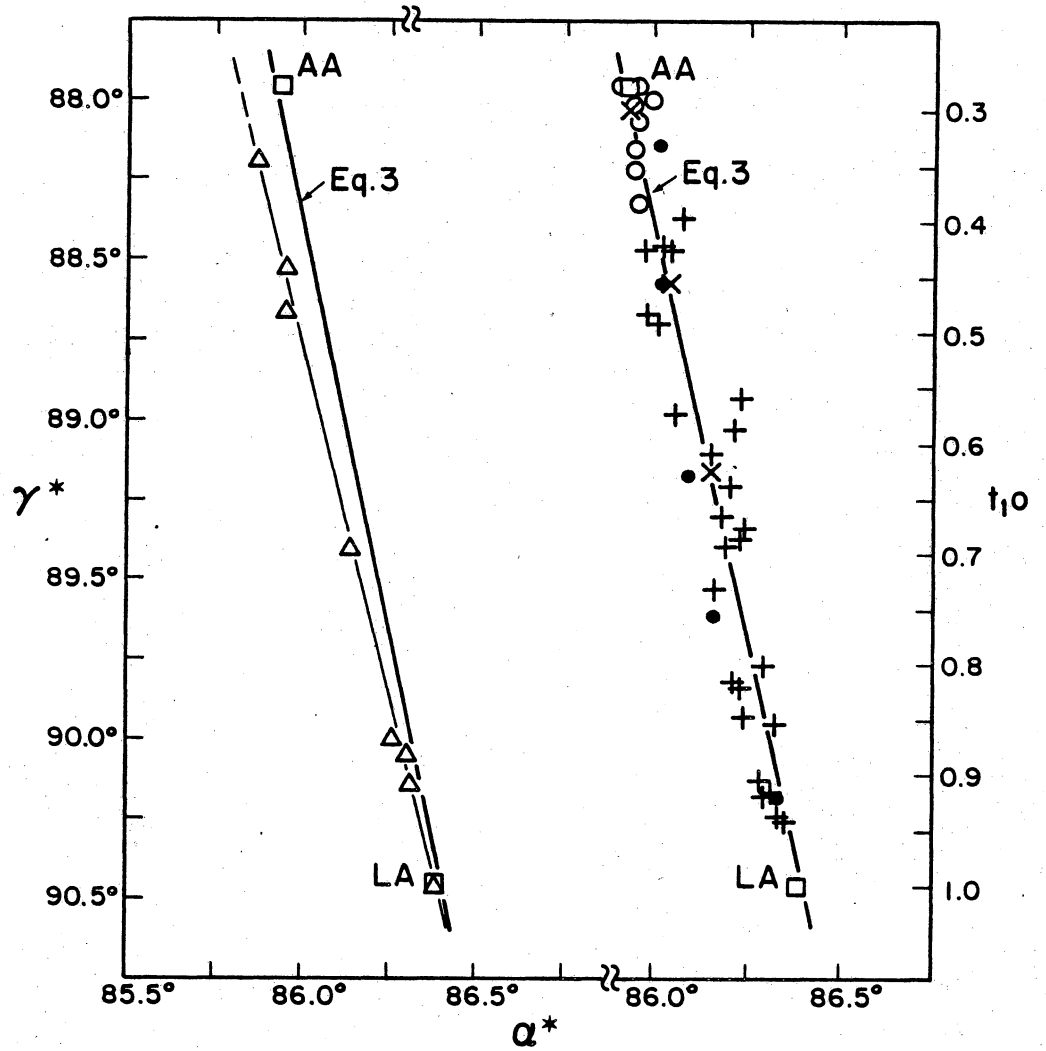

Figure 3.1. Reciprocal lattice angles, γ^* versus. α^* for albites: To the left is a plot of data for the Clear Creek albite suite of single crystals (Δ) with end members AA (analbite) and LA (low albite) (□) from Kroll and Ribbe (1983) shown for comparison. To the right is a plot of similar data for synthetic albites: (x) Wright and Stewart (1968), (•) Raase and Kern (1969), (+) Martin (1970), (o) Kroll et al. (1980), and (□) Kroll and Ribbe's AA and LA. The t_1o scale to the right was calculated using Equation (5).

where t_1o and t_1m are the Al contents of the T_1o and T_1m tetrahedral sites. Smith et al. (1985) have recently clarified a nagging uncertainty about the degree of order in low albite by refining its crystal structure at 13 K using neutron diffraction. They demonstrated unequivocally that it is completely ordered (within the limit of error) with 0.997(4) Al in T_1o, and 1.001(3), 1.002(3), 1.006(4) Si in T_1m, T_2o, T_2m, respectively. This result verifies the assumption of complete order implicit in recent structural studies of low albite.

All X-ray and neutron diffraction refinements of feldspar structures have shown that, to a first approximation, $t_2o = t_2m$. It is therefore necessary to determine only one more occupancy value in addition to Δt_1 to obtain a complete estimation of Al,Si distribution of all four tetrahedral sites. A study of the lattice parameters of the 43 synthetic albites indicated that t_1o is linearly related to γ^* as shown by the straight line (in Fig. 3.1) representing the regression equation

$$t_1o = -25.15(15) + 0.2892(17)\gamma^* \quad [r^2 = 0.999] \ . \tag{3}$$

In Equation (3) t_1o is determined by combining $(t_1o - t_1m)$, as estimated from α^* and γ^* (Eqn. 2), with $(t_1o + t_1m)$, as estimated by the equation for triclinic feldspars,

$$\Sigma t_1 \equiv (t_1o + t_1m) = \frac{b - 21.5398 + 53.8405c^*}{2.1567 - 15.8583c^*} \tag{4}$$

(Kroll and Ribbe, personal communication).

At present, Equation (3) is thought to be the best one to estimate t_1o of albites from γ^*. However, because Equation (2) was calculated using only the data from the four alkali feldspar end members LA (low albite), AA (analbite), LM (low microcline) and HS (high sanidine) (Kroll and Ribbe, 1983, Table 3.4), the following equation (similar to Eqn. (3) but based solely on the data of Kroll and Ribbe's end members LA [α^*

= 86.39°, γ^* = 90.46°, t_1o = 1.0, Δt_1 = 1.0] and AA [α^* = 85.94°, γ^* = 87.96°, t_1o = 0.28, Δt_1 = 0]), was used henceforth in our calculations to ensure internal consistency of the estimations:

$$t_1o = -25.05 + 0.2880\gamma^* \quad . \tag{5}$$

If drawn in Figure 3.1, Equation (5) would be represented by a straight line precisely joining the points labelled LA and AA; it is statistically identical to and nearly coincident with the bold line representing Equation (3).

Using Equations (2) and (5) plus the observed α^* and γ^* values, and assuming $t_2o = t_2m$, we can calculate the Al,Si distribution among all four tetrahedral sites as well as the configurational entropy,

$$S_c = -R\Sigma[X_i \, ln X_i + (1 - X_i) \, ln(1 - X_i)] \quad ,$$

where R is the gas constant and X_i is mole fraction of Al in tetrahedral sites T_i as calculated above. See Table 3.1. The diffusive order parameter used by Salje (1985) can also be calculated, because $Q_{od} = \Delta t_1/\Sigma t_1$. It is evident that all these calculations involving Al,Si occupancies, although the best estimates currently available, are strongly model-dependent. Thus caution must be exercised in their use and interpretation.

It should be noted in Table 3.1 that none of our samples are analbites having $t_1o = t_1m$ and $t_2o = t_2m$. Thus, we use the term high albite (HA) for the most disordered of our series.

Refractive indices

The principal refractive indices for light vibrating most nearly parallel to crystallographic axes *a*, *b* and *c* -- respectively symbolized n_a (= n_α), n_b (= n_γ), and n_c (= n_β) as suggested by Su et al. (1984) and Bloss (1985) -- were determined for Fraunhofer lines F, D and C (Table 3.2), but only those for D have been plotted versus γ^* and Δt_1 in Figure 3.2. The resultant trends, linear within the limits of measurement, show that as γ^*, Δt_1, and Σt_1 and thus the degree of Al,Si order increases from HA to LA, n_b increases, n_c decreases, and n_a increases. Consequently, as Figure 3.2 illustrates, the optic sign changes from negative to positive at $(t_1o - t_1m) \cong 0.71$. The relationship between the principal refractive indices and the structural states can be explained by analogy with the interpretation proposed by Stewart and Ribbe (1969) and Su et al. (1984) for K-rich alkali feldspars. From HA (or AA) to LA, the number of Al atoms encountered in the tetrahedral framework along the *b* axis direction (Al_b) decreases from 1.5 to 1.0, and the number of Al atoms encountered along the *c* axis direction (Al_c) increases from 0.75 to 1.0. In fact,

$$Al_b = 2 - \Sigma t_1 \quad \text{and} \quad Al_c = (1 + \Sigma t_1)/2$$

(Su et al., 1984, Fig. 3 and Eqns. 4 and 5). Thus the variations of Al_b and Al_c with Al,Si ordering cause the *b* cell edge to decrease in length by about twice as much as the *c* cell edge increases. Because the three principal vibration directions X, Z and Y of the albite indicatrix are subparallel to crystallographic axes, *a*, *b* and *c*, respectively, the variations of the corresponding indices n_a , n_b, and n_c (in that order; Fig. 3.2), can be accounted for, to a first approximation, by contraction of *a* and *b* and by expansion of *c* from HA to LA. Linear Equations (12)-(14), relating n_α, n_β and n_γ at 589 nm to γ^*, Δt_1, and Σt_1 are

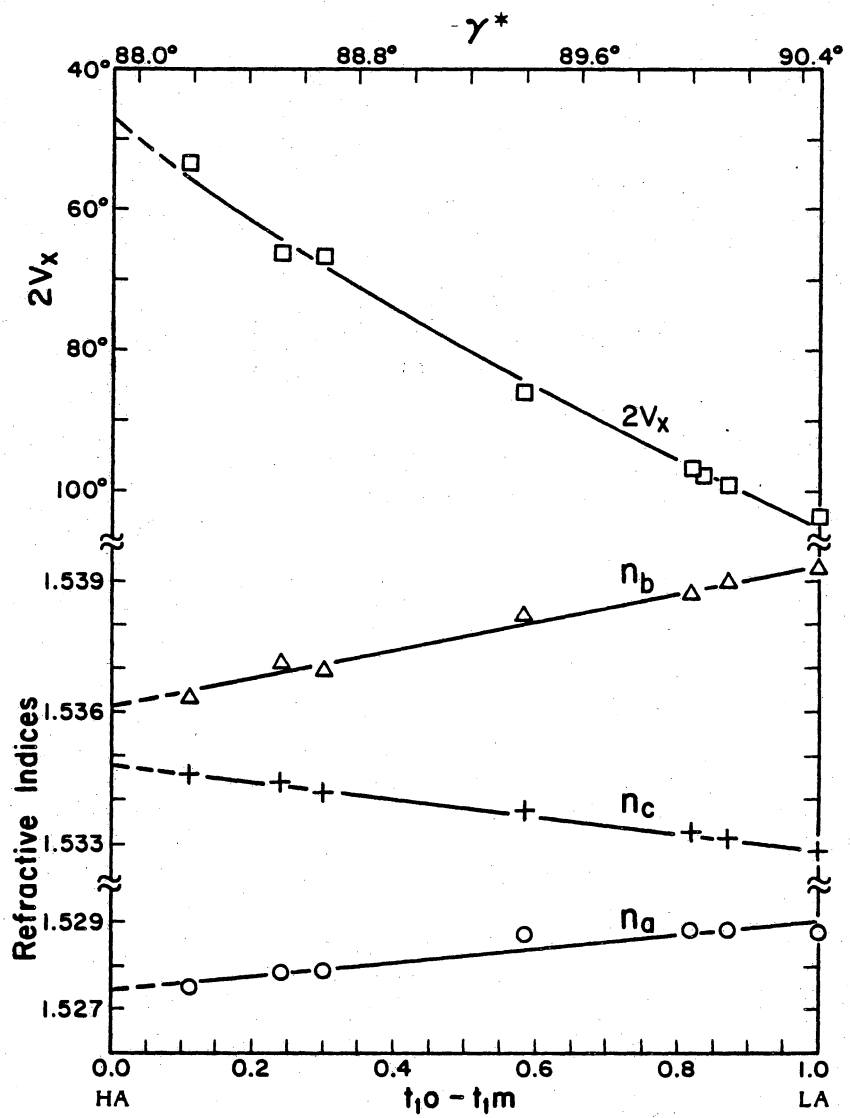

Figure 3.2. Refractive indices and $2V_x$ at 589 nm plotted versus Δt_1 and γ^* for Clear Creek albites: The curve for $2V_x$ is calculated from the linear regression equations (12b, 13b, 14b in Table 3.4) relating n_α, n_β and n_γ to Δt_1.

Table 3.2 Observed (*o*) and calculated (*c*) optic axial angles $2V_x$, extinction angles X′Λ[100] on (010) and on (001) (degrees), and refractive indices of the Clear Creek albites.

Sample	589 nm (D)			486 nm (F)				589 nm (D)				656 nm (C)			
	$2V_x(o)$	(010)	(001)	α	β	γ	$2V_x(c)$	α	β	γ	$2V_x(c)$	α	β	γ	$2V_x(c)$
MAB177	53.6	7.8	9.0	1.5333	1.5408	1.5426	52.0	1.5276	1.5346	1.5364	53.6	1.5251	1.5322	1.5340	53.2
MAB169	66.1	9.7	7.5	1.5338	1.5405	1.5434	66.4	1.5279	1.5344	1.5372	66.3	1.5255	1.5321	1.5348	65.0
MAB176	66.7	10.4	7.4	1.5334	1.5402	1.5431	66.0	1.5279	1.5342	1.5370	67.1	1.5257	1.5318	1.5346	68.0
MAB171	85.9	15.5	6.2	1.5346	1.5397	1.5444	87.4	1.5288	1.5338	1.5383	86.7	1.5265	1.5314	1.5360	87.9
MAB167	96.6	17.5	3.8	1.5351	1.5394	1.5449	96.8	1.5289	1.5333	1.5388	96.1	1.5267	1.5310	1.5364	96.2
MAB172A	97.4	19.4	3.8												
MAB151	98.8	18.0	4.6	1.5347	1.5391	1.5451	98.6	1.5289	1.5332	1.5391	98.7	1.5266	1.5308	1.5366	98.9
LA-CC	103.4	21.0	3.3	1.5347	1.5389	1.5455	102.5	1.5288	1.5329	1.5394	102.8	1.5264	1.5305	1.5368	101.9

listed in Table 3.4, which summarizes the results of a number of regressions performed on the data to obtain either linear or quadratic regression equations of the form

$$y = a_0 + a_1 x \quad \text{or}$$

$$y = a_0 + a_1 x + a_2 x^2 .$$

The dispersions of refractive indices

From the analysis of the refractive-index dispersion data for more than 100 ionic and covalent materials (solids and liquids), Wemple and DiDomenico (1969, 1971) used a single-oscillator description of the frequency-dependent dielectric constant, which equals the square of the refractive index n, to define a "dispersion-energy" parameter E_d. The analytical expression is

$$n^2 - 1 = E_d E_0 / (E_0^2 - h^2\omega^2) \quad , \tag{6}$$

where n is the refractive index at frequency ω, E_d is the dispersion energy, E_0 is the single oscillatory energy, and h is Planck's constant.

The parameter E_d, a measure of the strength of interband optical transition, is related to the charge distribution within each unit cell and thus is a quantity closely related to chemical bonding. E_d is found to obey the simple empirical relationship

$$E_d = \beta N_c Z_a N_e \quad ,$$

where β is a coefficient whose value depends on the nature of the chemical bonding (ionic or covalent), N_c is the coordination number of the cation nearest neighbor to the anion, Z_a is the formal chemical valency of the anion, and N_e is the effective number of valence electrons per anion. Wemple and DiDomenico (1969, 1971) state that the ob-

served simple dependence on coordination number and chemical valency suggests further that nearest-neighbor atomic-like quantities strongly influence the electronic optical properties of materials.

Values of E_d, E_0 and λ_0 can be easily calculated from the Sellmeier dispersion constants a_0 and a_1 using the following equations derived from Equation (6):

$$E_d = \sqrt{\frac{1239.8}{-a_0 \cdot a_1}} \quad , \quad E_0 = \sqrt{\frac{1239.8}{-(a_1/a_0)}} \quad , \quad \lambda_0 = \sqrt{-\frac{a_1}{a_0}} \quad . \qquad (7)$$

We strongly suggest that these quantities be reported in all optical investigations of non-opaque minerals so that a data base of dispersion parameters will be established. Ultimately, new insight may be gained into the optical properties of matter and their relationships to chemical bonding and other features of crystal structures.

The calculations of E_d, E_0, and λ_0 of the Clear Creek albites (Eqns. 7 and Table 3.3) show that these values are very insensitive to the distributions of Al,Si among the tetrahedral sites in albites. The grand mean values, i.e., the mean values of all the principal vibration directions, are E_d = 16.7 eV, E_0 = 12.7 eV and λ_0 = 97.7 nm. These may be compared to the values E_d = 19.1 eV, E_0 = 13.0 eV and λ_0 = 95.3 nm which was obtained from optical measurements on an anorthite ($An_{97.5}Ab_{2.4}Or_{0.1}$) from Mt. Somma, Vesuvius, Italy, by the author.

Optic axial angle

It should be emphasized that, because n_α, n_β and n_γ are linear functions of γ^*, Δt_1 or Σt_1, the optic axial angle $2V_x$ cannot be, since $\sin^2 V_x = (n_\gamma^{-2} - n_\beta^{-2})/(n_\gamma^{-2} - n_\alpha^{-2})$. A predicted $2V_x$ curve is calculated from Equations (12b), (13b) and (14b) in Table 3.4, which relate Δt_1 to n_α, n_β and n_γ at 589 nm; it is plotted in Figure 3.2 and fits the ob-

Table 3.3 Dispersion energy E_d (eV), single oscillator energy E_0 (eV), and single oscillator wavelength λ_0 (nm) associated with $n\alpha$, $n\beta$, and $n\gamma$ of the Clear Creek albites.

Sample	n_α			n_β			n_γ		
	E_d	E_0	λ_0	E_d	E_0	λ_0	E_d	E_0	λ_0
MAB177	16.7	12.9	96.4	16.5	12.5	99.1	16.6	12.6	98.6
MAB169	16.6	12.8	97.2	16.9	12.8	96.9	16.7	12.6	98.6
MAB176	17.1	13.2	94.3	16.6	12.6	98.2	16.6	12.5	98.9
MAB171	16.8	12.9	96.3	16.8	12.7	97.3	16.8	12.7	97.3
MAB167	16.4	12.6	98.1	16.6	12.7	97.9	16.9	12.7	97.4
MAB151	16.6	12.8	97.0	16.7	12.7	98.0	16.7	12.6	98.7
LA-CC	16.4	12.6	98.2	16.7	12.7	97.3	16.6	12.5	99.1

Table 3.4. Equations relating α^* to γ^* and some optical properties to γ^*, Δt_1 and Σt_1, as derived by least-squares regression methods: The numbers in parentheses are the standard errors of estimate referring to last digit(s). The term a_0 is the intercept, and a_1 and a_2 are coefficients of γ^* (or Δt_1 or Σt_1) and Δt_1^2, respectively. Coefficient of determination r^2, square root of mean square errors s, and predicted values for the end members LA ($\gamma^* = 90.46°$, $\Delta t_1 = 1.0$, $\Sigma t_1 = 1.0$) and AA ($\gamma^* = 87.96°$, $\Delta t_1 = 0.0$, $\Sigma t_1 = 0.5$) are also listed.

Eqn. no.	Dep. var.	Ind. var.	a_0	a_1	a_2	r^2	s	Pred. LA $\Sigma t_1 = 1.0$	Pred. AA $\Sigma t_1 = 0.5$
11	α^*	γ^*	65.73 (53)	0.2284 (59)		0.996	0.014		
12a	$n\alpha$	γ^*	1.4748 (89)	0.00060 (10)		0.878	0.0002	1.5291	1.5276
12b	$n\alpha$	Δt_1	1.52754 (17)	0.00154 (26)		0.877	0.0002	1.5291	1.5275
12c	$n\alpha$	Σt_1	1.52584 (43)	0.00323 (53)		0.879	0.0002	1.5291	1.5275
13a	$n\beta$	γ^*	1.5992 (22)	-0.00073 (2)		0.995	0.0001	1.5332	1.5350
13b	$n\beta$	Δt_1	1.53483 (4)	-0.00188 (6)		0.995	0.0001	1.5330	1.5348
13c	$n\beta$	Σt_1	1.53689 (11)	-0.00394 (15)		0.993	0.0001	1.5330	1.5350
14a	$n\gamma$	γ^*	1.4228 (69)	0.00129 (78)		0.982	0.0002	1.5395	1.5363
14b	$n\gamma$	Δt_1	1.53617 (13)	0.00330 (21)		0.981	0.0002	1.5395	1.5362
14c	$n\gamma$	Σt_1	1.53253 (30)	0.00696 (38)		0.985	0.0002	1.5395	1.5360

(to be continued)

(continued)

Eqn. no.	Dep. var.	Ind. var.	a_0		a_1		a_2	r^2	s	Pred. LA $\Sigma t_1 = 1.0$	Pred. AA $\Sigma t_1 = 0.5$
15a	Ext.(010)	γ^*	-492	(28)	5.7	(3)		0.983	0.7	20.8	6.6
15b	Ext.(010)	Δt_1	6.2	(6)	14.6	(8)		0.982	0.7	20.8	6.2
15c	Ext.(010)	Σt_1	-9.8	(1.3)	30.6	(1.6)		0.984	0.7	20.8	5.5
16a	Ext.(001)	γ^*	222	(19)	-2.4	(2)		0.958	0.5	3.1	9.2
16b	Ext.(001)	Δt_1	9.4	(4)	-6.2	(5)		0.958	0.5	3.2	9.4
16c	Ext.(001)	Σt_1	16.2	(9)	-13.0	(1.1)		0.957	0.5	3.2	9.7
17	Θ	Δt_1	68.7	(6)	15.5	(9)		0.980	0.8	84.2	68.7
18	Ψ	Δt_1	128.5	(1.5)	-49.4	(7)	28.1 (6.0)	0.981	1.1	107.2	128.5
19	Φ	Δt_1	99.3	(4)	-10.5	(6)		0.981	0.5	88.8	99.3
20	I	Δt_1	43.4	(1.3)	-49.5	(6.1)	24.1 (5.4)	0.990	1.0	18.0	43.4
21	Lα	Δt_1	151.1	(3.5)	-32	(16)	43.0 (15)	0.873	2.6	162.1	151.1
22	R	Δt_1	31.3	(3.8)	33	(17)	-48.0 (15)	0.910	2.7	16.3	31.3
23	N	Δt_1	125.9	(1.4)	-44.0	(6.3)	25.2 (5.6)	0.979	1.0	107.1	125.9
24	Kα	Δt_1	155.5	(7)	18.9	(1.1)		0.982	0.9	174.4	155.5
25	D	Δt_1	-5.5	(7)	15.1	(3.1)	-12.8 (2.8)	0.830	0.5	-3.2	-5.5

served $2V_x$ data points quite well. In albites the Y-Z plane is very close to the *b-c.* plane. The structural inhomogeneity within the *b-c* plane, which is mainly determined by the Al,Si distribution among the four nonequivalent tetrahedral sites, is the least for HA (or AA) and the greatest for LA. This accounts for the smaller difference between n_β and n_γ for HA (or AA) and the greater difference between n_β and n_γ for LA. Accordingly, from HA (AA) to LA, $2V_x$ increases with ordering.

The $2V_x$ values for ordered low albite in the literature include 102.8°(Ramona, CA; J.R. Smith, 1958), 103.0° and 102.5° (Tiburon, CA; Crawford, 1966, and Su, personal communication), and 102.9° (Amelia, VA; Wolfe, 1976). For heated Amelia albites, Tuttle and Bowen (1950) reported $2V_x$ values of 45-55°, and Laves and Chaisson (1950) reported 40° and 60°; the former measured 45° and the latter $56 \pm 3°$ on synthetic albites. J.R. Smith (1958) determined mean $2V_x$ values of 46.9° on heated Ramona, CA and 45.3 and 46.7° on heated Amelia, VA albite crystals. With one exception, it would appear that 45° is the limiting $2V_x$ value for most highly disordered albite. We cannot be sure which samples were HA or which AA, although if any are **completely** disordered, they must be analbites.

These optic axial angles are close to values we obtained: 103.4° (observed) and 102.8° (calculated from refractive indices) for the Clear Creek, CA low albite (Table 3.2) and an extrapolated value of 45° for the most disordered albite. The latter was arrived at by assuming $\Sigma t_1 = 0.5$ in Equation (8), as given below.

For K-rich feldspars, Su et al. (1984) observed that Σt_1, the Al content of the T_1 sites, was linearly related to $\sin^2 V_x$ Their Equations (13a) and (13b) permitted Σt_1 to be closely estimated from the optical axial angle $2V_x$, of a K-rich feldspar, a quantity much more easily determined than the lattice parameters *b* and *c**. Similar regression equations permit Σt_1, Δt_1 and Q_{od} to be estimated for albites provided $2V_x$ is known:

$$\Sigma t_1 = +0.353(17) + 1.014(37)\sin^2 V_x \quad [r^2 = 0.992, s = 0.02] \ , \qquad (8)$$

$$\Delta t_1 = -0.353(39) + 2.121(83)\sin^2 V_x \quad [r^2 = 0.991, s = 0.03] \ , \qquad (9)$$

$$Q_{od} = -0.169(27) + 1.910(57)\sin^2 V_x \quad [r^2 = 0.995, s = 0.02] \ . \qquad (10)$$

For these equations the numbers in parentheses that follow each number represent the standard error of that number in terms of its least units cited. Thus 0.353(17) indicates a standard error of 0.017 for 0.353; r^2 is the coefficient of determination, and s is the square root of the mean square errors. The high r^2 values and small s values for regression Equations (8)-(10) indicate that $2V_x$, an easily measured quantity, may also serve to estimate the Al,Si distributions over the tetrahedral sites of albites. Indeed, the precision is comparable to that obtainable by use of lattice parameters.

Extinction angles X′∧[100] on (010) and X′∧[100] on (001)

Extinction angles were calculated by combining data on the orientation of the optical indicatrix, as obtained by spindle stage techniques, with data on the crystallographic axis orientation as obtained by X-ray precession photography on the same crystal (see Table 3.2 and Fig. 3.3). Because we did not measure $2\theta(131) - 2\theta(1\bar{3}1)$ for this suite of albites, it is not possible to compare the results of this study directly with the extinction angles of the suite of synthetic intermediate albites studied by Raase (1978).

Both extinction angles show linear relationships with Δt_1, Σt_1 and γ^* (Eqns. (15a,b,c) and (16a,b,c) in Table 3.4). The extrapolated values are 6.2° on (010) and

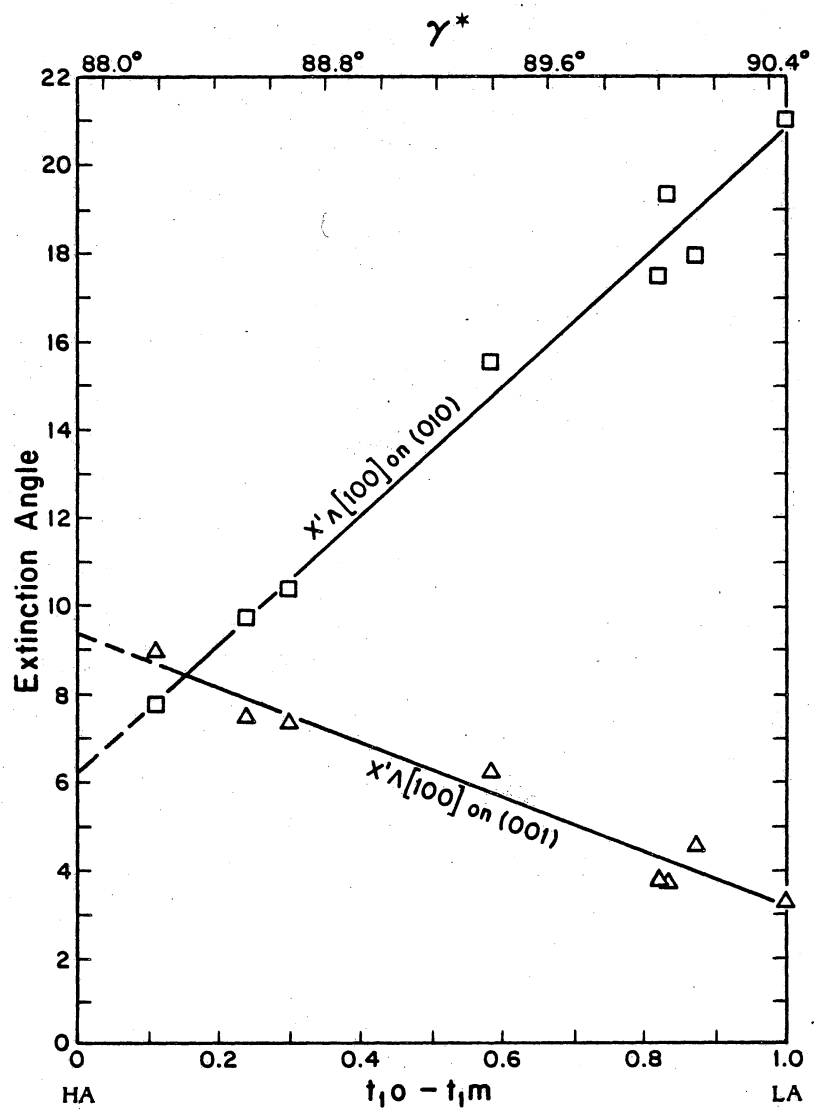

Figure 3.3. Extinction angles X′Λ[100] on (001) and X′Λ[100] on (010) versus γ* and Δt_1 for Clear Creek Albites: The lines represent Equations (15a,b) and (16a,b) in Table 3.4.

9.4° on (001) for HA (or AA) with $\Sigma t_1 = 0.5$ and 20.8° on (010) and 3.2° on (001) for LA. Raase's extrapolated values are 7.7°, 8.1° and 19.9°, 2.8°, respectively.

In Figure 3.3 the variation of X'Λ[100] on (010) with order-disorder is greater than that of X'Λ[100] on (001) because the migration trend for X from HA to LA is subparallel to (010) and nearly perpendicular to (001) (cf. Fig. 3.4).

Optical orientation

The universal stage was once the major tool for determining optical orientations of feldspars. Because the crystallographic directions were derived indirectly from twinning (twin planes, composition planes, and twin axes) or cleavages, the results were less precise (and less accurate) than those obtained by spindle stage techniques, which are capable of locating an optical direction to within a few tenths of a degree, and which are capable of working in concert with the X-ray precession method, which is in turn capable of locating both direct and reciprocal crystallographic axes to within 0.1°.

As the Clear Creek albite is increasingly disordered, its three principal vibration axes X, Y and Z and its two optic axes A_1 and A_2 for the wavelength 589 nm change orientation relative to the crystallographic directions *c* and *b** (large hollow arrows, Fig. 3.4, numerical data are listed in Table 3.5). A similar plot of the Burri et al. (1967, Plate V) data for low albite (labelled LA in Fig. 3.4) conforms to that for the natural Clear Creek albite. In contrast, their data points for high albite (HA) appear discrepant relative to the Clear Creek trends for A_1, Y, and particularly for Z. For Z the discrepancy approximates 17°, which seems beyond errors of measurement.

The Y-Z planes of albites of differing structural states are all nearly parallel to the *b*-*c* or (100) plane. Consequently, it is not surprising that, as disordering changes the Al,Si distribution among the tetrahedral sites (and thus the relative dimensions along *b*

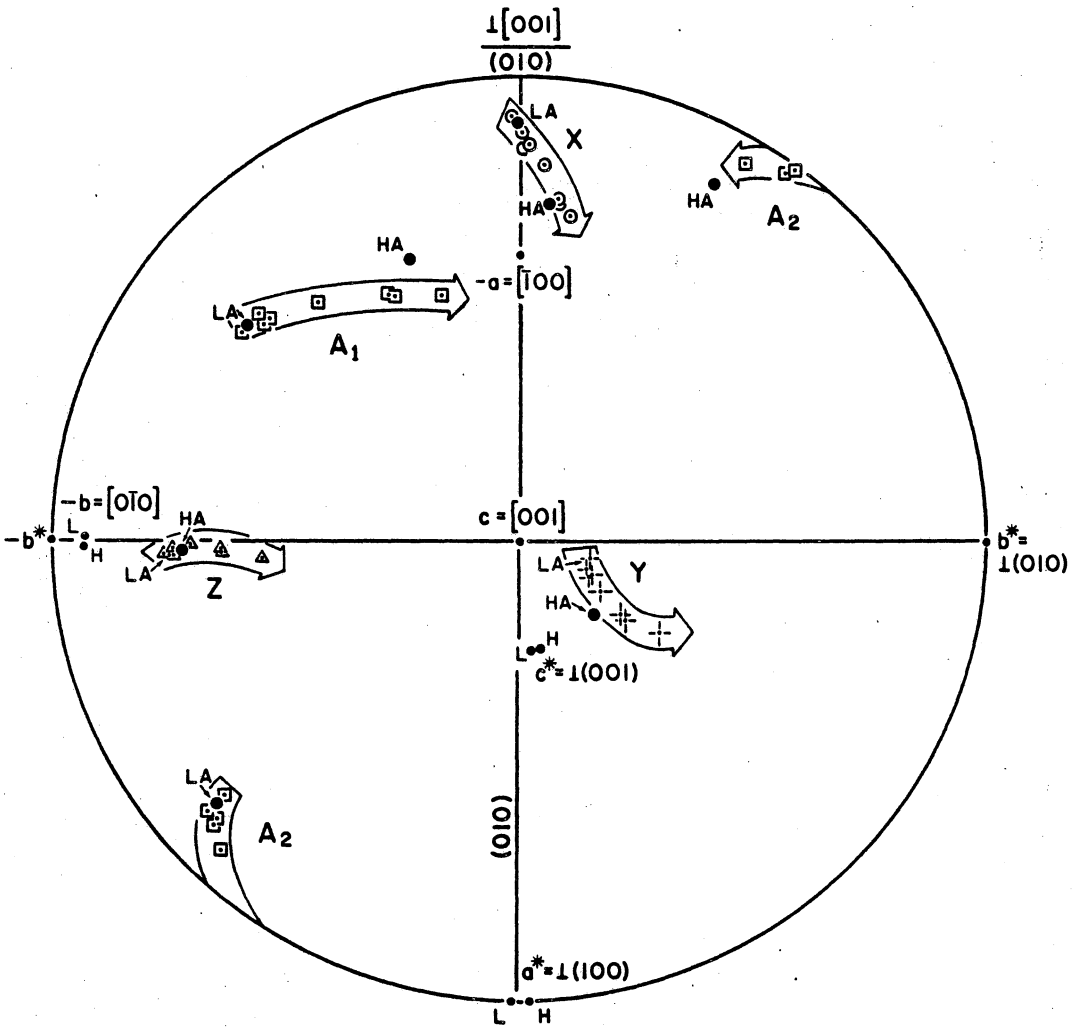

Figure 3.4. Optical orientations of the Clear Creek albites at λ = 589 nm: The projection plane is perpendicular to $+c$ with $+b^*$ pointing E (east). The large dots labeled LA and HA are the end members LA (low albite) and HA (high albite) of Burri et al. (1967). [The symbols of LA from Burri et al. (1967) for Y and Z fall right on the Clear Creek albite points and are thus omitted from this diagram for clarity.] The direct and reciprocal crystallographic axes of the Clear Creek albites are represented by small dots. The labels L and H correspond to the samples LA-CC and MAB177, respectively (Tables 3 and 4). The hollow arrows show the migration trends from low to high albite. The points of the arrows do not necessarily represent the extrapolated positions of completely disordered high albites.

Table 3.5 The spherical coordinates of two optic axes A_1 and A_2 and the principal vibration directions X, Y and Z (degrees) of the Clear Creek albites at 589 nm: The projection plane is perpendicular to $+c$ and $+b^*$ is toward the E (east) direction as in Figure 3.4 LA(BPW) and HA(BPW) refer to the end-member data of Burri et al. (1967, p. 271), which are listed here for comparison. The spherical coordinate angle φ counts clockwise starting from $+b^*$.

Sample	A_1		A_2		X		Y		Z	
	φ	ρ	φ	ρ	φ	ρ	φ	ρ	φ	ρ
HA(BPW)	248.5	66.0	298.3	82.1	274.5	72.5	45.0	25.9	178.5	71.5
MAB177	252.3	57.6	300.3	86.8	278.4	70.7	34.3	38.8	175.7	57.8
MAB169	242.4	61.0	305.5	88.8	276.3	72.5	37.4	31.5	177.8	64.8
MAB176	241.5	61.6	306.3	89.6	276.2	73.1	36.9	30.7	178.1	65.1
MAB171	229.8	67.6	133.3	85.3	273.5	78.2	32.3	23.4	179.1	70.1
MAB167	221.5	71.2	136.3	83.7	270.4	80.8	28.0	19.3	177.6	73.2
MAB172A	221.1	73.0	136.6	82.8	270.1	82.7	23.4	17.8	177.9	73.8
MAB151	220.8	71.2	138.4	83.1	271.1	81.0	28.2	19.2	178.4	73.2
LA-CC	217.2	73.5	138.3	79.9	268.6	85.0	14.6	17.8	177.1	72.9
LA(BPW)	218.2	73.4	138.1	81.2	269.2	84.0	18.6	17.5	177.4	73.6

Table 3.6 Euler angles I, II and III as defined by Burri et al. (1967) and the spherical coordinates φ and ρ (degrees) of the crystallographic axes *-a*, *-b*, *+a** and *+c**: The projection plane is perpendicular to *+c* and *+b** is toward the E (east) direction as in Figure 3.4. The spherical coordinate angle φ counts clockwise starting from *+b**.

Sample	I			II			III			*-a*		*-b*		*a**		*c**	
	Θ	Ψ	Φ	I	Lα	R	N	Kα	D	φ	ρ	φ	ρ	φ	ρ	φ	ρ
MAB177	70.7	124.3	98.4	38.8	148.1	34.3	122.2	157.0	-4.3	270.0	63.5	178.2	86.3	88.2	90.0	80.8	26.7
MAB169	72.5	116.5	96.3	31.5	144.7	37.4	115.2	160.5	-2.2	270.0	63.5	178.5	86.2	88.5	90.0	81.0	26.7
MAB176	73.1	116.1	96.2	30.7	145.4	36.9	114.9	161.3	-1.9	270.0	63.6	178.7	86.2	88.7	90.0	81.0	26.7
MAB171	78.2	110.3	93.5	23.4	149.0	32.3	109.9	167.5	-0.9	270.0	63.5	179.4	86.0	89.4	90.0	81.4	26.8
MAB167	80.8	107.0	90.4	19.3	151.0	28.0	106.8	170.4	-2.4	270.0	63.4	179.8	85.9	89.8	90.0	81.7	26.8
MAB172A	82.7	106.3	90.1	17.8	155.6	23.4	106.2	172.4	-2.1	270.0	63.4	180.0	85.9	90.0	90.0	81.8	26.8
MAB151	81.0	107.0	91.1	19.2	151.6	28.2	106.8	170.6	-1.6	270.0	63.4	179.9	85.8	89.9	90.0	81.8	26.8
LA-CC	84.9	107.1	88.6	17.8	163.3	14.6	107.1	174.7	-2.9	270.0	63.4	180.5	85.7	90.5	90.0	82.0	26.8

and *c*), the concomitant changes in the values of n_b and n_c will be accompanied by changes in the orientation of Z and Y. Quantitative data for the changes in optic orientation caused by increasing order in the Clear Creek albite are summarized in Table 3.6 (Euler angles I, II and III and spherical coordinates for *-a*, *-b*, *a** and *c**) and in Table 3.5 (spherical coordinates of A_1, A_2, X, Y and Z for 589 nm).

Note that in Table 3.4 Euler angles Θ, Φ and K_α, as defined by Burri et al. (1967), appear linearly related to Δt_1 whereas angles Ψ, L_α , I, R, N and D (Burri et al., 1967) bear a quadratic relationship to Δt_1.

REFERENCES

Bloss, F.D. (1981) The Spindle Stage: Principles and Practice. Cambridge University Press, Cambridge, England, 340 p.

Bloss, F.D. (1985) Labelling refractive index curves for mineral series. American Mineralogist, 70, 428-432.

Bloss, F.D. and Riess, D. (1973) Computer determination of 2V and indicatrix orientation from extinction data. American Mineralogist, 58, 1052-1061.

Burri, C., Parker, R.L., and Wenk, E. (1967) Die optische Orientierung der Plagioklase -- Unterlagen und Diagramme zur Plagioklase-bestimmung nach der Drehtischemethode. Birkhäuser, Basel und Stuttgart, 334 p.

Goldsmith, J.R. and Jenkins, D.M. (1985) The high-low albite relations revealed by reversal of degree of order at high pressures. American Mineralogist, 70, 911-923.

Kroll, H. and Ribbe, P.H. (1983) Lattice parameters, composition and Al,Si order in alkali feldspars. In P.H. Ribbe, Ed., Feldspar Mineralogy, Reviews in Mineralogy, 2, 2nd Edition, 57-100. Mineralogical Society of America, Washington, D.C., 362 p.

Kroll, H., Bambauer, H.-U., and Schirmer, U. (1980) The high albite-monalbite and analbite-monalbite transitions. American Mineralogist, 65, 1192-1211.

Martin, R.F. (1970) Cell parameters and infra-red absorption of synthetic high to low albites. Contributions to Mineralogy and Petrology, 26, 62-74.

Raase, P. (1978) Extinction angles of synthetic intermediate albites. American Mineralogist, 63, 466-469.

Raase, P. and Kern, H. (1969) Über die synthese von Albiten bei Temperaturen von 250 bis 700°C. Contributions to Mineralogy and Petrology, 21, 225-237.

Salje, E. (1985) Thermodynamics of sodium feldspar I. Order parameter treatment and strain induced coupling effects. Physics and Chemistry of Minerals, 12, 93-98.

Smith, J.V., Artioli, G., and Kvick, Å (1986) Low albite NaAlSi3O8: neutron diffraction study of crystal structure at 13 K. American Mineralogist, 71, in press.

Stewart, D.B. and Ribbe, P.H. (1969) Structural explanation for variations in cell parameters of alkali feldspar with Al/Si ordering. American Journal of Science, 267-A, 144-462.

Su, S.C., Bloss, F.D., Ribbe, P.H., and Stewart, D.B. (1984) Optic axial angle, a precise measure of Al,Si ordering in T_1 tetrahedral sites of K-rich alkali feldspars. American Mineralogist, 69, 440-448.

Wemple, S.H. and DiDomenico, M., Jr. (1969) Optical dispersion and the structure of solids. Physical Review Letters, 23, 1156-1160.

Wemple, S.H. and DiDomenico, M., Jr. (1971) Behavior of the electronic dielectric constant in covalent and ionic materials. Physical Review B, 3, 1338-1351.

Wright, T.L. and Stewart, D.B. (1968) X-ray and optical study of alkali feldspars: I. Determination of compositions and structural state from refined unit-cell parameters and 2V. American Mineralogist, 53, 38-87.

CHAPTER 4. OPTICAL PROPERTIES OF THE HIGH ALBITE (ANALBITE)-HIGH SANIDINE SOLID SOLUTION SERIES

Introduction

Many attempts have been made to characterize the variation of the refractive indices (and 2V) of alkali feldspars of "high" structural state (see a review of early literature by Hewlett, 1959, p. 534). The classic work of Spencer (1937) on what he called the "thermal stability of the potash-soda feldspars" produced excellent sets of optical data on naturally-occurring perthitic specimens and their heat-treated and presumably homogenized equivalents that have been used widely in subsequent studies. Adding six sets of data, only one of which was collected on a homogeneous specimen, Tuttle (1952, Fig. 2, p. 559; cf. Deer et al., 1963, Fig. 30, p. 60) drew straight lines through α, β and γ, delineating a "sanidine-anorthoclase" series and an "orthoclase-low albite" series. Smith's Figure 8-9 (1974, p. 386) is a modified version of Tuttle's drawing with a few additional data points, but it gives limiting curves only for the low series.

To date, the careful study by Hewlett (1959) of a suite of chemically analyzed sanidines and anorthoclases is the best documented, because he not only measured refractive indices and corrected the α values for effects of minor components, but he also checked crystals for homogeneity by single-crystal X-ray methods and reported d-spacings determined from powder diffraction patterns. He used d($\bar{2}$01) as an independent measure of Ab-content (note that strain may affect this parameter) and was the first to use d(001) and d(010) as measures of Al,Si order-disorder. Hewlett combined some of Spencer's data with his own to prepare a semiquantitative picture of the relationships among optical properties, composition and degree

of Al,Si ordering in alkali feldspars. A notable contribution was his recognition that structural state is directly related to partial birefringence "b"-α, where "b" is the principal refractive index whose vibration direction is most nearly parallel to the *b* crystallographic axis.

However, as far as the high albite-high sanidine series is concerned, the relationships between refractive indices and composition have remained confusing, at best, and the various attempts to summarize and/or simplify them for determinative purposes (e.g., Bambauer et al., 1979, Fig. 223-232, p. 123; Shelley, 1985, Fig. 9.61, p. 182; Phillips and Griffen, 1981, Fig. 7-20, p. 342) are misleading and incorrect except perhaps for the α vs. mol % Or curves.

Factors Affecting Refractive Indices

In addition to minor chemical constituents, a number of factors have combined to obscure the correct relationship between refractive indices and mol % Or in the high albite-high sanidine series. First, one must define what is meant by "high" structural state.

Definitions

The symbols t_1o, t_1m, t_2o, t_2m are used to designate the aluminum contents of the T_1o, T_1m, T_2o, T_2m tetrahedral sites of triclinic alkali feldspars (where t_i = the number of Al atoms in T_i sites divided by the total number of T_i sites). Thus, **high albite** (HA) is defined as $t_1o > t_1m \geq t_2o = t_2m$, where $(t_1o + t_1m) > (t_2o + t_2m)$. There is no convention to exactly define "high" albite as opposed to "in-

termediate" albite. However, we have designated $\Sigma t_1 \equiv (t_1o + t_1m)$ as a measure of structural state and used only specimens with $0.5 \leq \Sigma t_1 \leq 0.65$ in this study. **Analbite** (AA) is also highly disordered and metrically triclinic, but it has $t_1o = t_1m$ and $t_2o = t_2m$, thus making it possible for AA to invert displacively to metrically monoclinic **monalbite** above the transition temperature (~980°C for pure, highly disordered $NaAlSi_3O_8$). The distinction between HA and AA is unimportant at this stage of our investigation.

For the K-rich series, monoclinic **high sanidine** (HS) has been defined traditionally on the basis of having its optic axial plane parallel to (010) [shorthand: O.A.P. = (010)]. Using data from crystals whose average composition was 90 mol % Or, Su et al. (1984) established the fact that $0.5 \leq \Sigma t_1 \leq 0.67$ for K-rich high sanidines.

Methods of determining structural state

To determine Σt_1 it is most desirable to have a neutron diffraction refinement of the Al,Si distribution among nonequivalent tetrahedral sites or, failing that, an x-ray structure refinement. The latter involves interpretation of bond lengths in terms of Al content t_i of site T_i, and this is described at length in a review by Kroll and Ribbe (1983), who also prescribed methods of quantitatively estimating Σt_1 using demonstrated relationship among lattice parameters, mean T_i-O bond lengths, and Al contents of tetrahedral sites or pairs of sites, namely $\Sigma t_1 = (t_1o + t_1m)$ [note that $\Sigma t_2 = 1 - \Sigma t_1$]. The Kroll-Ribbe equations (10a and 10b, p. 77) recently have been revised using additional structural data and a better algorithm for regression analysis, so we will use the following to calculate Σt_1 for specimens whose lattice parameters are available:

for monoclinic feldspars,

$$\Sigma t_1 = 2t_1 = 72.245 - 3.1130b - 200.785c^* \ ;$$

for triclinic feldspars,

$$\Sigma t_1 = t_1o + t_1m = \frac{b - 21.5398 + 53.8405c^*}{21.1567 - 15.8583c^*} \ .$$

(standard error of estimate is ± 0.01 for assumed errors of $\pm$ 0.002 Å in b and ± 0.00002 Å^{-1} in c^*; Kroll and Ribbe, pers. comm.).

In the absence of lattice parameters, we have used the optic axial angle $2V_x$ to determine relative structural state. A full discussion is consigned to the following chapter. Fortunately, it is not extremely important for the present study that structural state be precisely known, because refractive indices are not extremely sensitive to variation in Σt_1, varying from as little as 0.00001 to a maximum 0.00006 per 0.01 Σt_1 in any isocompositional series.

Labelling principal refractive indices

Probably the factor that has most obscured the true relationships among optical properties and composition in the HA(AA)-HS series is the same one that plagued the relationships among refractive indices and structural state for the K-rich alkali feldspar series, low microcline-high sanidine. The principal refractive index of a feldspar should be labelled, not α, β, γ or n_α, n_β, n_γ in the traditional manner, but n_a, n_b, n_c according to which crystallographic axis a, b or c the vibration direction most nearly parallels. Hewlett's (1959) "b" corresponds to n_b, and in all alkali feldspars n_a a. For monoclinic high sanidines with O.A.P. = (010),

$n_b = \beta$ and $n_c = \gamma$, but these are reversed for **all other** alkali feldspars, i.e., those with O.A.P. $\perp$(010) or $\sim \perp$ (010) (Su et al., 1984; Bloss, 1985).

The Data Base

Choice of specimens

The 32 chemically analyzed alkali feldspars with $0.50 \leq \Sigma t_1 \leq 0.65$ were selected for this study and are listed in Table 4.1. They include a heated high albite from Ramona, CA (J.R. Smith, 1958), two high albite single crystals prepared by heating a Clear Creek, CA, specimen at high pressures (Su et al., 1986), a highly disordered anorthoclase (the structure of which was determined by DePieri and Quareni, 1973), a homogeneous Eifel sanidine (Tuttle, 1952), the 14 homogenized and "sanidinized" specimens of Spencer (1937) which had been heated for 100 to 300 hours at 1075°C, and nine sanidines and one anorthoclase from Hewlett (1959). New data were added for a heated Eifel sanidine (7002H) and two natural volcanic specimens (439 and 1909-261; Carmichael, 1965) by Warner et al. (abstr., 1984), who determined optical properties and lattice parameters on the same single crystal. Because submicroscopic intergrowths have some small effects on refractive indices, we have attempted to use homogeneous feldspars for our investigation. To our knowledge we have allowed only two exceptions to this, namely Hewlett's specimens 4 and 15, which are described as having less than 5% exsolved Na-feldspar component (his Table 8, p. 527; see also powder diffraction studies of the Hewlett specimens by Emerson and Guidotti, 1974).

Table 4.1. Data of homogeneous alkali feldspars with $\Sigma t_1 \leq 0.65$: For each sample, the corrected composition Or/(Or+Ab) and Ab/(Or+Ab) and the corrected refractive indices are listed below their respective observed values. The negative sign of 2V value indicates that optic axial plane is parallel to (010). The Σt_1 values were derived either from lattice parameters *b* and *c** (w/o *) as described in the text. or from 2V and mol % Or (with *) using Figure 5.2 in Chapter 5. Ref = reference, as listed at the bottom of the table.

No.	Sample	Or	Ab	An	Cn	Srf	Rbf	Fef	n_a	n_c	n_b	$2V_x$	Σt_1	Ref
1	MAB177	0.3	99.7	0.0	0.0	0.0	0.0	0.0	1.5276	1.5346	1.5364	53.6	0.59	7
		0.3	99.7						1.5276	1.5346	1.5364			
2	MAB169	0.3	99.7	0.0	0.0	0.0	0.0	0.0	1.5279	1.5344	1.5372	66.1	0.64	7
		0.3	99.7						1.5279	1.5344	1.5372			
3	RAMONA(H)	1.1	98.7	0.2	0.0	0.0	0.0	0.0	1.5273	1.5344	1.5357	46.9	0.51*	4
		1.1	98.9						1.5272	1.5343	1.5356			
4	DQ-1	25.2	67.9	6.5	0.4	0.0	0.0	0.0	1.5275	1.5324	1.5337	56.0	0.54	1
		27.1	72.9						1.5237	1.5289	1.5303			
5	HEW-10	27.9	69.3	1.4	0.5	0.9	0.0	0.0	1.5258	1.5313	1.5328	55.5	0.61	2,3
		28.7	71.3						1.5242	1.5298	1.5314			
6	SP-R(H)	39.6	56.9	3.4	0.1	0.0	0.0	0.0	1.5222	1.5282	1.5293	49.8	0.62*	5,6
		41.0	59.0						1.5201	1.5263	1.5274			
7	SP-P(H)	43.4	56.5	0.1	0.0	0.0	0.0	0.0	1.5209	1.5265	1.5267	15.0	0.50*	5,6
		43.4	56.6						1.5208	1.5264	1.5266			

(to be continued)

(continued)

No.	Sample	Or	Ab	An	Cn	Srf	Rbf	Fef	n_a	n_c	n_b	$2V_x$	Σt_1	Ref
8	439	43.8	51.4	3.8	0.0	0.1	0.0	0.9	1.5238	1.5292	1.5306	53.3	0.59	5,9
		46.0	54.0						1.5210	1.5266	1.5281			
9	SP-N(H)	50.7	48.6	0.5	0.2	0.0	0.0	0.0	1.5202	1.5255	1.5258	34.0	0.57*	5,6
		51.1	48.9						1.5198	1.5251	1.5254			
10	SP-M(H)	52.2	46.0	1.8	0.0	0.0	0.0	0.0	1.5206	1.5255	1.5263	45.0	0.63*	5,6
		53.2	46.8						1.5195	1.5245	1.5253			
11	HEW-15	52.7	42.4	3.2	1.2	0.3	0.2	0.0	1.5223	1.5269	1.5274	41.3	0.63	2,3
		55.4	44.6						1.5193	1.5242	1.5247			
12	HEW-4	57.6	38.9	2.0	1.1	0.3	0.1	0.0	1.5226	1.5269	1.5275	41.8	0.60	2,3
		59.7	40.3						1.5204	1.5249	1.5255			
13	1909-261	59.7	37.1	1.7	1.1	0.3	0.0	0.1	1.5221	1.5268	1.5273	35.3	0.59	5,9
		61.7	38.3						1.5200	1.5249	1.5254			
14	SP-J(H)	61.2	37.8	0.7	0.0	0.3	0.0	0.0	1.5191	1.5240	1.5240	-16.0	0.52*	5,6
		61.8	38.2						1.5185	1.5234	1.5235			
15	SP-I(H)	64.0	35.2	0.8	0.0	0.0	0.0	0.0	1.5190	1.5237	1.5237	0.0	0.55*	5,6
		64.5	35.5						1.5185	1.5233	1.5233			
16	SP-K(H)	66.2	32.0	1.6	0.0	0.2	0.0	0.0	1.5198	1.5246	1.5251	20.0	0.58*	5,6
		67.4	32.6						1.5187	1.5236	1.5241			
17	HEW-13	66.7	31.3	1.7	0.0	0.0	0.3	0.0	1.5194	1.5239	1.5240	21.8	0.61	2,3
		68.0	32.0						1.5184	1.5230	1.5231			
18	HEW-5	67.7	26.9	1.8	1.3	2.2	0.1	0.0	1.5235	1.5277	1.5283	42.5	0.62	2,3
		71.6	28.4						1.5203	1.5247	1.5253			

(to be continued)

(continued)

No.	Sample	Or	Ab	An	Cn	Srf	Rbf	Fef	n_a	n_c	n_b	$2V_x$	Σt_1	Ref
19	HEW-3	69.8	27.1	0.1	2.8	0.2	0.0	0.0	1.5211	1.5253	1.5258	35.8	0.65	2,3
		72.0	28.0						1.5189	1.5232	1.5237			
20	SP-G(H)	71.1	26.2	0.1	2.2	0.4	0.0	0.0	1.5199	1.5247	1.5242	-29.0	0.53*	5,6
		73.1	26.9						1.5180	1.5229	1.5224			
21	SP-H(H)	71.1	25.1	1.9	1.7	0.2	0.0	0.0	1.5203	1.5250	1.5248	-17.0	0.56*	5,6
		73.9	26.1						1.5178	1.5226	1.5224			
22	SP-F(H)	72.8	25.2	1.6	0.2	0.2	0.0	0.0	1.5192	1.5240	1.5236	-28.0	0.54*	5,6
		74.3	25.7						1.5180	1.5229	1.5225			
23	HEW-2	74.0	24.9	0.8	0.1	0.1	0.1	0.0	1.5191	1.5237	1.5237	0.0	0.60	2,3
		74.8	25.2						1.5185	1.5231	1.5231			
24	T-1	76.4	22.3	0.8	0.0	0.0	0.0	0.4	1.5201	1.5252	1.5248	-17.0	0.59*	8
		77.4	22.6						1.5193	1.5245	1.5241			
25	HEW-1	77.4	19.6	1.6	0.9	0.4	0.1	0.0	1.5206	1.5248	1.5248	0.0	0.59	2,3
		79.8	20.2						1.5187	1.5230	1.5230			
26	HEW-12	79.2	17.5	2.2	0.6	0.2	0.3	0.0	1.5199	1.5241	1.5241	-10.0	0.57	2,3
		81.9	18.1						1.5179	1.5223	1.5223			
27	SP-D(H)	80.9	17.4	1.2	0.3	0.2	0.0	0.0	1.5189	1.5236	1.5233	-33.0	0.56*	5,6
		82.3	17.7						1.5178	1.5226	1.5223			
28	HEW-11	79.0	15.3	1.7	1.2	2.4	0.4	0.0	1.5228	1.5269	1.5270	28.0	0.61	2,3
		83.8	16.2						1.5195	1.5239	1.5240			
29	7002H	83.1	14.2	0.5	1.3	0.0	0.0	0.9	1.5196	1.5243	1.5237	-42.6	0.54	5,9
		85.4	14.6						1.5177	1.5226	1.5220			

(to be continued)

(continued)

No.	Sample	Or	Ab	An	Cn	Srf	Rbf	Fef	n_a	n_c	n_b	$2V_x$	Σt_1	Ref
30	SP-E(H)	85.6	12.2	0.9	1.1	0.2	0.0	0.0	1.5190	1.5235	1.5232	-29.0	0.60*	5,6
		87.5	12.5						1.5175	1.5221	1.5218			
31	SP-C(H)	90.5	8.4	0.7	0.2	0.2	0.0	0.0	1.5187	1.5233	1.5227	-44.8	0.56*	5,6
		91.5	8.5						1.5180	1.5227	1.5220			
32	SP-A(H)	92.6	7.4	0.0	0.0	0.0	0.0	0.0	1.5192	1.5240	1.5230	-53.8	0.52*	5,6
		92.6	7.4						1.5192	1.5240	1.5230			

1. DePieri & Quareni (1973)
2. Emerson & Guidotti (1974)
3. Hewlett (1959)
4. Smith (1958)
5. Smith & Ribbe (1966)
6. Spencer (1937)
7. Su et al. (1986)
8. Tuttle (1952)
9. Warner et al. (1984)

Corrections for minor constituents

Chemical factors that obscure the relationship between refractive indices and mol % Or are the nonbinary constituents commonly found in minor amounts in high temperature alkali feldspars. Hewlett (1959, p. 520f.) devised a simple linear method to correct his n_a indices (only) for the effects of iron content plus Ca-, Ba-, Sr- and Rb-feldspar components. Our sources of mean refractive indices $\bar{n}_i$ were the same as his for $SrAl_2Si_2O_8$ (Srf), but differed for anorthite (An), celsian (Cn), $RbAlSi_3O_8$ (Rbf) and $KFeSi_3O_8$ (Fef); see Table 4.2. We used the following approach to calculate the corrected indices:

$$n^{corr}_{a,b,c} = n^{obs}_{a,b,c} - [(\bar{n}_i - \bar{n}^{obs}_{a,b,c})M_i/100] \quad ,$$

where M_i is mol % of the ith component and $\bar{n}^{obs}_{a,b,c}$ is the value of n_a, n_b or n_c appropriate to the mol % Or of a feldspar as determined from regression lines fitted to the observed indices (plotted in the upper portions of Figs. 4.1a,b,c; lines not shown).

More refined values for $\bar{n}^{obs}_{a,b,c}$ could have been attained by iterative methods, and we tested two of the more "impure" specimens (Hew-11 and Hew-15) only to find that the final values of $n^{corr}_{a,b,c}$ changed insignificantly (by ± 0.00015 or less). Corrected indices are listed below their respective observed values in Table 4.1. These are plotted in the lower portions of Figures 4.1a,b,c as a function of Or/(Or + Ab), whereas the observed values are plotted in the upper portions as a function of Or/(Or + Ab + An + Cn + Srf + Rbf).

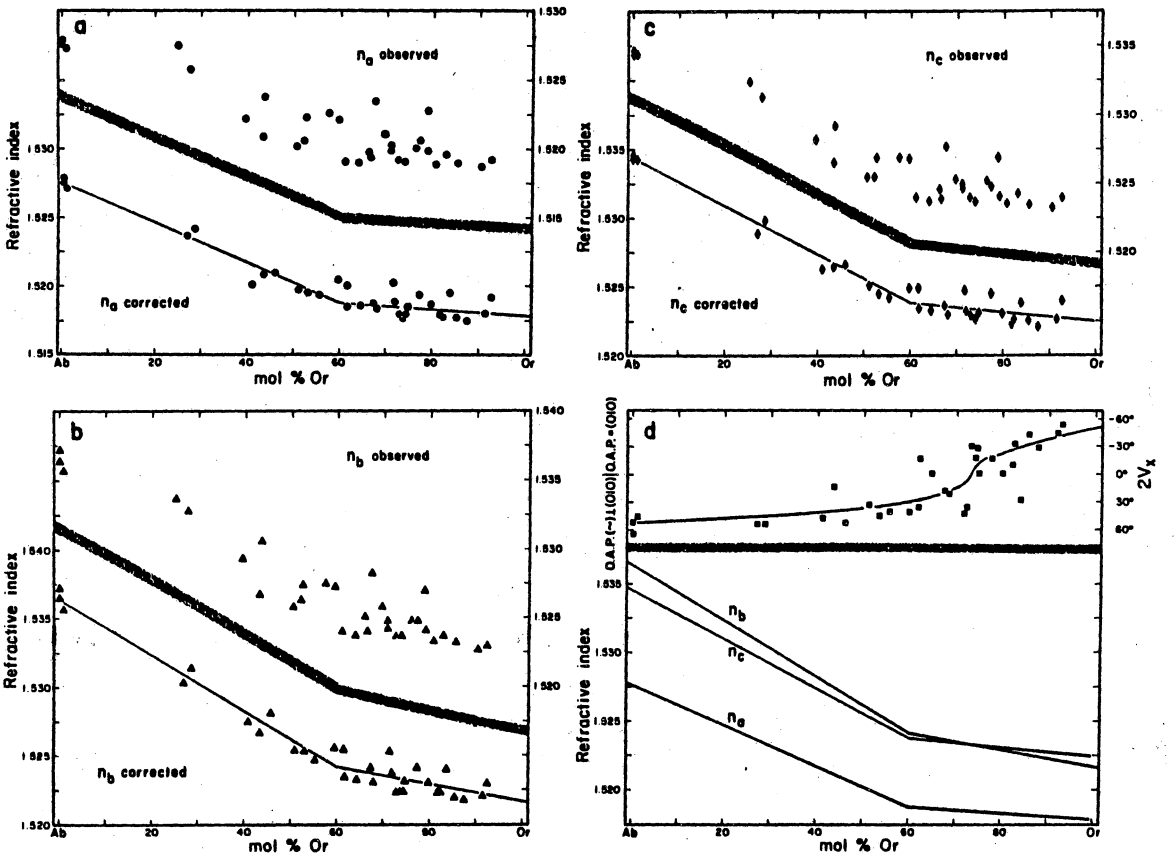

Figure 4.1. The principal refractive indices as a function of composition for alkali feldspars with $\Sigma t_1 \leq 0.65$: (a) n_a, (b) n_b, and (c) n_c. The upper portion of each figure displays the observed refractive indices; the lower portions have indices corrected for minor constituents. Regression lines are drawn through the corrected data sets, segmented at Or_{60} . (d) The regression lines for HA-HS series from the three separate figures a,b,c on the same scale, together with the observed $2V_x$ data points and the $2V_x$ curve calculation from the regression lines for refractive indices. Data in Tables 4.1 and 4.3.

Table 4.2. Refractive indices of some end member feldspars: The "average" structures of the alkaline earth feldspars are disordered (see Ribbe, 1984, p.16-21), the structural state of the Rb-feldspar is not known, and the Fe-feldspar is an "iron sanidine." Ref = references, as listed at the bottom of the table.

End member	n_a	n_b	n_q	n	Ref
$CaAl_2Si_2O_8$	1.5751	1.5838	1.5886	1.5825	2
$BaAl_2Si_2O_8$	1.589	1.593	1.599	1.594	4
$SrAl_2Si_2O_8$	1.574	1.582	1.586	1.581	3
$RbAlSi_3O_8$	1.520	.	1.529	1.525	1
$KFeSi_3O_8$	1.554	1.595	1.605	1.585	5

1. Boratskaya and Vlasova (1975)*
2. Burri et al. (1967)
3. Eskola (1922)
4. Roy (1965)
5. Wones and Appleman (1961)

* Brown, W. L. (pers. comm.)

Variation of Refractive Indices with Composition

Warner et al. (abstr., 1984) attempted to correlate n_a, n_b, n_c with mol % Or for a few analyzed single crystals whose lattice parameters had been determined. In that preliminary study effects of minor constituents were ignored, and linear regression lines showed that n_b and n_c crossed between 70 and 80 mol % Or. However, it was observed that the n_c data were significantly better fit with a quadratic equation than a linear one. Numerous unresolved questions led to this broader investigation using the 32 data sets described above. For only five of these were indices, composition, and structural state all measured on the same crystal, so it is obvious that some scatter in the relationships is to be expected. Moreover, scatter is inevitable because a rather wide range of structural states ($0.50 \leq \Sigma t_1 \leq 0.65$) was intentionally allowed and some chemical zoning and variation in structural state are expected from grain to grain within any bulk-analyzed sample (see especially Table 5 of Hewlett, 1959).

In first examining the trends with Or content of both observed and corrected n_a, n_b, n_c indices in Figures 4.1a,b,c, it was obvious that they were nonlinear. For the corrected values there are relatively steep negative slopes from 0 to ~60 mol % Or, with flatter trends to 100 mol % Or. This was evident in Hewlett's plots of corrected n_a indices for homogenized alkali feldspars of high structural state. His own data extended only from Or_{53} to Or_{93} (for some reason he did not plot existing high albite data or the Or_{28} specimen in his Fig. 2a), although Spencer's (1937) data covered a broader range, $Or_{\sim 40}$ to Or_{92} (see Hewlett's Fig. 2b). These nonlinear trends required a physical explanation, and after recalling the nonlinear variations in lattice parameters and unit cell volume (see Kroll and

Ribbe, 1983, Fig. 2, p. 72-73) the answer became apparent: density is a controlling factor for refractive indices. The well known Gladstone-Dale relationship is

$$\frac{\bar{n} - 1}{\rho} = \Sigma k_i \xi_i \quad ,$$

where $\bar{n}$ is the mean refractive index, ρ is density, k_i the Gladstone-Dale "constant" and u_i the weight fraction of the *i*th oxide (see Larsen, 1921).

Spencer (1937, Fig. 3, p. 459) showed that specific gravity varied nearly linearly for his "orthoclase microperthite" series, but he had no data between Or_{40} and Or_2 (albite) and in any case, microperthites are essentially mechanical mixtures of the end members. Spencer indicated that specific gravities increased for his Na-K homogenized equivalents (short heating times at 850°C), but he did not measure them for his feldspars "sanidinized" at 1075°C. Barth (1969, Fig. 3.21, p. 590) produced a density vs. mol % Or curve from Orville's (1967) series of synthetic high alkali feldspars, and Smith (1974, Fig. 12-15, p. 590) plotted those data and the densities calculated from Orville's (1967) LA-LM alkali exchange series.

We used unit cell volumes and compositions from the well characterized LA-LM and AA-HS exchange series (Kroll et al., 1986, Tables 4 and 5) and calculated theoretical densities for these solid solution specimens. The trends in Figure 4.2 are similar to those in Smith's Figure 12-15. Of course, polynomial curves will best fit these data, but we arbitrarily chose Or_{60} as a flexure point in the AA-HS density curves and decided to use that point to break the refractive index trends in Figures 4.1a,b,c into two distinct segments.

Least-squares linear regression analyses of data between Or_0 and Or_{60} and Or_{60} and Or_{100} produced the six lines shown in Figures 4.1,a,b,c and plotted on a single graph in 4.1d. Slopes, intercepts and related statistical data are listed in Ta-

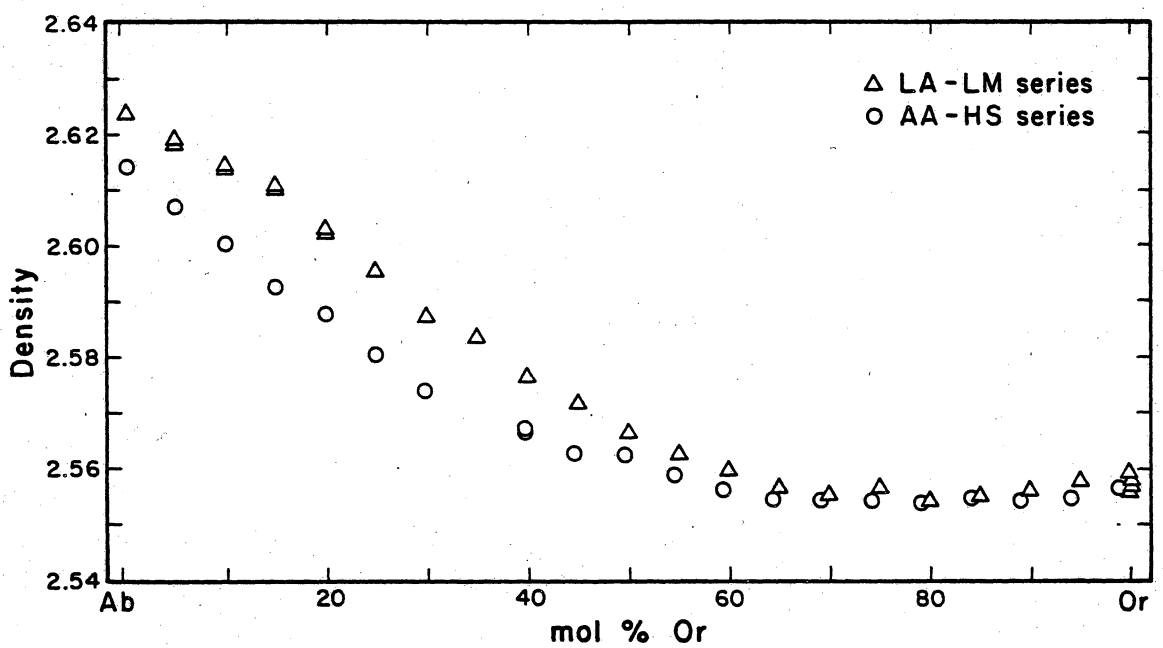

Figure 4.2. Variations of density with mol % Or for the LA-LM and the AA-HS alkali-exchange series: Densities were calculated from unit cell volumes and compositions reported by Kroll et al. (1986, Tables 4 and 5).

Table 4.3. Statistics for equations relating principal refractive indices to mole fraction of Or, X_{Or}, for the samples in Table 4.1, as derived by linear least-squares regression methods: The numbers in parentheses are standard errors referring to last digit(s) of the intercept a_0 and the coefficient a_1 of the independent variable X_{Or}. Coefficient of determination r^2, square root of mean square errors s, and predicted values for end and intermediate members Or_0 , Or_{60} and Or_{100} are also listed.

Eqn. no.	Or range mol %	Dep. var.	a_0	a_1	r^2	s	Predicted n Or_0	Or_{60}	Or_{100}
1	0 - 60	n_a	1.5276(5)	-0.0146(11)	0.951	0.0008	1.5276	1.5188	
2	0 - 60	n_c	1.5345(3)	-0.0180(8)	0.984	0.0006	1.5345	1.5237	
3	0 - 60	n_b	1.5365(5)	-0.0205(11)	0.973	0.0008	1.5365	1.5242	
4	60 -100	n_a	1.5205(15)	-0.0026(19)	0.091	0.0008		1.5189	1.5179
5	60 -100	n_c	1.5257(14)	-0.0032(19)	0.137	0.0008		1.5238	1.5225
6	60 -100	n_b	1.5280(17)	-0.0063(22)	0.319	0.0009		1.5242	1.5217

ble 4.3. There is excellent agreement (± 0.0001) between refractive index values, n_a, n_b, n_c, predicted for Or_{60} from each of the three pairs of regression equations, indicating that the flexure point is well chosen.

Note that in Figure 4.1d the n_b and n_c curves cross at about Or_{73}, where $2V_x = 0°$ and the optic axial plane changes from O.A.P. $\sim \perp(010)$ to O.A.P. = (010). This intersection will vary, depending on the average structural state of the data set (see Fig. 5.2 in Chapter 5). In this case Or_{73} is the value for specimens which have an average Σt_1 of 0.60.

Discussion of Results

It is interesting to note that from high albite (Or_0) to high sanidine (Or_{100}) the mean corrected refractive index varies from 1.5329 to 1.5207, which amounts to a relative change of 2.32% in $(\bar{n} - 1)$, and the density calculated from the data of Kroll et al. (1986) varies between 2.615 and 2.555, also a relative change of 2.32%. Furthermore, it is obvious that the variation of $\bar{n}^{corr}_{a,b,c}$ with Or/(Or + Ab) closely follows the density curves. Compare Figures 4.1d and 4.2. Although we feel that our fitting of two linear segments to the indices is a simplification, it is probably all that the data can substantiate. More sophisticated treatment would require a series of data sets for which indices, 2V, structural state, and bulk composition each had been measured on the same crystal. The work involved in such an undertaking would seem unjustified in the light of the present results. Even if better curves for n_a, n_b, n_c vs. Or were to be produced, they would have no practical application.

The curve plotted in Figure 4.1d represents the variation of optic axial angle $2V_x$ with Or/(Or + Ab) as calculated from the equations of n_a, n_b, n_c vs.

Or/(Or + Ab) summarized in Table 4.3. If the observed $2V_x$ values for specimens 1-32 (Table 4.1) are plotted in Figure 4.1d, the scatter is great and is due almost exclusively to differences in the structural states of the specimens used for determining the refractive index curves. This will be demonstrated in the following chapter.

REFERENCES

Bambauer, H.U., Taborszky, F., and Trochim, H.D. (1971) Optical Determination of Rock-Forming Minerals. Part 1. Determinative Tables. Schweizerbart'sche Verlagsbuchhandlung, Stuttgart, 188 p.

Barth, T.F.W. (1969) Feldspars. New York and London: Wiley, Interscience, 261 p.

Bloss, F.D. (1985) Labelling refractive index curves for mineral series. American Mineralogist, 70, 428-432.

Brown, B.E. and Bailey, S.W. (1964) The structure of maximum microcline. Acta Crystallographica, 17, 1391-1400.

Burri, C., Parker, R.L. and Wenk, E. (1967) Die optische Orientierung der Plagioclase – Unterlagen und Diagramme zur Plagioklasbestimmung nach der Drehtischemethode. Birkhauser, Basel and Stuttgart, 334 p.

Carmichael, I.S.E. (1965) Trachytes and their feldspar phenocrysts. Mineralogical Magazine, 34, 107-125.

Deer, W.A., Howie, R.A. and Zussman, J. (1963) Rock Forming Minerals. 4. Framework Silicates. London: Longmans, Green and Co., Ltd., 435 p.

DePieri, R. and Quareni, S. (1973) The crystal structure of an anorthoclase: an intermediate alkali feldsspar. Acta Crystallographica, B29, 1483-1487.

Eskola, P. (1922) The silicates of strontium and barium. American Journal of Science, Series 5, 4, 331-375.

Emerson, R.W. and Guidotti, C.F. (1974) New x-ray and chemical data on Hewlett's 1959 feldspar suite. American Mineralogist, 59, 615-617.

Hewlett, C.G. (1959) Optical properties of potassic feldspars. Bulletin of the Geological Society of America, 70, 511-538.

Kroll, H. and Ribbe, P.H. (1983) Lattice parameters, composition and Al,Si order in alkali feldspars. Reviews in Mineralogy, 2, 2nd edition, 57-100, Mineralogical Society of America, Washington, D.C., 362 p.

Kroll H., Schmiemann, I. and Cölln, G. von (1986) Feldspar solid solutions. American Mineralogist, 71, 1-16.

Orville, P.M. (1967) Unit-cell parameters of the microcline-low albite and the sanidine-high albite solid solution series. American Mineralogist, 52, 55-86. Correction 346-347.

Phillips, W.R. and Griffen, D.T. (1981) Optical Mineralogy. The Nonopaque Minerals. Freeman, San Francisco, 677 p.

Ribbe, P.H. (1984) Average structures of plagioclase and alkali feldspars: systematics and applications. In W.L. Brown, ed., Feldpars and Feldspathoids: Structures, Properties and Occurences. D. Riedel, Dordrecht, 541p.

Roy, N.N. (1965) The mineralogy of the potassium-barium feldspars series. I. The determination of the optical properties of natural members. Mineralogical Magazine, 35, 508-518.

Shelley, D. (1985) Manual of Optical Mineralogy. Second Edition. Elsevier, New York, 321 p.

Smith, J.R. (1958) Optical properties of heated plagioclases. American Mineralogist, 43, 1179-1194.

Smith, J.V. (1974) Feldspar Minerals. I. Crystal Structure and Physical Properties. Springer-Verlag, Heidelberg, 627 p.

Spencer, E. (1937) The potash-ash feldspars I. Thermal stability. Mineralogical Magazine, 24, 453-494.

Su, S.C., Bloss, F.D., Ribbe, P.H., and Stewart, D.B. (1984) Optic axial angle, a precise measure of Al,Si ordering in T_1 tetrahedral sites of K-rich alkali feldspars. American Mineralogist, 69, 440-448.

Su, S.C., Ribbe, P.H., Bloss, F.D., and Goldsmith, J.R. (1986) Optical properties of single crystals in the order-disorder series low-high albite. American Mineralogist, 71, in press.

Tuttle, O.F. (1952) Optical studies on alkali feldspars. American Journal of Science, Bowen Volume, 553-568.

Warner, J.K., Su, S.C., Ribbe, P.H., and Bloss, F.D. (1984) Optical properties of the analbite-high sanidine solid solution series. Geological Society of America, Abstracts with Programs, 16, 687.

Wones, D.R. and Appleman, D.E. (1961) X-ray crystallography and optical properties of synthetic monoclinic $KFeSi_3O_8$, iron-sanidine. U. S. Geological Survey Professional Paper 424-C, 309-310.

CHAPTER 5. ALKALI FELDSPARS: STRUCTURAL STATE DETERMINED FROM COMPOSITION AND OPTIC AXIAL ANGLE 2V

Introduction

Quantitative measures of the structural state of alkali feldspars have been employed in geological investigations for many years. Kroll and Ribbe (1983, p. 95) listed 30 studies in the period 1975 to 1982 that involved use of unit cell parameters for that purpose. Wright and Stewart (1968) introduced the now familiar *b-c* plot, which was quantified by Stewart and Ribbe (1969) in terms of $\Sigma t_1 = 2t_1$ or $(t_1o + t_1m)$, depending on whether the feldspar is monoclinic C2/m or triclinic $C\bar{1}$. [The symbols t_1, t_1o and t_1m indicate the Al content of the T_1, T_1o and T_1m tetrahedral sites in the structure of the alkali feldspar.] Kroll and Ribbe (manuscript in preparation) have summarized the more recent equations for determining structural state from lattice parameters. However, separating feldspar from rocks and indexing x-ray powder diffraction patterns for least-squares refinement of unit cell parameters is tedious at best. Short cuts involving d-spacings of a certain few peaks in a powder pattern were introduced by Hewlett (1959), refined by Wright (1968), and put in equation form by Kroll and Ribbe (manuscript in preparation). All the while and for decades preceding the development of X-ray methods, use of optic axial angle 2V as a quantitative measure of structural state (where composition is known) has tantalized petrologists. Stewart (1974) concluded that 2V depended "on the Al content of the T_1sites" (Σt_1) in isocompositional series, and Su et al. (1984) confirmed this quantitatively for the K-rich low microcline-high sanidine series. The very careful work of Bertelmann et al. (1985) demonstrated the interdependence of composition, Σt_1 and $2V_x$ for a limited range of monoclinic K-rich feldspars ($69 \leq Or \leq 82$).

This chapter attempts to relate quantitatively the relationships among compositions, structural states (Σt_1) and optic axial angles 2V for the **entire** range of homogeneous alkali feldspars. In order to do this, the optical properties of the limiting series around the periphery of the quadrilateral on a *b-c* plot were first established.

Optical properties of the limiting series of alkali feldspars

The assumption that refractive indices vary linearly with $\Sigma t_1 = 2t_1$ or $(t_1o + t_1m)$ in the series low microcline-high sanidine (LM-HS) was substantiated by Su et al. (1984). Fortunately, for purposes of comparison with this order-disorder series, the refractive indices of the low albite-high albite (LA-HA) series were also found to vary linearly with Σt_1 (Su et al., 1986; see Chapter 3 for details). Preliminary optical and X-ray investigation of the highly disordered high albite-high sanidine (HA-HS) solid solution series (Warner et al., abstr., 1984) led to somewhat misleading conclusions that since have been superceded by the study described in Chapter 4.

In all three of these studies n_a, n_b, n_c were defined as the principal refractive indices for light vibrating most nearly parallel to the *a*, *b*, *c* crystallographic axes, respectively (Su et al., 1984; Bloss, 1985). Accordingly, $n_a = n_\alpha$ for all alkali feldspars, $n_b = n_\beta$ and $n_c = n_\gamma$ for those high-temperature, monoclinic, K-rich sanidines whose optic axial planes (O.A.P.) are parallel to (010), and $n_b = n_\gamma$ and $n_c = n_\beta$ for all the triclinic and some of the monoclinic alkali feldspars whose O.A.P.'s are perpendicular or approximately perpendicular to (010). Recognition of this switch in optical identity obviates the confusion that has long surrounded the variation of optical properties of different series in the system $NaAlSi_3O_8$-$KAlSi_3O_8$. It has been particularly useful in delineating the variation of the optic axial angle 2V, which must vary sigmoidally (approximately linearly with $\sin^2V_x$, see Su et al., 1984) if the refractive indices vary linearly within an iso-

compositional order-disorder series or if they vary linearly within an alkali-exchange or a solid solution series of felspars which have a particular structural state.

The low albite-low microcline (LA-LM) solid solution series has eluded detailed optical investigation because no natural single crystals exist except for nearly pure end members. However, 2V has been measured on a few minute grains of alkali-exchanged specimens whose lattice parameters were determined by X-ray powder diffractometry (Rankin, 1967 on specimens of Orville, 1967). The assumptions involved in arriving at a trend for the refractive indices of this series will be discussed at a later point in this chapter.

Variation of 2V with composition and structural state

The optic angle 2V is of particular interest for the alkali feldspars. Minor substitutions of [(Ca,Ba,Sr) + Al] for [(Na,K) + Si] and Fe^{3+} for Al all tend to increase the refractive indices (Hewlett, 1959; Plas, 1966; Smith, 1974), but effects on birefringences (and thus 2V) are relatively small. Although some scatter possibly due to these effects was unaccounted for, Stewart (1974, updated by Stewart and Ribbe, 1983) found that a plot of the *b* and *c* unit cell parameters for more than 80 alkali feldspars whose 2V values were known could be contoured with straight lines for 2V rather well. Because the *b*-*c* plot has long been established as a quantitative indicator of structural state (Σt_1) for the entire range of alkali feldspars (Stewart and Ribbe, 1969), it is obvious that there exists some **quantitative** relationship among 2V, Σt_1 and composition. This was implied by Tuttle (1952) and again by Hewlett (1959), both of whom used optical data from Spencer (1937) as well as their own.

Smith (1974, Fig. 8-5, p. 380) plotted 2V as a function of mol % Or for synthetic and for perthitic, non-perthitic, and heated natural alkali feldspars. In so doing, he

traced the approximate location of the solvus and roughly indicated (with straight lines) the limiting HA-HS and LA-LM series, as did Bambauer et al. (1979, Fig. 223-232, p. 123). Smith's Figure 8-6 (p. 383) summarizes the 2V versus mol % Or data of Wright and Stewart (1968) and Rankin (1967) for natural and ion-exchanged alkali feldspars. Smith asked, "Is it possible to go further and make a quantitative structural interpretation of the 2V,Or diagram? Unquestionably, there is a strong tendency for the vertical position on the diagram to correlate with Si,Al order-disorder, but it seems the correlation is somewhat imperfect." Certainly part of the imperfection may have resulted from compositional impurities and from poorly characterized specimens [for example, wide ranges of 2V on grains from an alkali-exchanged powder must indicate that either bulk composition and/or structural state differ from grain to grain (cf. Rankin, 1967)]. Submicroscopic twinning, exsolution and strain will also affect 2V. But much of the imperfection must be attributed to the model that has been used until now. The effects of Al,Si ordering and composition on 2V in homogeneous feldspar can be properly interpreted only in terms of their effects on refractive indices which, in turn, determine the magnitude and sign of 2V, as well as the orientation of the optic axial plane. Based on this approach, we have developed a quantitative model for this system.

Assumptions for a Model Relating 2V to Structural State and Composition

As documented in Chapters 2 and 3 and discussed above, our model for the variation of $2V_x$ with structural state at constant composition in alkali feldspars assumes that

(i) n_a, n_b, n_c vary linearly with total Al (Σt_1) in the two T_1tetrahedral sites of monoclinic and in the T_1O plus T_1m sites of triclinic feldspars in (a) the LA-HA series and (b) the LM-HS series, and that

(ii) by extension of (i), n_a, n_b, n_c vary linearly with Σt_1 for **all** isocompositional series of alkali feldspars, without regard to the symmetry of individual members.

As documented in Chapter 4, our model for the variation of 2V with composition for a series of high alkali feldspars with $0.50 \leq \Sigma t_1 \leq 0.65$ (mean $\Sigma t_1 = 0.60$) assumes that

(iii) n_a, n_b, n_c each vary in two linear segments with mol % Or/(Ab+Or) for the HA(AA)-HS series, reflecting the variation in density with mol % Or of the same series (see Fig. 4.2, Chapter 4). The first line segment has a relatively steep negative slope between Or_0 and Or_{60} and the second is much flatter between Or_{60} and Or_{100}. See Figure 5.1.

The variation of $2V_x$ with composition for the LA-LM solid solution series ($\Sigma t_1 = 1.0$) assumes that

(iv) n_a, n_b, n_c vary with mol % Or in the same manner as for the HA-HS series and mimic the variation in density for the LA-LM alkali-exchange series. The assumed trends of the two-segment model (Fig. 5.1) are discussed below.

Among the above, only assumption (iv) is not directly supported by refractive index data. This is because data are nonexistent, except for the end members. The two-segment model in Figure 5.1 is based by analogy on the variation of the indices with composition in the HA-HS series. The Gladstone-Dale relationship and the density curve for

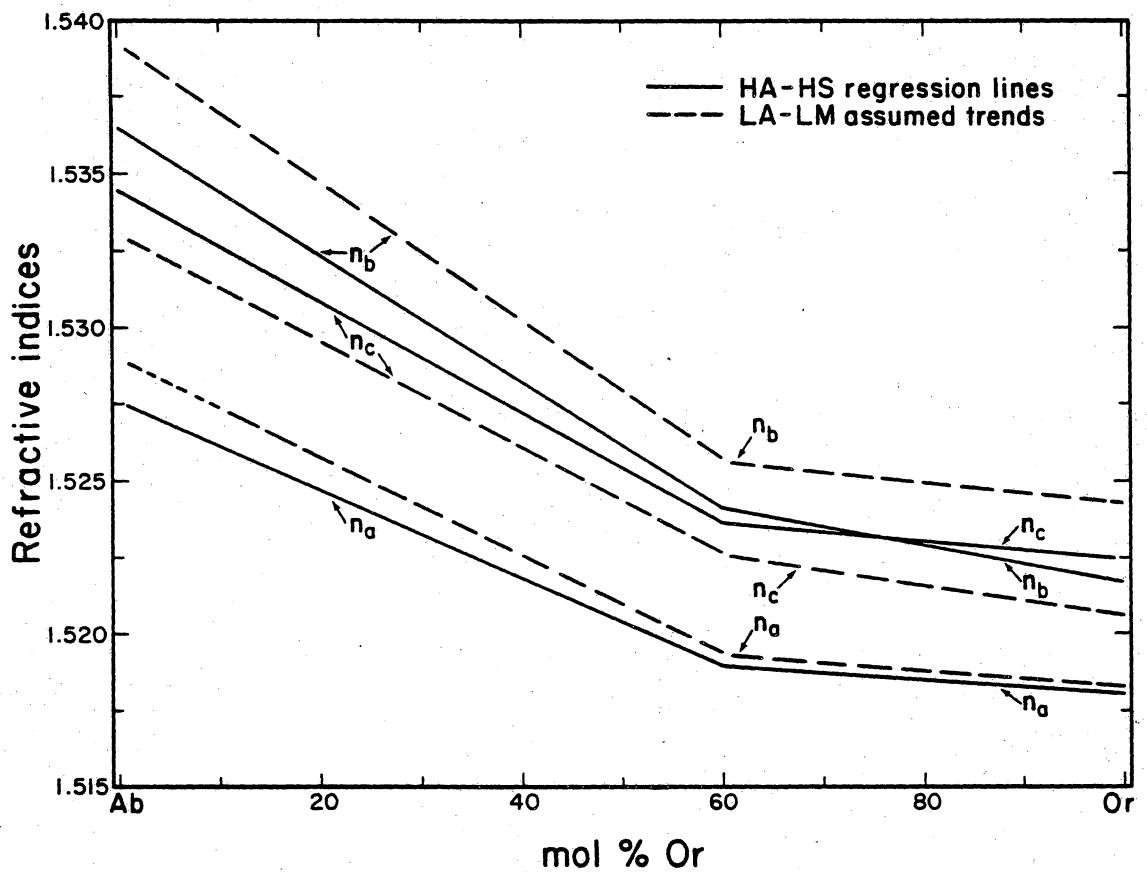

Figure 5.1. Variation trend of refractive indices of alkali feldspars versus mol % Or: Solid lines are the observed trends for HA-HS series with $\Sigma t_1 = 0.60$. Dashed lines are the assumed trend for LA-LM series with $\Sigma t_1 = 1.00$.

the LA-LM series (Fig. 4.2, Chapter 4) give us reason to expect that the analogy is valid and that the Or_{60} point is at or near the point at which the slopes of the linear segments change.

Additional support is found in the fact that the highest $2V_x$ value measured by Rankin (1967) in each sample of the alkali-exchanged feldspars of Orville (1967) plots very nearly on the $2V_x$ vs. mol % Or curve calculated from (iv) for Σt_1 (see the solid triangle symbols on Fig. 5.2). This would not be true, for example, if one assumed straight-line variations in n_a, n_b, n_c with mol % Or between LA and LM. Furthermore, small adjustments to the slopes of the segments or even the point of flexure would not change partial birefrigences substantially and thus would affect the calculated $2V_x$ curve only slightly. Bambauer et al. (1979, Fig. 228-232, p. 123) obtained a 2V curve similar to ours, but gave no justification for it.

Selection of 2V and refractive indices of end members

If assumptions (i-iv) are valid, then the immediate problem is to choose refractive indices and 2V for the LA, HA(AA), HS and LM end members and the Or_{60} flexure point (Table 5.1) that will permit calculation of a working diagram of 2V versus mol % Or contoured for Σt_1 (Fig. 5.2). Of course, this determinative diagram must reproduce Σt_1 values calculated by lattice parameter methods on the same specimens. Our requirement is that the standard error of estimate for Figure 5.2 be about the same as that for determining Σt_1 from lattice parameters, i.e., 0.02 (Kroll and Ribbe, 1983).

The following additional constraints were observed.

(a) The optic axial angles calculated from these hypothetical refractive indices must be in agreement with $2V_x$ values of 103° for LA and 45°for HA(AA)

Table 5.1. Optical data of some natural and heated alkali feldspars and extrapolated values for end members from other sources: These are used as reference values in selecting refractive indices and optic angles (degrees) of "hypothetical" end members (LA,LM,HA,HS) and Or_{60} members. The values for the "hypothetical" reference points are the ones used to construct Figure 5.2. Ref = references, as listed at the bottom of the table.

Σt_1	Or mol	An %	Description	n_a	n_c	n_b	$2V_x$ (°)	Ref
1.00	0.3	0.0	Low albite Clear Creak, CA	1.5288 (1)	1.5329 (2)	1.5394 (2)	103.4	5
0.99	0.5	0.2	Low albite Tiburon, CA	1.5290 (2)	1.5331 (2)	1.5395 (1)	102.5	7,8
1.00	0.8	1.2	Low albite Amelia, VA	1.5290 (2)	1.5330 (2)	1.5388 (2)	102.9	3,9
	1.1	0.2	Low albite Ramona, CA	1.5286 (3)	1.5326 (3)	1.5388 (3)	103.0	4
1.00	0.0	0.0	Low albite Hypothetical	1.5289	1.5329	1.5393	103.0	
1.00	60.0	0.0	Na microcline Hypothetical	1.5194	1.5226	1.5257	89.2	

(to be continued)

(continued)

Σt_1	Or mol	An %	Description	n_a	n_c	n_b	$2V_x$ (°)	Ref
1.00	95.0	0.0	Low microcline Pellatsalo, USSR	1.5178 (?)	1.5217 (?)	1.5247 (?)	82.5	1
0.99	98.0	0.0	Low microcline Pontiskalk, Switzerland	1.5178 (?)	1.5218 (?)	1.5243 (?)	77.0	2
1.00	100.0	0.0	Low microcline Hypothetical	1.5183	1.5217	1.5243	82.2	
0.60	0.0	0.0	High albite Extrapolated	1.5276 (8)	1.5345 (6)	1.5264 (8)		4
0.60	0.0	0.0	High albite Hypothetical	1.5276	1.5344	1.5267	60.3	
0.60	60.0	0.0	Na high sanidine Extrapolated	1.5188 (8)	1.5238 (8)	1.5242 (9)		6
0.60	60.0	0.0	Na high sanidine Hypothetical	1.5186	1.5238	1.5243	33.4	
0.60	100.0	0.0	High sanidine Extrapolated	1.5179 (8)	1.5225 (8)	1.5217 (9)		6

(to be continued)

(continued)

Σt_1	Or mol	An %	Description	n_a	n_c	n_b	$2V_x$ (°)	Ref
0.60	100.0	0.0	High sanidine Hypothetical	1.5176	1.5227	1.5220	-44.1	
0.50	0.0	0.0	High albite Hypothetical	1.5273	1.5348	1.5361	45.0	
0.50	60.0	0.0	Na high sanidine Hypothetical	1.5185	1.5242	1.5240	-21.4	
0.50	100.0	0.0	High sanidine Hypothetical	1.5174	1.5229	1.5214	-64.0	

1. Bailey (1969)
2. Finney & Bailey (1964)
3. Harlow & Brown (1980)
4. Smith (1959)
5. Su (see Chapter 3)
6. Su (see Chapter 4)
7. Su (unpublished data)
8. Wainwright & Starkey (1968)
9. Wolfe (1976)

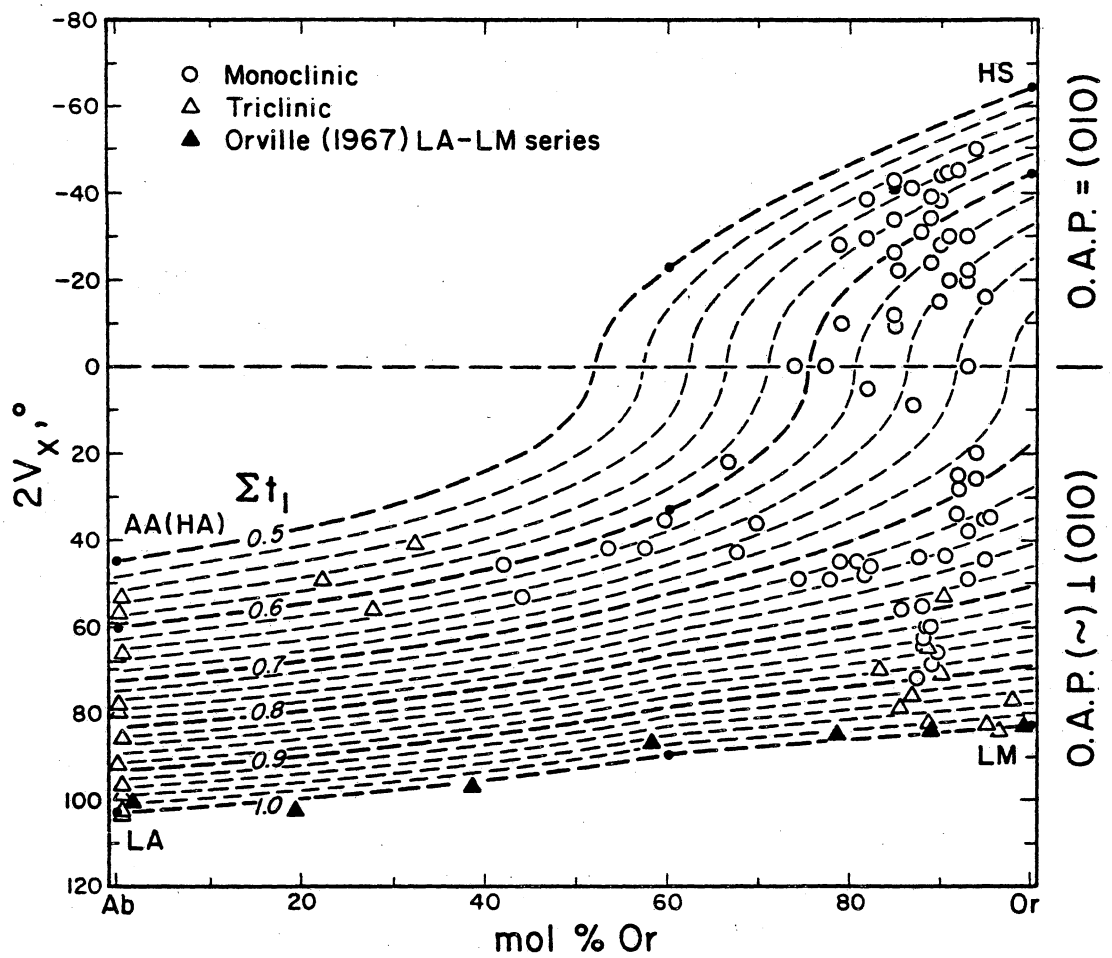

Figure 5.2. Plot of $2V_x$ versus mol % Or contoured for Σt_1: AA = analbite, i.e., a disordered albite with $t_1o = t_1m$ and $t_2o = t_2m$ which will invert to monoclinic symmetry at temperatures above 980°C; other symbols as elsewhere in text. The 109 data from Table 5.1 are plotted here. Solid triangles represent the largest $2V_x$ value measured by Rankin (1967) on each of the compositions in the LA-LM alkali-exchange series of Orville (1967).

[both pure $NaAlSi_3O_8$ with Σt_1 = 1.0 and 0.5, respectively] and 82.2° for LM and 64° for HS [both pure $KAlSi_3O_8$ with Σt_1 = 1.0 and 0.5, respectively].

The choice of 103° for LA is based on the following data: 103° (Ramona, CA; Smith, 1958), 103.4° (Clear Creek, CA; Su et al., 1986 – see Chapter 3), 103° and 102.9° (Amelia, VA; Tuttle, 1952, and Wolfe, 1976), 103° and 102.5° (Tiburon, CA; Crawford, 1966, and this author). Burri et al. (1967) and Marfunin (1966) also chose 103° for LA.

Tuttle and Bowen (1950) obtained $2V_x$ = 45°-55° for heated albite and ~45° for synthetic albites, Laves and Chaisson (1950) measured 64°and 40° on heated Amelia albites and Schneider (1957) 50° on a heated vein albite. In addition, Smith (1958) measured 45° and 47° on heated Amelia and Ramona albites, respectively, and extrapolation to completely disordered albite of Raase and Kern's (1969, Fig. 2, p. 229) data gave 47°. Burri et al. (1967) and Bambauer et al. (1971) chose $2V_x$ = 50° for their hypothetical end-member high albites, but based on the above evidence, 45° is probably a better value. In fact, our choice of 45° for HA is based both on this and on the extrapolated $2V_x$ of 44.8° determined for the series of heated Clear Creek albites using Equation 8 in Chapter 3.

A value of $2V_x$ = 82.2° was chosen for LM in part because it is near the $2V_x$ observed in the structurally-analyzed, fully ordered low microclines, from Pellatsalo (Or_{95}, 82.5°; Brown and Bailey, 1974; cf. a new refinement by Blasi et al., 1985). Furthermore, it was found that in ultimately testing the $2V_x$-Or-Σt_1model, use of 83° and 84° for hypothetical LM consistently underestimated $\Sigma t_1$for the more ordered K-rich feldspars, whereas use of values lower than 82° had the opposite effect.

The choice of $2V_x$ = 64° value for the HS end member was based in part on the $2V_x$ = 63°, O.A.P. = (010)) , for a synthetic K-feldspar measured by Tuttle (1952, p. 557) and on an extrapolated $2V_x$ = 63° at 100 mol % Or for 23 heated alkali feldspars

studied by Spencer (1937; also see Tuttle, 1952, Fig. 1). Tuttle (1952) did not publish any X-ray data for his synthetic K-feldspar, so it is not known whether it is completely disordered ($\Sigma t_1 = 0.5$). Spencer (1937) mentioned that some of the feldspars he heated had not reached equilibrium. Therefore, the 63° value might not represent a completely disordered HS end member. Ultimately, the choice of 64° was made in the process of testing our $2V_x$-Or-Σt_1 model (as discussed below). It was found that if 63° is chosen, the model tends to underestimate slightly the Σt_1 of sanidines with O.A.P. = (010), i.e., the Σt_1 values read from an early version of Figure 5.2 were usually lower than Σt_1 calculated from lattice parameters. However, if 64° is chosen, a noticeably (though only slightly) better fit resulted for sanidines.

(b) Hypothetical n_a, n_b, n_c values chosen for each end member must exactly reproduce the $2V_x$ values in (a) and agree with observed or extrapolated refractive indices accepted for HA, LA, LS, LM to within the standard error of routine measurements.

Discussion of this constraint is complicated by the fact that specimens in the HA-HS series investigated in Chapter 4 had an average structural state of $\Sigma t_1 = 0.60$ rather than 0.50 for theoretically complete disordered series. The indices for the end members of the 0.60 series are predicted from the regression equations given in Table 4.3 of Chapter 4, but the hypothetical values used in constructing Figure 5.2 (see Table 5.1) had to be slightly adjusted from the predicted indices. Adjustments amount to ± 0.0003 or less and are well within the standard errors of estimates of the regression equations and also within twice the standard error ($2\sigma = 0.0006$) for careful refractive index measurement using conventional double variation methods.

For the LA-LM series, data are only available for the LA and LM end members. The refractive indices and the calculated $2V_x$ values chosen for the hypothetical LA are

very close to the arithmetic mean values obtained for the four natural low albites listed as reference values in Table 5.1. Only two sets of refractive indices were available for LM, one from Pellatsalo, Lake Lagoda, USSR [Or_{95}, $\Sigma t_1 = 1.0$ (Brown and Bailey, 1964; Blasi et al., 1985)] and the other from the Pontiskalk formation, Switzerland [Or_{98}, $\Sigma t_1 = 0.99$ (Finney and Bailey, 1964)]. Since the composition of Pontiskalk microcline is closer to Or_{100} , its n_b and n_c values were assigned to hypothetical LM. However, in order to obtain a calculated $2V_x$ of 82.2°, a hypothetical n_a value had to be chosen that is 0.0005 higher than that of the Pontiskalk microcline.

The index values for hypothetical HA and HS at $\Sigma t_1 = 0.50$ were obtained by linear extrapolation from LA and LM through the HA and HS points at $\Sigma t_1 = 0.60$ (assumptions (i) and (ii)) to reproduce $2V_x$ values of 45° and 64°. See Table 5.1.

(c) Hypothetical n_a, n_b, n_c values for the Or_{60} flexure points must agree within the related standard errors of estimates with those predicted by the regression equations in Table 4.3 of Chapter 4 for the $\Sigma t_1 = 0.60$ series.

This constraint was easily accommodated by the values listed in Table 5.1. However, the corresponding values for Or_{60} in the $\Sigma t_1 = 1.0$ series (Table 5.1) were chosen rather subjectively from the LA-LM curves in Figure 5.1. Their values were affirmed by the fact that $2V_x = 89°$ agrees reasonably well with Rankin's (1967) value of 86° for Or_{58}. The reference n_a, n_b, n_c indices for Or_{60} at $\Sigma t_1 = 0.5$ were obtained by linear extrapolation of their respective values at $\Sigma t_1 = 1.0$ and 0.6, based on assumptions (i) and (ii).

Construction of the Determinative Diagram

A $2V_x$ vs. Or diagram (Fig. 5.2) was contoured for Σt_1 using the refractive indices for the hypothetical LA, HA(AA), HS, and LM end members and those of low and high Or_{60} (Table 5.1). The calculations used in constructing this diagram are given in detail in the Appendix, as is the derivation of the following equation relating Σt_1 to the mole fraction (**not** mol %) $KAlSi_3O_8$ and one-half the angle $2V_x$:

$$\Sigma t_1 = \frac{b_0 + b_1X_{Or} + b_2X_{Or}\sin^2V_x + b_3\sin^2V_x}{a_0 + a_1X_{Or} + a_2X_{Or}\sin^2V_x + a_3\sin^2V_x} \quad . \qquad (1)$$

Because a two-segment linear model was adopted for the variation of refractive indices with Or content and two different orientations of optic axial plane exist for K-rich members, three sets of coefficients for Equation (1) are required to account for the three cases (A) where Or $\leq$ Or 60% mol or $X_{Or} \leq 0.6$; (B) where Or $>$ 60% or $X_{Or} > 0.6$ and O.A.P. (~) $\perp$ (010) and (C) where Or $>$ 60% or $X_{Or} > 0.6$ and O.A.P. = (010). They are listed in Table 5.2.

For those who are undertaking systematic investigation of the structural states of alkali feldspars in certain geological terraines, Equation (1) should prove useful if a computer is employed to process the experimental data.

Evaluation of the Determinative Diagram

Data for a total of 109 natural, heated natural and synthetic alkali feldspars are plotted in Figure 5.2 and are listed in Table 5.3 together with their compositions, measured $2V_x$ angles, selected lattice parameters (where available), and structural states as

Table 5.2. Coefficients of Equation 1 for calculating Σt_1 from X_{Or} and $2V_x$.: Case A = Or ≤ 60% mol; Case B = Or > 60% and O.A.P. (~) ⊥ (010) and Case C = Or > 60% and O.A.P. = (010).

Coefficient	Case A	Case B	Case C
a_0	0.00408	0.00169	-0.00169
a_1	-0.00235	0.00163	-0.00163
a_2	0.00095	-0.00233	-0.00070
a_3	-0.00128	0.00069	0.00238
b_0	0.00152	0.00011	-0.00011
b_1	-0.00018	0.00217	-0.00217
b_2	-0.00174	-0.00270	-0.00053
b_3	0.00288	0.00346	0.00357

Table 5.3. Alkali feldspars, their compositions (mol %), $2V_x$ (degrees), and direct and reciprocal cell edges b (Å) and c^* (Å^{-1}), and Al content of the T_1 tetrahedral site, Σt_1: For 2V values, a minus sign indicates that the optic axial plane is parallel to (010). Sym = symmetry (M = monoclinic, T = triclinic). $\Sigma t_1(b,c^*) = \Sigma t_1$ derived from observed b and c^*. Σt_1(2V,Or) = Σt_1 estimated from 2V and mol % Or using Figure 5.3. $\Delta = \Sigma t_1(b,c^*) - \Sigma t_1$(2V,Or). Ref = references, as listed at the bottom of the table.

No.	Sample	Or	Non-alkali	Sym	$2V_x$	b	c^*	Σt_1 (b,c^*)	Σt_1 (2V,Or)	Δ	Ref
1	5A1	94.0	2.0	M	-50.0	13.032	0.15503	.55	.55	0	14
2	1B1	92.0	2.0	M	-45.0	13.031	0.15498	.57	.56	.01	14
3	SAN-SP-C	90.8	1.1	M	-44.5	13.030	0.15506	.55	.56	-.01	3
4	S1A33-4	90.0	1.0	M	-44.0	13.032	0.15498	.56	.56	0	27
5	7002H	85.0	0.5	M	-42.6	13.033	0.15510	.54	.54	0	13,24
6	SAGT-N	85.0	1.0	M	-42.0	13.033	0.15501	.55	.55	0	9
7	SANN-R	85.0	1.0	M	-42.0	13.033	0.15501	.55	.55	0	9
8	SANI-R	85.0	1.0	M	-41.5	13.033	0.15501	.55	.55	0	9
9	SVG3-N	85.0	1.0	M	-41.5	13.033	0.15501	.55	.55	0	9
10	SV-17T	87.0	2.0	M	-41.0	13.037	0.15496	.55	.56	-.01	25
11	S1A33-3	89.0	1.0	M	-39.0	13.032	0.15498	.56	.58	-.02	27
12	SV-1050	82.0	2.0	M	-38.4	13.034	0.15502	.54	.55	-.01	12
13	S1A43-4	90.0	1.0	M	-38.0	13.026	0.15491	.59	.58	.01	27
14	S1A44-2	89.0	1.0	M	-34.0	13.023	0.15494	.60	.59	.01	27
15	SAND-R	85.0	1.0	M	-33.8	13.026	0.15494	.59	.58	.01	9

(to be continued)

(Continued)

No.	Sample	Or	Non-alkali	Sym	$2V_x$	*b*	*c**	Σt_1 (*b*,*c**)	Σt_1 (2V,Or)	Δ	Ref
16	SANG-N	85.0	1.0	M	-33.8	13.026	0.15494	.59	.58	.01	9
17	SAAT-R	85.0	1.0	M	-33.6	13.026	0.15494	.59	.58	.01	9
18	S1A43-3	88.0	1.0	M	-31.0	13.019	0.15496	.61	.60	.01	27
19	S1A33-2	91.0	1.0	M	-30.0	13.025	0.15490	.60	.61	-.01	27
20	2A4	93.0	2.0	M	-30.0	13.017	0.15488	.63	.62	.01	14
21	SV-850	82.0	2.0	M	-29.5	13.026	0.15498	.58	.58	0	12
22	HEW-11	79.0	5.3	M	-28.0	13.015	0.15500	.61	.57	.04	6,11
23	S1A43-2	90.0	1.0	M	-28.0	13.025	0.15491	.60	.62	-.02	27
24	SATO-R	85.0	1.0	M	-26.3	13.026	0.15492	.59	.60	-.01	9
25	S1A44-1	89.0	1.0	M	-24.0	13.021	0.15487	.62	.62	0	27
26	7002	85.4	1.0	M	-22.0	13.015	0.15497	.62	.61	.01	13
27	2B4-2	93.0	2.0	M	-22.0	13.018	0.15480	.64	.64	0	14
28	S1A33-1	91.0	1.0	M	-20.0	13.024	0.15483	.61	.64	-.03	27
29	2B4-1	93.0	2.0	M	-20.0	13.017	0.15489	.63	.65	-.02	14
30	2B15-2	95.0	2.0	M	-16.0	13.014	0.15473	.66	.66	0	14
31	S1A43-1	90.0	1.0	M	-15.0	13.020	0.15484	.63	.64	-.01	27
32	SAGA-R	85.0	1.0	M	-11.8	13.019	0.15488	.62	.63	-.01	9
33	SANU-N	85.0	1.0	M	-11.8	13.019	0.15488	.62	.63	-.01	9
34	SVG1-N	85.0	1.0	M	-11.8	13.019	0.15488	.62	.63	-.01	9
35	HEW-12	79.2	3.0	M	-10.0	13.018	0.15515	.57	.61	-.04	6,11
36	STOT-R	85.0	1.0	M	-9.0	13.019	0.15488	.62	.63	-.01	9

(to be continued)

(Continued)

No.	Sample	Or	Non-alkali	Sym	$2V_x$	*b*	*c**	Σt_1 (*b*,*c**)	Σt_1 (2V,Or)	Δ	Ref
37	HEW-2	74.0	1.0	M	0.0	13.010	0.15511	.60	.59	.01	6,11
38	HEW-1	77.4	2.9	M	0.0	13.017	0.15508	.59	.61	-.02	6,11
39	2B15-1	93.0	2.0	M	0.0	13.011	0.15478	.66	.66	0	14
40	SV-0	82.0	2.0	M	5.2	13.023	0.15486	.61	.63	-.02	12
41	SV-17	87.0	2.0	M	9.0	13.028	0.15481	.61	.65	-.04	25
42	2B-6	94.0	2.0	M	20.0	13.008	0.15471	.69	.69	0	14
43	HEW-13	66.7	1.7	M	22.0	13.010	0.15506	.61	.59	.02	6,11
44	2B11-2	92.0	2.0	M	25.0	13.003	0.15473	.70	.69	.01	14
45	2B12	94.0	2.0	M	26.0	13.005	0.15466	.71	.70	.01	14
46	2B131	92.0	2.0	M	28.0	13.004	0.15469	.70	.70	0	14
47	2B31	92.0	2.0	M	34.0	12.997	0.15462	.74	.71	.03	14
48	SP-A	95.4	2.0	M	34.8	12.989	0.15462	.76	.73	.03	17,18,19
49	2B11-1	95.0	2.0	M	35.0	13.003	0.15458	.73	.73	0	14
50	1909-261	59.8	3.1	M	35.3	13.004	0.15528	.59	.61	-.02	13,24
51	HEW-3	69.8	3.1	M	36.0	13.002	0.15500	.65	.65	0	6,11
52	P2B	93.1	1.5	M	38.0	12.995	0.15460	.75	.73	.02	4
53	GC-2	32.5	0.8	T	40.9	12.966	0.15605	.55	.55	0	9,23
54	HEW-15	53.6	4.7	M	42.0	12.984	0.15537	.63	.62	.01	6,11
55	HEW-4	57.6	3.4	M	42.0	12.999	0.15529	.60	.63	-.03	6,11
56	HEW-5	67.7	5.3	M	43.0	12.998	0.15522	.62	.67	-.05	6,11
57	SP-C	90.5	1.1	M	43.6	12.996	0.15469	.73	.75	-.02	17,18,19

(to be continued)

(Continued)

No.	Sample	Or	Non-alkali	Sym	$2V_x$	*b*	*c**	Σt_1 (*b*,*c**)	Σt_1 (2V,Or)	Δ	Ref
58	P50-56	87.7	0.4	M	44.0	12.995	0.15465	.74	.74	0	26
59	BENSON	95.0	0.0	M	44.5	12.997	0.15451	.76	.76	0	26
60	FOX-86	79.0	5.0	M	45.0	12.996	0.15468	.73	.72	.01	8
61	FOX-46	80.9	3.1	M	45.0	12.994	0.15465	.74	.72	.02	8
62	PUYE	42.0	1.2	M	45.5	12.974	0.15566	.60	.60	0	26
63	SP-D	82.3	1.4	M	46.2	12.982	0.15488	.73	.73	0	17,18,19
64	FOX-18	81.7	2.7	M	48.0	12.994	0.15466	.74	.74	0	8
65	SP-F	74.5	1.5	M	49.0	12.976	0.15504	.72	.73	-.01	17,18,19
66	FOX-82	77.9	5.4	M	49.0	12.994	0.15469	.73	.74	-.01	8
67	P2A	93.1	1.5	M	49.0	12.989	0.15455	.78	.78	0	4
68	MT.GIBELE	22.3	6.9	T	49.2	12.936	0.15642	.56	.57	-.01	10,22
69	A1D	90.4	1.4	T	53.0	12.984	0.15453	.81	.79	.02	4
70	439	44.1	3.9	M	53.3	12.993	0.15574	.59	.65	-.06	13,24
71	MAB177	0.3	0.0	T	53.6	.	.	.58	.55	.03	21
72	SH1070	88.0	0.0	M	55.5	12.983	0.15458	.79	.79	0	6,11
73	DQ-1	25.2	6.5	T	56.0	12.953	0.15625	.54	.62	-.08	5
74	HEW-10	27.9	2.8	T	56.0	12.935	0.15623	.61	.62	-.01	6,11
75	FOX-B	85.8	2.3	M	56.0	12.988	0.15452	.79	.79	0	8
76	I-5	0.0	0.0	T	57.0	.	.	.58	.57	.01	16
77	I-1	0.0	0.0	T	58.0	.	.	.60	.58	.02	16
78	I-3B	0.0	0.0	T	58.0	.	.	.59	.58	.01	16

(to be continued)

(Continued)

No.	Sample	Or	Non-alkali	Sym	$2V_x$	*b*	*c**	Σt_1 (*b*,*c**)	Σt_1 (2V,Or)	Δ	Ref
79	CA1A	88.6	1.9	M	60.0	12.984	0.15448	.81	.82	-.01	4
80	FOX-C	88.9	1.4	M	60.0	12.976	0.15443	.84	.82	.02	8
81	HIMALAYA	88.1	0.0	M	63.0	12.963	0.15441	.88	.84	.04	15
82	SP-V	88.0	1.4	M	63.5	12.973	0.15450	.84	.84	0	17,18,19
83	FOX-D	88.1	1.0	M	64.0	12.971	0.15443	.85	.85	0	8
84	7007	88.1	1.0	M	65.0	12.967	0.15451	.85	.85	0	13
85	CA1B	88.6	1.9	T	65.0	12.976	0.15433	.88	.86	.02	4
86	HEW-6	89.4	0.8	M	66.0	12.976	0.15449	.83	.86	-.03	6,11
87	MAB169	0.3	0.0	T	66.1	.	.	.64	.64	0	21
88	MAB176	0.3	0.0	T	66.7	.	.	.66	.65	.01	21
89	I-12	0.0	0.0	T	67.0	.	.	.66	.65	.01	16
90	SP-B	89.0	1.3	M	68.5	12.970	0.15439	.87	.88	-.01	17,18,19
91	FOX-E	83.3	0.7	T	70.0	12.970	0.15442	.88	.88	0	8
92	P1C	90.0	1.4	T	71.0	12.971	0.15431	.90	.90	0	4
93	SP-Z	87.4	1.1	M	71.8	12.965	0.15442	.88	.90	-.02	17,18,19
94	SP-U	86.8	1.1	T	76.0	12.960	0.15425	.95	.93	.02	17,18,19
95	PONTISKALK	98.0	0.0	T	77.0	12.962	0.15404	.99	.96	.03	7
96	I-3A	0.0	0.0	T	78.0	.	.	.79	.75	.04	16
97	RC20C	85.5	1.3	T	78.5	12.961	0.15417	.96	.95	.01	4
98	V-3	0.0	0.0	T	80.0	.	.	.77	.76	.01	16
99	CA1E	88.6	1.9	T	82.0	12.963	0.15408	.98	.98	0	4

(to be continued)

(Continued)

No.	Sample	Or	Non-alkali	Sym	$2V_x$	*b*	*c**	Σt_1 (*b*,*c**)	Σt_1 (2V,Or)	Δ	Ref
100	PELLOTSALO	95.0	0.0	T	82.5	12.964	0.15399	1.00	.99	.01	1
101	PRILEP	96.5	0.0	T	84.0	12.964	0.15400	1.00	1.01	-.01	20
102	MAB171	0.3	0.0	T	85.9	.	.	.80	.82	-.02	21
103	III-16	0.0	0.0	T	92.0	.	.	.92	.88	.04	16
104	MAB167	0.3	0.0	T	96.6	.	.	.92	.93	-.01	21
105	MAB172A	0.3	0.0	T	97.4	.	.	.93	.94	-.01	21
106	III-47	0.0	0.0	T	98.0	.	.	.95	.94	.01	16
107	MAB151	0.3	0.0	T	98.8	.	.	.95	.95	0	21
108	TIBURON	0.3	0.0	T	102.5	12.781	0.15653	.99	.99	0	22,23
109	LA-CC	0.3	0.0	T	103.4	.	.	1.00	1.00	0	21

1. Bailey (1969)
2. Brown & Bailey (1964)
3. Cole et al. (1949)
4. DePieri (1979)
5. DePieri & Quareni (1973)
6. Emerson & Guidotti (1974)
7. Finney & Bailey (1964)
8. Fox & Moore (1969)
9. Gering (1985)
10. Harlow (1982)
11. Hewlett (1959)
12. Ott (1982)
13. Phillips & Ribbe (1973)
14. Priess (1981)
15. Prince et al. (1973)
16. Raase & Kern (1969)
17. Smith & Ribbe (1966)
18. Spencer (1973)
19. Stewart & Wright (1974)
20. Strob (1983)
21. Su et al. (1986)
22. Su (unpublished data)
23. Wainwright & Starkey (1968)
24. Warner et al. (1984)
25. Weitz (1972)
26. Wright & Stewart (1968)
27. Zeipert & Wondratschek (1981)

expressed by Σt_1, the total Al content of the two T_1 tetrahedral sites. Values of Σt_1 are, of course, model-dependent, and this has been reviewed in detail by Kroll and Ribbe (1983). The now familiar *b-c* plot of Wright and Stewart (1968) has been used for more than 15 years to obtain estimates of Σt_1 for alkali feldspars, but there has always been a flaw in its use: plots of *b* versus *c* for alkali exchange series are nonlinear, leading to systematic misestimates in Σt_1 of up to 0.05 (see e.g., Luth, 1974; Hovis, 1984).

Recently Kroll and Ribbe (personal communication) have found that a plot of *b* versus c^* linearizes the exchange series (to about 0.01) and makes them parallel to Σt_1 contours on a b-c^* quadrilateral. They derived equations for determining Σt_1 based on crystal structure analyses of 21 monoclinic and 16 triclinic alkali feldspars and a different algorithm for calculating Σt_1 from lattice parameter data.

For monoclinic feldspars,

$$\Sigma t_1 = 2t_1 = 72.245 - 3.1130b - 200.785c^* \quad . \tag{2}$$

For triclinic feldspars,

$$\Sigma t_1 = t_1o + t_1m = \frac{b - 21.5398 + 53.8405c^*}{21.1567 - 15.8583c^*} \quad . \tag{3}$$

We used these equations to calculate Σt_1 for the 93 samples in Table 5.3 whose unit cell dimensions were known.

For the eight intermediate synthetic albites studied by Raase and Kern (1969), Σt_1 was calculated using his reported values of $\Delta 131 \equiv 2\theta(131) - 2\theta(1\bar{3}1)$ for CuKα radiation and the equation $\Sigma t_1 = t_1o + (1 - t_1o)/3$, where $t_1o = 1.965 - 0.849(\Delta 2\theta)$ and where $(1 - t_1o)/3 = t_1m = t_2o = t_2m$ is implicitly assumed. Similar values for Σt_1 are given by Smith (1974, Fig. 8.7) in his interpretation of Raase and Kern's results. For the eight

albite crystals in the Clear Creek series, Σt_1 values were calculated using reciprocal lattice angles α^* and γ^*, as described in Chapter 3.

For each sample in Table 5.3, an estimated Al content of the T_1tetrahedral sites, Σt_1(2V,Or), was obtained from its position relative to the Σt_1 contours in Figure 5.2, based on its $2V_x$ value and composition. Nearly 83% of the Σt_1(2V,Or) values are within ± 0.02 of their corresponding $\Sigma t_1(b,c^*)$ values, i.e., Σt_1 calculated from lattice parameters, and 97% are within ± 0.04 of their corresponding $\Sigma t_1(b,c^*)$, as displayed on histogram in Figure 5.3. This remarkable agreement substantiates the linear model for variation of refractive indices in the series LA-HA and LM-HS and the two-segment models for HA-HS and LA-LM. In particular it justifies the choices of $2V_x$ and refractive indices for the hypothetical end members and low and high Or_{60} . And one can conclude from this test that the standard error for estimating Σt_1 from 2V and Or using this diagram is about 0.02, which is the same as that attained by estimation using lattice parameters refined from X-ray powder diffraction data.

Also marked in Figure 5.3 are the numbers of samples containing totals of > 2 mol % non-alkali feldspar components. It seems that high non-alkali content tends to cause an underestimate of Σt_1 if we treat the Σt_1 estimated from lattice parameters b and c^* as the "true" values. This may be due to the fact that $\Sigma t_1 > 1.00$ in feldspars with An, Cn and Srf components.

It should be recalled that the final $2V_x$ values (and thus the refractive indices) for hypothetical LM and HS as well the Or_{60} reference points were adjusted a few degrees one way or the other to attain a best fit of the model to the **entire** data set, and this represents one degree of empiricism inherent in the present model. The others are the models relating lattice parameters to Σt_1 and for that matter, those relating results of crystal structure analyses, i.e., Al,Si-O bond lengths, to lattice parameters. Further refinement of Figure 5.2 for use in determining structural states may be anticipated as new,

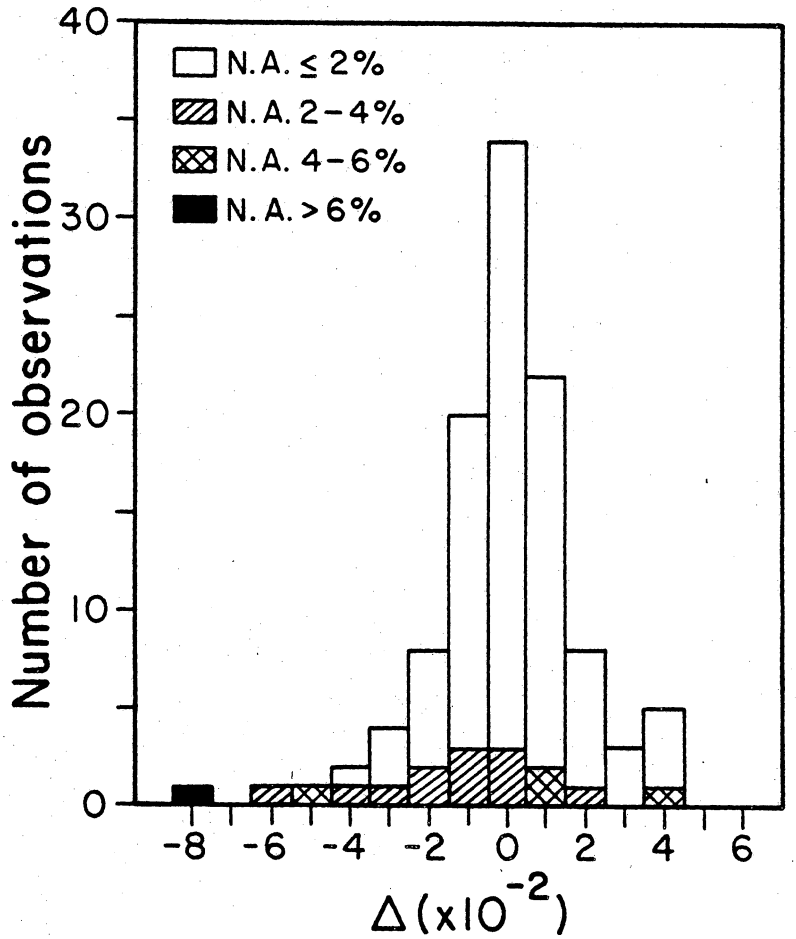

Figure 5.3. Histogram showing frequency distribution of Δ values from Table 5.2: N.A. (non-alkali) refers to mol % of end members other than Ab and Or.

more precise data become available, but for the moment this diagram should prove very useful in routine petrographic investigations of alkali exchange series, natural and heat-treated homogeneous alkali feldspars. On the other hand, it may also be reasonably anticipated that, even if there are refinements, the actual adjustments will be relatively minor, because most of the samples used in evaluating this model are representative of alkali feldspars in terms of their geological occurrences or conditions of formation, and their ranges of chemical compositions in terms of both major and minor constituents.

Case Study of Alkali Exchange Series

Wright and Stewart (1968) described six alkali-exchange series. For each they measured $2V_x$ and the unit cell parameters on (1) a starting material of known composition, (2) its K-exchanged equivalent, and (3) its Na-exchanged equivalent. They estimated compositions of exchanged materials from unit cell volumes. See Table 5.4. We calculated $\Sigma t_1(b,c^*)$ from the b and c^* lattice parameters, using Equations (2) and (3) above. Note in the far right column of Table 5.5 that structural state does not vary significantly [± 0.02 in Σt_1] among any three members of a series, indicating that the Al,Si distribution has remained almost unaffected during the exchange experiments. This is an expected result, and one that has been demonstrated in dozens of similar experiments.

For the five sanidine and orthoclase specimens, the mean values of Σt_1(2V,Or), i.e., those determined from 2V and mol % Or using Figure 5.2, agree within ± 0.02 with $\Sigma t_1(b,c^*)$ for the natural and K-exchanged specimens only. For all the Na-exchanged members, however, mean Σt_1(2V,Or) is systematically less than $\Sigma t_1(b,c^*)$ by 0.06 to as much as 0.11. A possible explanation for these discrepancies is the fact that the starting

Table 5.4. Compositional, optical and structural state data for six feldspars that were alkali-exchanged by Wright and Stewart (1968): The range and the mean value of $2V_x$ for each sample and the corresponding Σt_1 values estimated from Figure 3 using $2V_x$ and Or are listed. These are compared to Σt_1 estimated from lattice parameters *b* and *c**, using an equation from Kroll and Ribbe (in preparation) as expalined in the text.

Sample type	Sample name	Or mol %	$2V_x$ (°) min	$2V_x$ (°) max	$2V_x$ (°) mean	Σt_1(2V,Or) min	Σt_1(2V,Or) max	Σt_1(2V,Or) mean	Σt_1 (*b*,*c**)
Sanidine	Puye	42	40.5	49.0	45.5	0.57	0.62	0.60	0.60
	Puye + KCl	95	-52.0	19.0	-17.0	0.55	0.70	0.63	0.61
	Puye + NaCl	2	42.5	52.0	48.0	0.50	0.54	0.52	0.62
Orthoclase	P50-56	86	41.5	52.0	44.5	0.72	0.77	0.74	0.74
	P50-56 + KCl	95	35.0	42.0	39.0	0.73	0.75	0.74	0.74
	P50-56 + NaCl	8	61.5	67.0	65.0	0.62	0.66	0.65	0.71
Orthoclase	Benson	95	37.5	51.5	44.5	0.74	0.79	0.76	0.76
	Benson + NaCl + KCl	97	38.5	45.5	42.0	0.74	0.77	0.75	0.76
	Benson + NaCl	7	64.0	67.0	66.0	0.64	0.67	0.66	0.72
Orthoclase	SH1070	88	50.0	60.0	55.5	0.77	0.82	0.80	0.79
	SH1070 + KCl	96	48.0	48.5	48.0	0.78	0.78	0.78	0.79
	SH1070 + NaCl	4	66.5	74.5	69.5	0.65	0.72	0.68	0.76
Orthoclase	Spencer-B	89	.	.	68.4	.	.	0.87	0.87
	Spencer-B + NaCl	11	72.5	77.0	75.0	0.72	0.76	0.74	0.85
Microcline	Spencer-U	84	69.0	72.0	71.0	0.87	0.89	0.88	0.95
	Spencer-U + KCl	94	67.5	71.0	70.0	0.88	0.91	0.90	0.94
	Spencer-U + NaCl	0	78.5	86.0	82.5	0.75	0.82	0.79	0.96

material is monoclinic and the Na-exchanged member triclinic. By analogy with the sanidine-microcline transformation, one might expect polysynthetic Albite (A) and/or Pericline (P) twins to develop with inversion. If the Na-exchanged member is submicrotwinned, the optical properties will be different from its untwinned equivalent (Marfunin, 1966, Table 21, p. 140; see also Smith, 1974, Table 8-1, p. 372).

With a program by Hauser and Wenk (1976) as modified by B.J. Cooper, we calculated the effects of both submicroscopic Albite (A) and Pericline (P) twinning on $2V_x$ of albite using the refractive indices and optic orientation of a high albite (Σt_1 = 0.59, specimen MAB-177 described by Su et al., 1986; see Chapter 3). The results in Table 5.5 indicate that $2V_x$ could be reduced by up to 20°, implying that a crystal is more disordered than it actually is, depending on the degree and type or mix of types of submicroscopic twinning.

This "comfortable" conclusion is, however, open to question, because the intermediate microcline (Spencer U, Table 5.5), that started as triclinic and presumably is no more twinned **after** Na-exchange than **before**, also shows too low a $2V_x$ value and thus appears to be significantly more disordered than is indicated by $\Sigma t_1(b,c^*)$. Of course, additional twinning may have been introduced by the exchange process. Note that even for unexchanged and K-exchanged Spencer U there is poor agreement between Σt_1(2V,Or) [= 0.88,0.90] and $\Sigma t_1(b,c^*)$ [= 0.95], and that the latter is further than the former from the Σt_1 value of 0.91 calculated by Kroll and Ribbe (1983, Table 3, p. 65) from a structural analysis by Bailey (1969). The fact that the original Spencer U specimen is not homogeneous but contains two phases (Stewart and Wright, 1974) may have some bearing on the confusion surrounding this specimen.

Table 5.5. Effects of submicroscopic twinning on 2V of high albite: The host material is MAB169, a high albite with $\Sigma t_1 = 0.59$ (see Table 3.1 in Chapter 3). Host = Percentage of untwinned host individual; Ab = Percentage of Albite law twin individual; Pe = Percentage of Pericline law twin individual; Ab-Pe = Percentage of Albite-Pericline law twin individual. $\Delta(2V_x)$ is the difference between the $2V_x$ of untwinned crystal and that of twinned crystal.

Twin law	Host	Ab	Pe	Ab-Pe	$2V_x$	$\Delta(2V_x)$
None	100	0	0	0	53.6	0.0
Albite	90	10	0	0	49.2	4.4
	80	20	0	0	44.5	9.1
	70	30	0	0	39.5	14.1
	60	40	0	0	35.1	18.5
	50	50	0	0	33.2	20.4
Pericaline	90	0	10	0	49.8	3.8
	80	0	20	0	45.9	7.7
	70	0	30	0	42.1	11.5
	60	0	40	0	39.2	14.4
	50	0	50	0	38.0	15.6
Albite-Pericline	40	40	10	10	35.1	18.5
	30	30	20	20	36.9	16.7
	25	25	25	25	37.8	15.8

REFERENCES

Bailey, S.W. (1969) Refinement of an intermediate microcline structure. American Mineralogist, 54, 1540-1545.

Bambauer, H.U., Taborszky, F., and Trochim, H.D. (1971) Optical Determination of Rock-Forming Minerals. Part 1. Determinative Tables. Schweizerbart'sche Verlagsbuchhandlung, Stuttgart, 188 p.

Bertelmann, D., Förtsch, E. and Wondratschek, H. (1985) Zum Temperverhalten von Sanidinen: Die Ausnahmerolle der Eifelsanidin- Megakristalle. Neues Jahrbuch für Mineralogie, Abhandlungen, 152, 123-141.

Bloss, F.D. (1985) Labelling refractive index curves for mineral series. American Mineralogist, 70, 428-432.

Brown, B.E. and Bailey, S.W. (1964) The structure of maximum microcline. Acta Crystallographica, 17, 1391-1400.

Cole, W.F., Sörum, H. and Kennard, O. (1949) The crystal structures of orthoclase and sanidinized orthoclase. Acta Crystallographica, 2, 280-287.

DePieri, R. (1979) Cell dimensions, optic axial angle and structural state in triclinic K-feldspar of the Adamello massif, Northern Italy. Memorie de Scienze Geologiche, Padova, 32.

DePieri, R. and Quareni, S. (1973) The crystal structure of an anorthoclase: an intermediate alkali feldsspar. Acta Crystallographica, B29, 1483-1487.

Emerson, R.W. and Guidotti, C.F. (1974) New x-ray and chemical data on Hewlett's 1959 feldspar suite. American Mineralogist, 59, 615-617.

Finney, J.J. and Bailey, S.W. (1964) Crystal structure of an authigenic maximum microcline. Zeitschrift für Kristallographie, 119, 413-436.

Fox, P.E. and Moore, J.M., Jr. (1969) Feldspars from Adamant pluton, British Columbia. Canadian Journal of Earth Sciences, 6, 1199-1209.

Gering, E. (1985) Silizium/Aluminium-Ordnung und Kristallperfektion von Sanidinen. Dissertation, Universität Karlsruhe.

Gunter, M. and Bloss, F.D. (1982) Andalusite-kanonaite series: lattice parameters and optical properties. American Mineralogist, 67, 1218-1228.

Hauser, J. and Wenk, H.-R. (1976) Optical properties of composite crystals (submicroscopic domains, exsolution lamellae, solid solution). Zeitschrift für Kristallographie, 143, 188-219.

Harlow, G.E. (1982) The anorthoclase structures: the effects of temperature and composition. American Mineralogist, 67, 975-996.

Harlow, G.E. and Brown, G.E., Jr. (1980) Low albite: an x-ray and neutron diffraction study. American Mineralogist, 65, 986-995.

Hewlett, C.G. (1959) Optical properties of potassic feldspars. Bulletin of the Geological Society of America, 70, 511-538.

Hovis, G.L. (1984) Characterization of Al-Si distributions in alkali feldspars. Bulletin of the Geological Society of America, 16, 544.

Kroll, H. and Ribbe, P.H. (1983) Lattice parameters, composition and Al,Si order in alkali feldspars. In P.H. Ribbe, Ed., Feldspar Mineralogy, Reviews in Mineralogy, 2, 2nd Edition, 57-100. Mineralogical Society of America, Washington, D.C., 362p.

Luth, W.C. (1974) Analysis of experimental data on alkali feldspars: unit cell parameters and solvi. In W.S. MacKenzie and J. Zussman, Eds., The Feldspars, p. 249-296. Manchester University Press, Manchester, 717p.

Marfunin, A.S. (1966) The feldspars: phase relations, optical properties, and geological distribution. (Translated from the Russian edition, 1962.) Israel Program for Scientific Translations, Jerusalem, 317p.

Orville, P.M. (1967) Unit-cell parameters of the microcline-low albite and the sanidine-high albite solid solution series. American Mineralogist, 52, 55-86.

Ott, G. (1982) Rötgenographische Strukturverfeinerungen an getemperten Eifelsanidinen zur Feststellung ihres Ordnungszustandes. Diplomarbeit, Universität Karlsruhe.

Phillips, M.W. and Ribbe, P.H. (1973) The structures of monoclinic potassium-rich feldspars. American Mineralogist, 58, 263-270.

Plas, L. van der (1966) The Identification of Detrital Feldspars. Elsevier, Amsterdam, 305p.

Priess, U. (1981) Untersuchungen zur Tief-Hoch-Umwandlung von Fe-hältigen Orthoklas-Kristallen aus Madagascar. Neues Jahrbuch für Mineralogie, Abhandlungen, 141, 17-29.

Prince, E., Donnay, G. and Martin, R.F. (1973) Neutron diffraction refinement of an ordered orthoclase structure. American Mineralogist, 58, 500-507.

Raase, P. and Kern, H. (1969) Über die Synthese von Albiten bei Temperaturen von 250 bis 700°C. Contributions to Mineralogy and Petrology, 21, 225-237.

Rankin, D.W. (1967) Axial angle determinations in Orville's microcline-low albite solid solution series. American Mineralogist, 52, 414-417.

Smith, J.R. (1958) Optical properties of heated plagioclases. American Mineralogist, 43, 1179-1194.

Smith, J.V. (1974) Feldspar Minerals. I. Crystal Structure and Physical Properties. Springer-Verlag, Heidelberg, 672p.

Smith, J.V. and Ribbe, P.H. (1966) X-ray-emission microanalysis of rock-forming minerals. III. Alkali feldspars. Journal of Geology, 76, 197-216.

Spencer, E. (1937) The potash-ash feldspars I. Thermal stability. Mineralogical Magazine, 24, 453-494.

Stewart, D.B. (1974) Optic axial angle and extinction angles of alkali feldspars related by cell parameters to Al/Si order and composition. In W.S. MacKenzie and J. Zussman, Eds., The Feldspars, p. 145-161. Manchester University Press, Manchester, 717p.

Stewart, D.B. and Ribbe, P.H. (1969) Structural explanation for variations in cell parameters of alkali feldspar with Al/Si ordering. American Journal of Science, 267-A, 144-462.

Stewart, D.B. and Ribbe, P.H. (1983) Optical properties of feldspars. In P.H. Ribbe, Ed., Feldspar Mineralogy, Reviews in Mineralogy, 2, 2nd Edition, 121-139. Mineralogical Society of America, Washington, D.C., 362p.

Stewart, D.B. and Wright, T.L. (1974) Al/Si order and symmetry of natural alkali feldspars, and the relationship of strained cell parameters to bulk composition. Bulletin de la Société française de Minéralogie et de Cristallographie, 97, 356-377.

Strob, W. (1983) Strukturverfeinerung eines Tief-Mikroklins, Zusammenhange zwischen <T-O> Abstanden und Al,Si-Ordnungsgrad und metrische Variation in einer Tief-Albit/Tief-Mikroklin-Mischkristallreihe. Diplomarbeit, Institut für Mineralogie, Westfälische Wilhelms-Universität, Münster.

Su, S.C., Bloss, F.D., Ribbe, P.H., and Stewart, D.B. (1984) Optic axial angle, a precise measure of Al,Si ordering in T_1 tetrahedral sites of K-rich alkali feldspars. American Mineralogist, 69, 440-448.

Su, S.C., Ribbe, P.H., Bloss, F.D., and Goldsmith, J.R. (1985) Structural states and properties of a low-high albite series of single crystals. Geological Society of America, Abstracts with Programs, 17, 729.

Su, S.C., Ribbe, P.H., Bloss, F.D., and Goldsmith, J.R. (1986) Optical properties of single crystals in the order-disorder series low-high albite. American Mineralogist, 71, in press.

Wainwright, J.E. and Starkey, J. (1968) Crystal structure of a metamorphic low albite. Program, Geological Society of America, Annual Meeting, Mexico City, 310.

Warner, J.K., Su, S.C., Ribbe, P.H., and Bloss, F.D. (1984) Optical properties of the analbite-high sanidine solid solution series. Geological Society of America, Abstracts with Programs, 16, 687.

Weitz, G. (1972) Die Struktur des Sanidins bei verschiedenen Ordnungsgraden. Zeitschrift für Kristallographie, 136, 418-426.

Wolfe, H.E. (1976) Optical and X-ray Study of the Low Plagioclases. M.S. thesis, Virginia Polytechnic Institute and State University. Blacksburg, Virginia.

Wright, T.L. and Stewart, D.B. (1968) X-ray and optical study of alkali feldspars: II. An X-ray method for determining the composition and structural state from measurement of 2Θ values for three reflections. American Mineralogist, 53, 88-104.

Wright, T.L. and Stewart, D.B. (1968) X-ray and optical study of alkali feldspars: I. Determination of compositions and structural state from refined unit-cell parameters and 2V. American Mineralogist, 53, 38-87.

Zeipert, C. and Wondratschek, H. (1981) Ein ungewöhnliches Temperverhalten bei Sanidin von Volkesfeld/Eifel. Neues Jahrbuch für Mineralogie Monatshefte, 407-415.

APPENDIX

Calculation of 2V-Or Diagram Contoured for Σt_1

Because a two-segment linear model was used to delineate the variations of refractive indices of alkali feldspar series with the same structural state, calculations were carried out separately for the ranges $Or_{0\text{-}60}$ and $Or_{60\text{-}100}$. For the latter, two orientations of the optic axial angle (O.A.P.) were also treated separately.

The refractive indices of end members and Or_{60} members are those listed in Table 5.1.

Symbols used in the following derivations are:

Or: mol % Or ($KAlSi_3O_8$);

Σt_1: Al content of T_1 sites;

A, B, C: principal refractive indices most nearly parallel to crystallographic directions *a*, *b*, *c*, respectively. The superscripts indicate the values of Σt_1 and subscripts the values of mol % Or. E.g., ${}^{0.6}A_{60}$ is n_a at $\Sigma t_1 = 0.6$ and Or = 60, and ${}^{1.0}B_{Or}$ is n_b at $\Sigma t_1 = 1.0$ and given Or.

Case 1. Or $\leq$ 60

(1) Refractive indices for the series with $\Sigma t_1 = 1.0$.

$$ {}^{1.0}A_{Or} = {}^{1.0}A_0 + ({}^{1.0}A_{60} - {}^{1.0}A_0)\,Or/60 \tag{1} $$

$$ {}^{1.0}B_{Or} = {}^{1.0}B_0 + ({}^{1.0}B_{60} - {}^{1.0}B_0)\,Or/60 \tag{2} $$

$$ {}^{1.0}C_{Or} = {}^{1.0}C_0 + ({}^{1.0}C_{60} - {}^{1.0}C_0)\,Or/60 \tag{3} $$

(2) Refractive indices for the series with $\Sigma t_1 = 0.6$.

$$ {}^{0.6}A_{Or} = {}^{0.6}A_0 + ({}^{0.6}A_{60} - {}^{0.6}A_0)\,Or/60 \tag{4} $$

$$ {}^{0.6}B_{Or} = {}^{0.6}B_0 + ({}^{0.6}B_{60} - {}^{0.6}B_0)\,Or/60 \tag{5} $$

$$ {}^{0.6}C_{Or} = {}^{0.6}C_0 + ({}^{0.6}C_{60} - {}^{0.6}C_0)\,Or/60 \tag{6} $$

(3) Refractive indices at Σt_1 and Or.

$$ A = {}^{1.0}A_{Or} - ({}^{0.6}A_{Or} - {}^{1.0}A_{Or})(\Sigma t_1 - 1.0)/0.4 \tag{7} $$

$$ B = {}^{1.0}B_{Or} - ({}^{0.6}B_{Or} - {}^{1.0}B_{Or})(\Sigma t_1 - 1.0)/0.4 \tag{8} $$

$$ C = {}^{1.0}C_{Or} - ({}^{0.6}C_{Or} - {}^{1.0}C_{Or})(\Sigma t_1 - 1.0)/0.4 \tag{9} $$

(4) Optic axial angle $2V_x$ at Σt_1 and Or.

$$ 2V_x = 2\sin^{-1}\sqrt{(C^{-2} - B^{-2})/(A^{-2} - B^{-2})} \tag{10} $$

Case 2. Or > 60 and O.A.P. (~) $\perp$ (010)

(1) Refractive indices for the series with $\Sigma t_1 = 1.0$.

$$^{1.0}A_{Or} = {}^{1.0}A_{60} + ({}^{1.0}A_{100} - {}^{1.0}A_{60})(Or - 60)/40 \quad (11)$$

$$^{1.0}B_{Or} = {}^{1.0}B_{60} + ({}^{1.0}B_{100} - {}^{1.0}B_{60})(Or - 60)/40 \quad (12)$$

$$^{1.0}C_{Or} = {}^{1.0}C_{60} + ({}^{1.0}C_{100} - {}^{1.0}C_{60})(Or - 60)/40 \quad (13)$$

(2) Refractive indices for the series with $\Sigma t_1 = 0.6$.

$$^{0.6}A_{Or} = {}^{0.6}A_{60} + ({}^{0.6}A_{100} - {}^{0.6}A_{60})(Or - 60)/40 \quad (14)$$

$$^{0.6}B_{Or} = {}^{0.6}B_{60} + ({}^{0.6}B_{100} - {}^{0.6}B_{60})(Or - 60)/40 \quad (15)$$

$$^{0.6}C_{Or} = {}^{0.6}C_{60} + ({}^{0.6}C_{100} - {}^{0.6}C_{60})(Or - 60)/40 \quad (16)$$

(3) Refractive indices at Σt_1 and Or.

$$A = {}^{1.0}A_{Or} - ({}^{0.6}A_{Or} - {}^{1.0}A_{Or})(\Sigma t_1 - 1.0)/0.4 \quad (17)$$

$$B = {}^{1.0}B_{Or} - ({}^{0.6}B_{Or} - {}^{1.0}B_{Or})(\Sigma t_1 - 1.0)/0.4 \quad (18)$$

$$C = {}^{1.0}C_{Or} - ({}^{0.6}C_{Or} - {}^{1.0}C_{Or})(\Sigma t_1 - 1.0)/0.4 \quad (19)$$

(4) Optic axial angle $2V_x$ at Or and Σt_1.

$$2V_x = 2\sin^{-1}\sqrt{(C^{-2} - B^{-2})/(A^{-2} - B^{-2})} \quad (20)$$

Case 3. Or > 60 and O.A.P. = (010)

In this case, the equations for A, B and C have the same forms as (17), (18) and (19), respectively, but C > B. Thus,

$$2V_x = 2\sin^{-1}\sqrt{(B^{-2} - C^{-2})/(A^{-2} - C^{-2})} \quad (21)$$

The above calculations were undertaken at increments of 1 mol % from 0 through 100% and for Σt_1 at increments of 0.01 from 0.5 through 1.0 to get $2V_x$ values at each Or,Σt_1 point. Then $2V_x$ was plotted versus mol % Or and contoured for Σt_1, as seen in Figure 5.2.

Derivation of Equation (1) in the Text

Case 1. Or $\leq$ 60.

Substituting (1) and (4) into (7), (2) and (5) into (8), (3) and (6) into (9), we can express the three principal refractive indices A, B, C as functions of Σt_1 and Or:

$$A = f_1(\Sigma t_1, Or) \ , \quad (22)$$

$$B = f_2(\Sigma t_1, Or) \ , \quad (23)$$

$$C = f_3(\Sigma t_1, Or) \ . \quad (24)$$

Because the birefringences of alkali feldspars are very low (≤ 0.011), the following approximate equation for calculating 2V from refractive indices can be used:

$$\sin^2 V_x = (B - C)/(B - A) \quad . \tag{25}$$

Substituting (22), (23) and (24) into (25) and rearranging the terms, we can express Σt_1 as a function of $\sin^2 V_x$ and or X_{Or} (mole fraction of $KAlSi_3O_8$; $X_{Or} = Or/100$).

$$\Sigma t_1 = \frac{b_0 + b_1 X_{Or} + b_2 X_{Or} \sin^2 V_x + b_3 \sin^2 V_x}{a_0 + a_1 X_{Or} + a_2 X_{Or} \sin^2 V_x + a_3 \sin^2 V_x} \quad , \tag{26}$$

where $a_0 = {}^{0.6}C_0 - {}^{1.0}C_0 - {}^{0.6}B_0 + {}^{1.0}B_0$,

$a_1 = 5/3[({}^{0.6}C_{60} - {}^{0.6}C_0) - ({}^{0.6}B_{60} - {}^{0.6}B_0) - ({}^{1.0}C_{60} - {}^{1.0}C_0) + ({}^{1.0}B_{60} - {}^{1.0}B_0)]$,

$a_2 = 5/3[({}^{1.0}A_{60} - {}^{1.0}A_0) - ({}^{1.0}B_{60} - {}^{1.0}B_0) - ({}^{0.6}A_{60} - {}^{0.6}A_0) + ({}^{0.6}B_{60} - {}^{0.6}B_0)]$,

$a_3 = {}^{1.0}A_0 - {}^{0.6}A_0 - {}^{1.0}B_0 + {}^{0.6}B_0$,

$b_0 = a_0 + 0.4({}^{1.0}C_0 - {}^{1.0}B_0)$,

$b_1 = a_1 + 2/3[({}^{1.0}C_{60} - {}^{1.0}C_0) - ({}^{1.0}B_{60} - {}^{1.0}B_0)]$,

$b_2 = a_2 + 2/3[({}^{1.0}B_{60} - {}^{1.0}B_0) - ({}^{1.0}A_{60} - {}^{1.0}A_0)]$,

$b_3 = a_3 + 0.4({}^{1.0}B_0 - {}^{1.0}A_0)$.

Case 2. Or > 60 and O.A.P. $(\sim) \perp (010)$

In this case, the equation has the same form as (26), but the coefficients are different.

$$a_0 = {}^{0.6}C_{60} - {}^{0.6}B_{60} - {}^{1.0}C_{60} + {}^{1.0}B_{60} + 2/3[({}^{0.6}C_{60} - {}^{0.6}C_{100}) - ({}^{0.6}B_{60} - {}^{0.6}B_{100}) - ({}^{1.0}C_{60} - {}^{1.0}C_{100}) + ({}^{1.0}B_{60} - {}^{1.0}B_{100})]$$

$$a_1 = 5/2[({}^{0.6}C_{60} - {}^{0.6}C_{100}) - ({}^{0.6}B_{60} - {}^{0.6}B_{100}) - ({}^{1.0}C_{60} - {}^{1.0}C_{100}) + ({}^{1.0}B_{60} - {}^{1.0}B_{100})]$$

$$a_2 = {}^{0.6}B_{60} - {}^{0.6}A_{60} - {}^{1.0}B_{60} + {}^{1.0}A_{60} + 2/3[({}^{0.6}A_{60} - {}^{0.6}A_{100}) - ({}^{0.6}B_{60} - {}^{0.6}B_{100}) - ({}^{1.0}A_{60} - {}^{1.0}A_{100}) + ({}^{1.0}B_{60} - {}^{1.0}B_{100})]$$

$$a_3 = 5/2[({}^{0.6}B_{60} - {}^{0.6}B_{100}) - ({}^{0.6}A_{60} - {}^{0.6}A_{100}) - ({}^{1.0}B_{60} - {}^{1.0}B_{100}) + ({}^{1.0}A_{60} - {}^{1.0}A_{100})]$$

$$b_0 = a_0 + 2/5({}^{1.0}C_{60} - {}^{1.0}B_{60}) + 3/5[({}^{1.0}C_{60} - {}^{1.0}C_{100}) - ({}^{1.0}B_{60} - {}^{1.0}B_{100})]$$

$$b_1 = a_1 + ({}^{1.0}B_{60} - {}^{1.0}B_{100}) - ({}^{1.0}C_{60} - {}^{1.0}C_{100})]$$

$$b_2 = a_2 + ({}^{1.0}A_{60} - {}^{1.0}A_{100}) - ({}^{1.0}B_{60} - {}^{1.0}B_{100})]$$

$$b_3 = a_3 + 2/5({}^{1.0}B_{60} - {}^{1.0}A_{60}) + 3/5[({}^{1.0}B_{60} - {}^{1.0}B_{100}) - ({}^{1.0}A_{60} - {}^{1.0}A_{100})]$$

Case 3. Or > 60 and O.A.P. = (010)

In this case, the equations still has the same form as (26), but the coefficients are different.

$$a_0 = {}^{0.6}B_{60} - {}^{0.6}C_{60} - {}^{1.0}B_{60} + {}^{1.0}C_{60} + 2/3[({}^{0.6}C_{60} - {}^{0.6}C_{100}) - ({}^{0.6}B_{60} - {}^{0.6}B_{100}) - ({}^{1.0}C_{60} - {}^{1.0}C_{100}) + ({}^{1.0}B_{60} - {}^{1.0}B_{100})]$$

$$a_1 = 5/2[({}^{0.6}B_{60} - {}^{0.6}B_{100}) - ({}^{0.6}C_{60} - {}^{0.6}C_{100}) - ({}^{1.0}B_{60} - {}^{1.0}B_{100}) + ({}^{1.0}C_{60} - {}^{1.0}C_{100})]$$

$$a_2 = 5/2[({}^{0.6}C_{60} - {}^{0.6}C_{100}) - ({}^{0.6}A_{60} - {}^{0.6}A_{100}) - ({}^{1.0}C_{60} - {}^{1.0}C_{100}) + ({}^{1.0}A_{60} - {}^{1.0}A_{100})]$$

$$a_3 = {}^{0.6}C_{60} - {}^{0.6}A_{60} - {}^{1.0}C_{60} + {}^{1.0}A_{60} + 2/3[({}^{0.6}A_{60} - {}^{0.6}A_{100}) - ({}^{0.6}C_{60} - {}^{0.6}C_{100}) - ({}^{1.0}A_{60} - {}^{1.0}A_{100}) + ({}^{1.0}C_{60} - {}^{1.0}C_{100})]$$

$$b_0 = a_0 + 2/5({}^{1.0}B_{60} - {}^{1.0}C_{60}) + 3/5[({}^{1.0}B_{60} - {}^{1.0}B_{100}) - ({}^{1.0}C_{60} - {}^{1.0}C_{100})]$$

$$b_1 = a_1 + ({}^{1.0}C_{60} - {}^{1.0}C_{100}) - ({}^{1.0}B_{60} - {}^{1.0}B_{100})]$$

$$b_2 = a_2 + ({}^{1.0}A_{60} - {}^{1.0}A_{100}) - ({}^{1.0}C_{60} - {}^{1.0}C_{100})]$$

$$b_3 = a_3 + 2/5({}^{1.0}C_{60} - {}^{1.0}A_{60}) + 3/5[({}^{1.0}C_{60} - {}^{1.0}C_{100}) - ({}^{1.0}A_{60} - {}^{1.0}A_{100})]$$

The 4 page vita has been removed from the scanned document

The 4 page vita has been removed from the scanned document

The 4 page vita has been removed from the scanned document

The 4 page vita has been removed from the scanned document